UNCLASSIFIED

SECURITY CLASSIFICATION OF THIS PAGE *(When Data Entered)*

REPORT DOCUMENTATION PAGE		READ INSTRUCTIONS BEFORE COMPLETING FORM
1 REPORT NUMBER AFGL-TR-82-0086	2 GOVT ACCESSION NO.	3 RECIPIENT'S CATALOG NUMBER
4 TITLE *(and Subtitle)* A REVIEW OF OPTICAL DATA ANALYSIS RELATED TO THE MODELLING OF VISIBLE AND OPTICAL INFRARED ATMOSPHERIC PROPERTIES		5 TYPE OF REPORT & PERIOD COVERED Final Report 1 OCT 78 - 30 SEP 81
		6 PERFORMING ORG REPORT NUMBER SIO 83-5
7 AUTHOR(s) Richard W. Johnson Jacqueline I. Gordon		8 CONTRACT OR GRANT NUMBER(s) F19628-78-C-0200
9 PERFORMING ORGANIZATION NAME AND ADDRESS University of California, San Diego Visibility Laboratory La Jolla, California 92093		10 PROGRAM ELEMENT, PROJECT, TASK AREA & WORK UNIT NUMBERS 62101F 7670-14-01
11 CONTROLLING OFFICE NAME AND ADDRESS Air Force Geophysics Laboratory Hanscom AFB, Massachusetts 01731 Contract Monitor: Major John D. Mill/OPA		12 REPORT DATE January 1982
		13 NUMBER OF PAGES 73
14 MONITORING AGENCY NAME & ADDRESS *(if different from Controlling Office)*		15 SECURITY CLASS *(of this report)* UNCLASSIFIED
		15a DECLASSIFICATION/DOWNGRADING SCHEDULE

16 DISTRIBUTION STATEMENT *(of this Report)*

Approved for public release; distribution unlimited.

17 DISTRIBUTION STATEMENT *(of the abstract entered in Block 20, if different from Report)*

18 SUPPLEMENTARY NOTES

19 KEY WORDS *(Continue on reverse side if necessary and identify by block number)*

Atmospheric Optical Properties
Atmospheric Volume Scattering Coefficients
Equilibrium Radiance
Models for Atmospheric Optical Properties
Contrast Transmittance Models

20 ABSTRACT *(Continue on reverse side if necessary and identify by block number)*

This Final Report under Contract No. F19628-78-C-0200 summarizes the results of a data analysis and modelling program addressing optical atmospheric properties in the western European environment. Two sets of data, one a series of surface measurements and the other an airborne set, were used in the analysis. The ground level data were collected by several host nation technical teams under the auspices of the NATO Research Study Group 8 of Panel IV, AC243, with the majority of that used in this analysis collected by the Physics Group of the

DD FORM 1 JAN 73 1473 EDITION OF 1 NOV 65 IS OBSOLETE
S/N 0102-014-6601

UNCLASSIFIED

SECURITY CLASSIFICATION OF THIS PAGE *(When Data Entered)*

20. ABSTRACT continued:

Physics Laboratory of the National Defense Research Organization - TNO at Ypenberg Air Base, Netherlands. The airborne data were collected by the Visibility Laboratory in cooperation with and under the sponsorship of the Air Force Geophysics Laboratory, Hanscom AFB, Massachusetts.

The Optical Data Analysis effort, task two under this two part research contract has concentrated on the analysis of selected sub-sets of surface and airborne data bases [Johnson *et al.* (1979)] and the application of these analyses toward the development of operationally useful models for the prediction of atmospheric optical properties.

Comparison of the surface visible and infrared extinction data, Shields (1981) with existing model predictions, primarily LOWTRAN 5, illustrated reasonable model performances on the average, but as one might expect, substantial shortcomings in the prediction of the high frequency variations in extinction which occur under the more turbid condition encountered during mist or fog episodes.

Analysis of the airborne data base has led to the development of the Hering model (Hering, 1981), a new operational technique for estimating visible spectrum contrast transmittance. The technique is relatively fast and easy to apply, yet is designed to take full advantage of the present limited capability to observe and predict the relevant atmospheric variables. To the extent that a climatological data base of conventional meteorological observations exists, the techniques in their present form can be used to estimate readily the frequency distributions of such quantities as spectral contrast transmittance, as a function of location and season. The model is used to demonstrate the change in target acquisition ranges as a function of variations in selected atmospheric parameters.

The Gordon clear day atmosphere model (Gordon, 1969), is evaluated against several other existing models defining Rayleigh atmospheric conditions, and is also compared with actual measurements of real atmospheres. Good agreement is illustrated in both instances, so the model concept is extended into the turbid atmosphere regime by a preliminary specification of a new cloud cover index, the cloud scalar irradiance ratio, and the introduction of a new model parameter, equilibrium reflectance. This generalization of the earlier model format is compared against airborne measurements and appears encouraging in its ability to address the more turbid atmospheric scenarios.

AFGL-TR-82-0086 SIO 83-5

A REVIEW OF OPTICAL DATA ANALYSIS RELATED TO THE MODELLING OF VISIBLE AND OPTICAL INFRARED ATMOSPHERIC PROPERTIES

Richard W. Johnson
Jacqueline I. Gordon

Visibility Laboratory
University of California, San Diego
Scripps Institution of Oceanography
La Jolla, California 92093

Approved:

Roswell W. Austin, Director
Visibility Laboratory

Approved:

William A. Nierenberg, Director
Scripps Institution of Oceanography

CONTRACT NO. F19628-78-C-0200
Project No. 7670
Task No. 7670-14
Work Unit No. 7670-14-01

Final Report
1 OCT 78 - 30 SEP 81

January 1982

Contract Monitor
Major John D. Mill, Atmospheric Optics Branch, Optical Physics Division

Prepared for

AIR FORCE GEOPHYSICS LABORATORY
AIR FORCE SYSTEMS COMMAND
UNITED STATES AIR FORCE
HANSCOM AFB, MASSACHUSETTS 01731

SUMMARY

This Final Report under Contract No. F19628-78-C-0200 summarizes the results of a data analysis and modelling program addressing optical atmospheric properties in the western European environment. Two sets of data, one a series of surface measurements and the other an airborne set, were used in the analysis. The ground level data were collected by several host nation technical teams under the auspices of the NATO Research Study Group 8 of Panel IV, AC243, with the majority of that used in this analysis collected by the Physics Group of the Physics Laboratory of the National Defense Research Organization - TNO at Ypenberg Air Base, Netherlands. The airborne data were collected by the Visibility Laboratory in cooperation with and under the sponsorship of the Air Force Geophysics Laboratory, Hanscom AFB, Massachusetts.

The Optical Data Analysis effort, task two under this two part research contract has concentrated on the analysis of selected sub-sets of surface and airborne data bases [Johnson *et al.* (1979)] and the application of these analyses toward the development of operationally useful models for the prediction of atmospheric optical properties.

Comparison of the surface visible and infrared extinction data, Shields (1981) with existing model predictions, primarily LOWTRAN 5, illustrated reasonable model performances on the average, but as one might expect, substantial shortcomings in the prediction of the high frequency variations in extinction which occur under the more turbid condition encountered during mist or fog episodes.

Analysis of the airborne data base has led to the development of the Hering model (Hering, 1981), a new operational technique for estimating visible spectrum contrast transmittance. The technique is relatively fast and easy to apply, yet is designed to take full advantage of the present limited capability to observe and predict the relevant atmospheric variables. To the extent that a climatological data base of conventional meteorological observations exists, the techniques in their present form can be used to estimate readily the frequency distributions of such quantities as spectral contrast transmittance, as a function of location and season. The model is used to demonstrate the change in target acquisition ranges as a function of variations in selected atmospheric parameters.

The Gordon clear day atmosphere model (Gordon, 1969), is evaluated against several other existing models defining Rayleigh atmospheric conditions, and is also compared with actual measurements of real atmospheres. Good agreement is illustrated in both instances, so the model concept is extended into the turbid atmosphere regime by a preliminary specification of a new cloud cover index, the cloud scalar irradiance ratio, and the introduction of a new model parameter, equilibrium reflectance. This generalization of the earlier model format is compared against airborne measurements and appears encouraging in its ability to address the more turbid atmospheric scenarios.

TABLE OF CONTENTS

LIST OF TABLES AND ILLUSTRATIONS

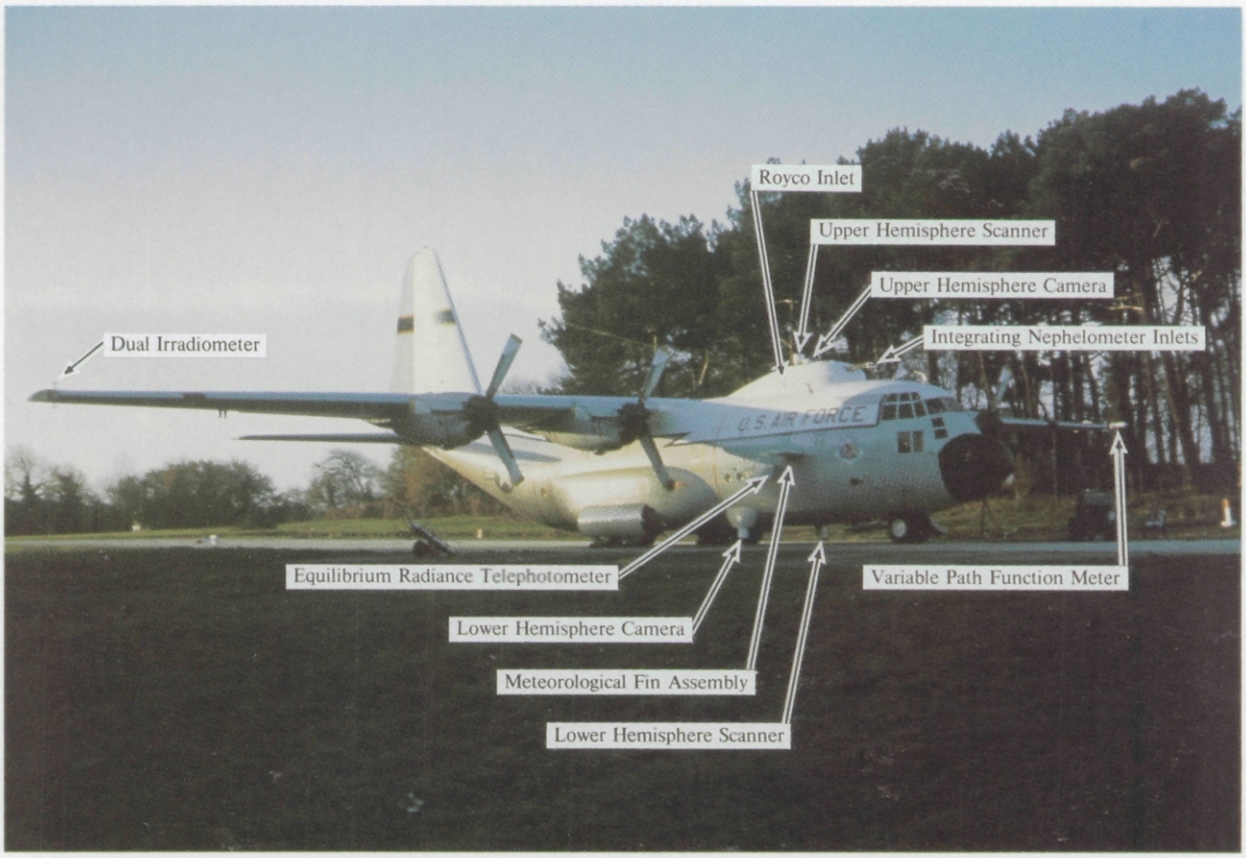

Frontispiece

Air Force C-130A, 550022, as deployed to Lann Bihoue Air Base, near Lorient, France during the summer of 1977. This aircraft, operated and maintained by Air Crews from the 4950th Test Wing, Wright Patterson AFB, Ohio, performed as the instrumented research vehicle for the data base collection described in this Final Report. The research was conducted by the Visibility Laboratory of the University of California, San Diego in cooperation with, and under the sponsorship of The Air Force Geophysics Laboratory, Hanscom AFB, Massachusetts.

A REVIEW OF OPTICAL DATA ANALYSIS RELATED TO THE MODELLING OF VISIBLE AND OPTICAL-INFRARED ATMOSPHERIC PROPERTIES

Richard W. Johnson
Jacqueline I. Gordon

1. INTRODUCTION

This Final Report under Contract No. F19628-78-C-0200 summarizes the results of a data analysis and modelling program addressing the optical atmospheric properties in the western European environment. Two sets of data, one a series of surface measurements and the other an airborne set, were used for most of the analytic effort. The ground level data were collected by several host nation technical teams under the auspices of the NATO Research Study Group 8 of Panel IV, AC243, and its Program OPAQUE, with the majority of that used in this analysis collected by the Physics Group of the Physics Laboratory of the National Defense Research Organization - TNO at Ypenberg Air Base, Netherlands. The airborne data were collected by the Visibility Laboratory of the University of California, San Diego in cooperation with, and under the sponsorship of the Air Force Geophysics Laboratory, Hanscom AFB, Massachusetts. These two data bases have been discussed in several preceding reports. The ground based data set and its conceptual organization is fully described by Fenn (1978), whereas a preliminary survey of the proposed use of both surface and airborne sets in the analysis and modelling effort is contained in Johnson *et al.* (1979).

The general European locale for the airborne and surface measurements used in this study is illustrated in Fig. 1-1 which indicates the six approximate flight tracks by short boldfaced lines such as that shown just north of Birkhof, Germany. The OPAQUE surface stations associated with each flight track are listed in Table 1.1 and described more specifically in Fenn (1978).

Table 1.1. Geographical Distribution of Project OPAQUE Data Flights.

Flight Track Ident	Attempted (and reported) Data Sequences				
	OPAQUE I Spring	OPAQUE II Fall	OPAQUE III Summer	OPAQUE IV Winter	OPAQUE V Summer
Sigonella, Sicily	0	0	0	2 (2)	0
Trapani, Sicily*	0	0	0	3 (3)	4 (4)
Bruz, France*	0	5 (5)	3 (3)	0	0
Birkhof, Germany*	0	0	0	8 (7)	5 (4)
Yeovil, England	5 (3)	0	0	5 (5)	3 (3)
Soesterberg, Netherlands	1 (1)	0	1 (0)	2 (2)	3 (3)
Mildenhall, England	0	0	0	2 (2)	0
Ahlhorn, Germany	0	0	2 (2)	0	0
Meppen, Germany*	5 (2)	4 (3)	3 (3)	3 (3)	3 (3)
Rodby, Denmark*	2 (2)	4 (4)	4 (4)	2 (2)	2 (2)
TOTAL	13 (8)	13 (12)	13 (12)	27 (26)	20 (19)
Technical Report No	AFGL-TR-77-0078	AFGL-TR-77-0239	AFGL-TR-78-0168	AFGL-TR 79-0159	AFGL-TR-80-0207

Note: OPAQUE surface stations located near cities identified with asterisk *, plus Christchurch, England 68 km ESE from Yeovil, and Ypenberg, Netherlands 69 km WSW from Soesterberg.

Since the basic data sets developed from both the airborne and surface measurement programs have been described at length in several preceding reports, Johnson *et al.* (1979), Fenn *et al.* (1979), Johnson (1981a), Johnson and Fitch (1981), and several of those listed in Appendix A, they will be summarized only briefly here. The primary measurements made by the airborne system are listed in Table 1.2. The profile measurements are described thoroughly in the reports listed in the bottom row of Table 1.1, and the constant altitude measurements, primarily those of sky and terrain radiances, are presented in Johnson (1981c), and Johnson and Hering (1981b). As noted in each of these earlier references, the airborne radiometric measurements were made in four separate spectral bands within the visible spectrum. One of these

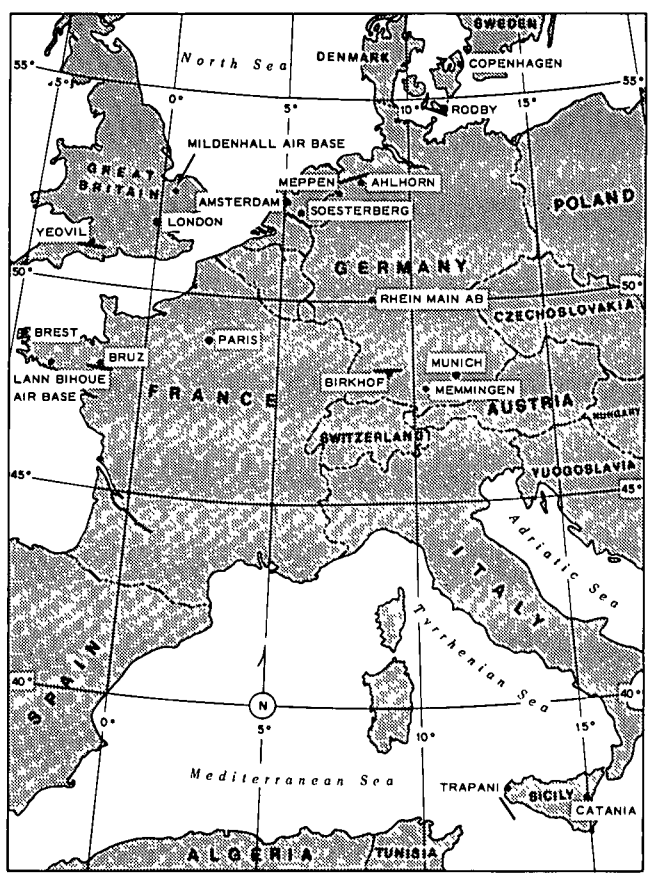

Fig. 1-1. Typical OPAQUE flight tracks and surface data sites.

Table 1.2. Typical Airborne Data.

Flight Mode & Item No	Measured Quantity	Quantity Description	Units
Profile			
1	$s(z)$	Volume Scattering Coefficient	m^{-1}
2	$E(z,d)$	Downwelling Flat Plate Irradiance	$Wm^{-2}\mu m^{-1}$
3	$E(z,u)$	Upwelling Flat Plate Irradiance	$Wm^{-2}\mu m^{-1}$
4	$L_o(z,\theta,\phi)$	Path Function	$(Wsr^{-1}m^{-2}\mu m^{-2})m^{-1}$
5	$t(z)$	Ambient Temperature	°C
6	$d^t(z)$	Dewpoint or Frostpoint Temperature	°C
7	$P(z)$	Atmospheric Pressure	mb
Constant Altitude			
1	$\sigma(z,\beta)$, β = 30° & 150°	Volume Scattering Function	$m^{-1}sr^{-1}$
2	$L^*_\infty(z,\theta,\phi)$, 90°>θ>0°	Sky Radiance, 5°FOV, 2π coverage	$Wsr^{-1}m^{-2}\mu m^{-1}$
3	${}_0L_t(z,\theta,\phi)$, 180°>θ>90°	Terrain Radiance, 5°FOV, 2π coverage	$Wsr^{-1}m^{-2}\mu m^{-1}$

Table 1.3. Typical OPAQUE Surface Data.

Item No	Measured		Time	Quantity Description	Units
1	SMAX & SMIN	vs	"	Visible Scattering Coefficient (nephelometer)	km^{-1}
2	SEMAX & SEMIN	vs	"	Visible Extinction Coefficient (transmissometer)	km^{-1}
3	T1 & T5	vs	"	Infrared Transmittance (3-5μm, First & Last)	%
4	T2 & T3	vs	"	Infrared Transmittance (8-12μm & 8-13μm)	%
5	TX	vs	"	Infrared Transmittance (4μm)	%
6	PRESS	vs	"	Atmospheric pressure	mb
7	TEMP	vs	"	Ambient Temperature	°C
8	RH	vs	"	Relative Humidity (or Dewpoint Temp)	% (°C)
9	NCLD	vs	"	Cloud Cover	Octals
10	WS10	vs	"	Wind Speed @ 10m	m/sec
11	EVN & EVS	vs	"	Illumination (Vertical Surface - North & South)	lux
12	EVE & EVW	vs	"	Illumination (Vertical Surface - East & West)	lux
13	EHMAX & EHMIN	vs	"	Illumination (Horizontal Surface)	lux
14	LPMAX & LPMIN	vs	"	Path Function (Night - East - 100m)	cd/m^2

bands was a pseudo-photopic response which is suitable for comparison with the visible spectrum optical measurements which were made at the OPAQUE surface stations. The primary surface measurements are listed in Table 1.3.

It is clear that there is a high degree of comparability between the two sets of visible spectrum optical and meteorological measurements, which of course was the intent and is the feature which makes the joint data set of such value in developing any modelled relationships. It is important therefore to have a clear visualization of the temporal relationship between these airborne and surface measurements such that they can be readily linked to their companion meteorological and other supporting data. This temporal link is illustrated in Fig. 1-2, where the OPAQUE surface data availability, during this contract interval, is represented by the heavily shaded horizontal bars in the seven horizontal rows, where each row represents one of the seven participating data stations. In this representation, each month long block of surface data is identified with a numerical index to identify the source tape from which it was extracted. A single number in this context, *e.g.* 9, indicates that the data for the associated month appears on source tape number 9, and has not been edited or updated. A dual number, on the other hand, *e.g.* 2/9 indicates that the data for the associated month first appeared on source tape number 2 and has most recently been edited and/or updated on source tape 9. The lightly shaded vertical bars represent the intervals during which the airborne measurements were being conducted, and the symbol "C" indicates the approximate time at which coincident airborne and surface measurements should occur within the two data sets. There are generally several flights associated with each "C" designation, and

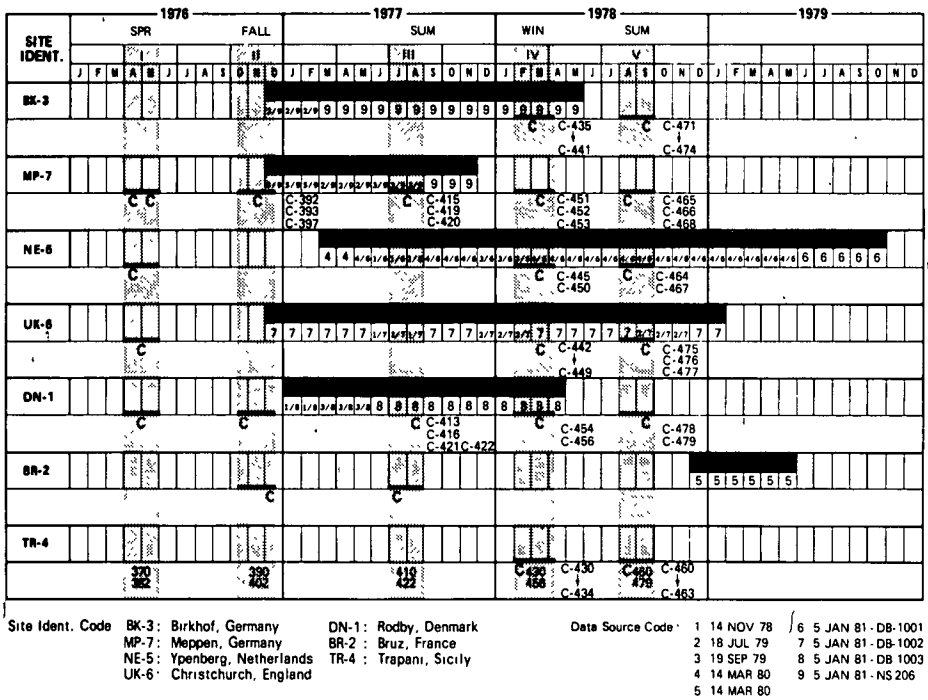

Fig. 1-2. Surface and Airborne Data: Temporal Alignments.

they are listed immediately to the right of each designator. The three digit numbers at the bottom of each lightly shaded bar designate the flight numbers for the missions conducted during the deployment interval, and are the same identification numbers used in the reports listed in Table 1.1.

The general experimental procedure around which the analyses of these OPAQUE related data has been oriented is illustrated in Fig. 1-3. In this schematic diagram an overall approach is presented to guide the selective analysis of those data most promising to yield the predictive correlations necessary for operational model development. As indicated in the preliminary report from which this figure has been reproduced, Johnson *et al.* (1979) the overall approach to the prediction of atmospheric aerosol effects upon optical/infrared extinctions from ground level observations is necessarily through this composite data base. This unique set, with its near simultaneous measurements within the three related regimes *i.e.* the visible and optical/infrared radiometric regimes plus the meteorological regime, represents our most powerful current tool for establishing the optical-meteorological relationships which will underlie our development of operationally useful predictive models.

The following sections of this report summarize the results obtained from establishing and pursuing the analytic approach illustrated by Fig. 1-3, and recommend the directions in which continuing effort might profitably be directed. The previously issued reports upon which this summary is based, and from which many of the recommendations have grown are listed in Table 1.4.

Table 1.4. OPAQUE Related Analysis and Modelling Reports.

Report Number	Type	Title
AFGL-TR-79-0285	Analysis	Preliminary Analysis and Modelling Based upon Project OPAQUE Profile and Surface Data
AFGL-TR-79-0257	Concepts	Daytime Visibility, A Conceptual Review
AFGL-TR-81-0198	Modelling	An Operational Technique for Estimating Visible Spectrum Contrast Transmittance
AFGL-TR-81-0251	Analysis	An Analysis of Infrared and Visible Atmospheric Extinction Measurements in Europe

2. TECHNICAL SUMMARY & REVIEW

In order to summarize the analysis efforts conducted during this contract interval in a relatively concise manner, each of the reports listed in Table 1.4 will be reviewed briefly and abstracts of their primary results and/or recommendations will be presented in the following several paragraphs.

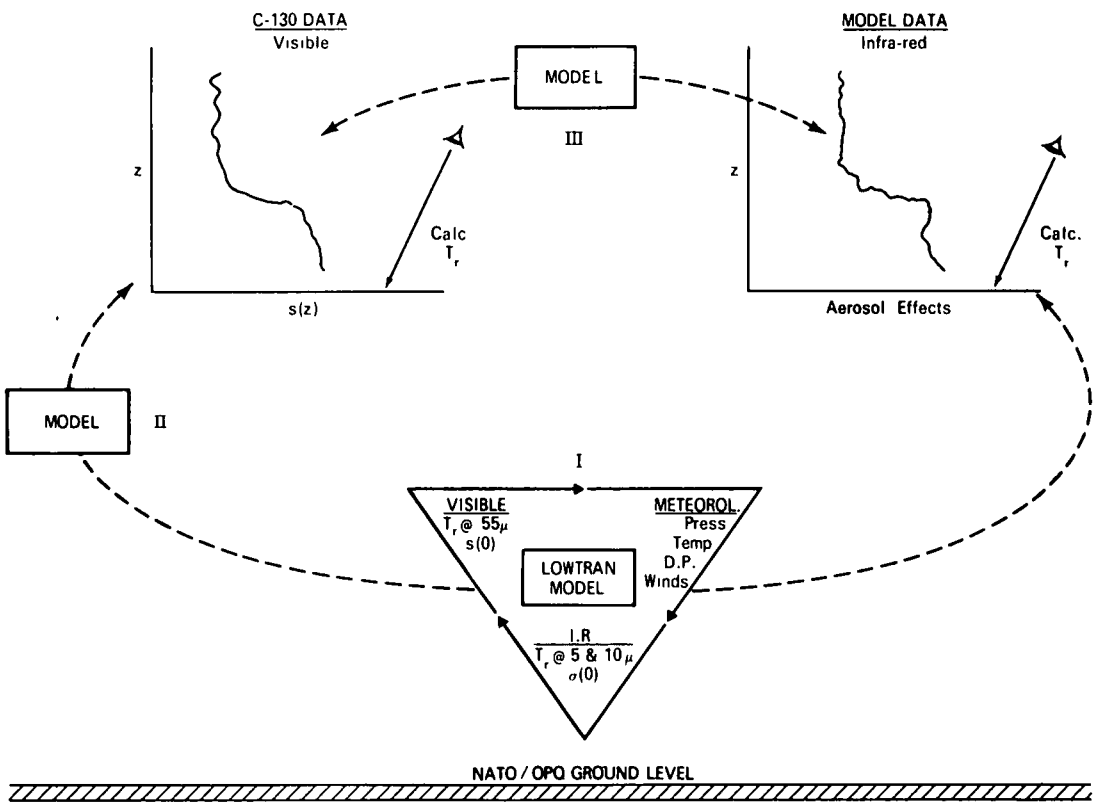

Fig. 1-3. General experimental procedure.

2.1 AFGL-TR-79-0285: Preliminary Analysis and Modelling Based Upon Project OPAQUE Profile and Surface Data

As noted in the preceding introductory section, the general experimental procedure around which the OPAQUE data analysis and modelling effort has been centered was presented in an earlier report, Johnson *et al.* (1979). This preliminary report provided an initial assessment of the OPAQUE surface data base, the OPAQUE related airborne data base, and a selection of proposed analytic approaches to the application of these data bases to the modelling effort. Summaries from three of the sections included in this preliminary report are reproduced below.

Development of Optical Forecasting Models
(Sec. 4, AFGL-TR-79-0285)

Preliminary test results suggest that a single haze layer model of variable depth for representation of the scattering ratio profile is a rational approach to the problem of slant path transmittance prediction in the lower troposphere. Additional development, test and evaluation studies are necessary to establish the validity of the model under a wide variety of environmental conditions and to refine and establish criteria for the specification and prediction of the model coefficients Z, $\bar{Q}_l$ and $\bar{Q}_u$, where Z is the depth of the low-level haze layer, $\bar{Q}_l$ is the average optical scattering ratio in the low level haze layer, and $\bar{Q}_u$ is the average optical scattering ratio in the upper region between the transition zone and z_{max} the highest altitude reached by the data profile.

Although the flight data included in the preliminary test sample were gathered in a variety of locations in northern Europe in all seasons, it is very important to realize that they are very limited in number and somewhat specialized with respect to weather conditions. In particular, all flights were made in the daylight hours in VFR flight conditions and the minimum altitude of the profile test sample was 100m. Accordingly, important complicating factors associated with the formation of ground based temperature inversions or stable layers due to radiational cooling of the ground surface at night did not significantly influence the initial test results. The modelling of the structure and behavior of scattering coefficient profiles within a thermally stable region adjacent to the surface is a prime subject for additional study with specialized high resolution optical and meteorological measurements.

Aside from the significant nocturnal boundary layer effects, we might expect that the relationships revealed by the flight test sample have general applicability. As we proceed with more complete tests based upon substantial additional flight data from Europe and the United States available in our data base, we anticipate the following:

(1) The simple model with a single low-level haze layer of variable depth will represent effectively the vertical profile of photopic scattering ratio in most daytime situations.

(2) A double haze layer model will be required for effective profile representation in some cases as identified by the presence of a significant ground based stable layer.

(3) Haze layer tops can be specified objectively and accurately by temperature lapse rate criteria which identify thermally stable layers in the lower troposphere. The relevant stable layers are of sufficient depth and strength in most cases to be identified with conventional radiosonde observations.

(4) To a good first approximation in the daytime, the optical scattering ratio can be assumed constant with height in a given haze layer and again in the altitude region above the transition zone and below the nominal flight altitude limit of 6 km. It follows, for example, that the average scattering ratio in a given layer may be estimated effectively by an observation or reliable forecast of scattering ratio at the base of the layer.

(5) For many purposes, the scattering ratio above the haze layer in the colder months over northern Europe may be assumed equal to a low average background level. Special forecasting techniques will be required to handle the much greater variability of scattering ratio above the low-level haze layer in the summer months.

Determination of Directional Optical Properties
(Sec. 5, AFGL-TR-79-0285)

One of the goals of Project OPAQUE is to develop the capability of predicting contrast transmittance in the visible on the basis of standard meteorological observations of visibility, cloud cover, temperature and pressure as a function of time. Also generally available are radiosonde measurements giving profiles of temperature and pressure as a function of altitude.

Procedures discussed in the previous sections of this report together with key sections from earlier reports, contain the necessary elements of a technique for predicting contrast transmission in the visible on the basis of these standard meteorological observations. They are summarized in the following outline:

(1) A recent report on daytime visibility (Gordon (1979)) describes the relationship between daytime visibility and the total volume scattering coefficient at ground level $s(o)$.

(2) Section 4, Development of Optical Forecasting Models, describes the development of a technique whereby values of total volume scattering coefficient at the base of the low level haze layer can be used with radiosonde measurements of temperature to produce a profile of $s(z)$ in the troposphere. This profile is expressed in the form of a profile of the visible scattering ratio $Q(z)$.

(3) Section 5.2, Directional Aspects from Nephelometer Data, indicates that the proportional volume scatter-

ing function $\sigma(\beta)/s$ can be reasonably predicted on the basis of the visible scattering ratio $Q(z)$ from the catalog of scattering functions of Barteneva (1960)

(4) Section 5 4, Directional Properties from Path Function Measurements, describes the evidence for assuming that equilibrium reflectance can be considered constant with altitude on many cloudy as well as clear days

(5) Section 5 5, Sky-Ground Ratio as a Modelling Parameter, contains the sky-ground ratio form of the contrast transmittance equation, with the sky-ground ratio in reflectance form

(6) The downwelling illuminance for a standard clear day can be computed from the Brown (1952) illuminance curve for any time of day or night given the time, latitude and longitude Subroutine ILLUM, developed by Drs M Ehrlich and Ir A C Van Bochove, The Netherlands, does this computation in full including the effect of moonlight It also computes the sun and moon zenith angles

(7) Table 2 5 of Duntley *et al* (1978b) indicates a preliminary relationship of cloud cover to the illuminances from Brown (1952) and Lumb (1964) relates total radiation to sun zenith angle and cloud cover, type and height Techniques must be developed to determine downwelling illuminance for both clear and cloudy days from Subroutine ILLUM in conjunction with cloud type and cover as a function of height These downwelling illuminances will then be used to obtain equilibrium reflectances from equilibrium radiances

(8) Prediction of the appropriate scalar irradiances for inclusion in the prediction of equilibrium radiance from $\sigma(\beta)/s$ can probably be done from a knowledge of the downwelling illuminance as derived above and the sun and moon zenith angles This relationship can be developed from the airborne scanner data, and the model atmosphere calculations using the Barteneva scattering functions

GENERAL RECOMMENDATIONS

(Sec 6, AFGL-TR-79-0285)

During the evolution of the various studies discussed in the preceding sections of this report, a consensus has developed among the several participants that are summarized here as general recommendations The recommendations involve the development of several procedural steps, each related to the general goals outlined in Section 1, but couched within the context of maximizing modelling progress through the utilization of the most available and reliable mix of profile and surface data bases

(a) OPAQUE Surface Data The surface data base, as illustrated in Section 2 and discussed in Section 3, was considered following its analysis in late 1979 to be too incomplete to develop broad-scale statistical-climatological studies for the European area However, as the volume of fully processed and edited data increases, they should be quite adequate for addressing a variety of specific statistical studies as required for the development of optical/IR models The quality of these early (*i e* prior to 1979) initial issue data sets appeared inadequate for direct application to the determination of causual relationships without significant amounts of pre-analysis and editing

The recommended course of action therefore, was to proceed first with the evaluation and partial editing of selected sub-sets of the surface data needed for meaningful analysis of optical/IR relationships When practicable, the five to ten day sub-sets selected for analysis should be coincident in time with profile measurements made during the OPAQUE IV and V deployment intervals The combined surface and flight data sets should then provide the primary base for application to the air-ground modelling and causual relationship studies

(b) Visible-Infrared Relationships An ultimate goal of the analysis related to the OPAQUE data bases is the development of models useful in predicting the optical influence of atmospheric aerosols upon infra-red transmittances Within the data base there are two experimental sub-sets germane to entry into the infra-red regime

They are the infra-red transmittance data and the aerosol size distribution data Both of these subsets were in November, 1979 extremely limited in both quantity and quality, however a fundamental approach to their use as outlined in Section 3 7 could be recommended The recommendation was predicated upon the initial premise that atmospheric scattering due to aerosols in both the visible and infra-red regions may be adequately linked through an adequate specification of the aerosol size distribution

The recommended course of action was therefore to develop a select library of infra-red transmittance data, which had been recalibrated via the LOWTRAN oriented calibration procedure as in the issue 5 data, and whose entries were coincident with sets of airborne and surface aerosol size distribution measurements Subsequently, re-index the library in terms of the aerosol extinction contributions and create the desired data base which associates visible spectrum scattering functions, aerosol size distribution, infra-red aerosol extinctions, and the local meteorological specifications related to aerosol source probabilities

(c) OPAQUE Profile Data The profile data base, as illustrated in Section 2 and discussed in Section 4, represented a statistically much smaller sample of the European environment than did the surface set, however it possessed a compensating advantage That is, it had already been reasonably well edited and evaluated, and was therefore ready for immediate user applications The procedures for modelling vertical aerosol scattering properties as presented in Section 4 appeared adequate for straight-forward application to the entire OPAQUE profile data base and thus immediately address a primary step in the overall research plan, the prediction of vertical aerosol structure from meteorological parameters

The recommended course of action therefore, was to proceed with the development of this modelling approach and immediately expand its application to the entire OPAQUE profile library, and subsequently to the overall profile library in order to enhance both the size and generality of the sample.

(d.) Directional Properties. The development of predictive models for atmospheric volume scattering coefficient is a necessary but obviously insufficient accomplishment for the prediction of contrast transmittance. It is essential that the directional scattering properties of the atmosphere also be predicted. As discussed in Section 5, the elements necessary for addressing the prediction of these directional properties, at least within the visible spectrum, appear to exist plentifully within the currently available airborne data base, and to a somewhat lesser degree within the surface set. In both sets, the validation of the quantitative relationships between total volume scattering coefficient and the directional properties specified in the Barteneva catalog is the key initial element.

Assuming that the encouraging initial results on the modelling approximations for the scattering ratio profile and for the angular scattering properties are confirmed by more complete evaluation, it is important to begin parallel investigations of the other factors that determine path radiance and background radiance, as defined by Eq. (5-2). In particular, effective models are required to describe the distribution and variability of illuminance, which in turn depends upon the cloud amount and type as a function of altitude. Here again, the extensive flight data base supplemented with the surface OPAQUE data offer an excellent opportunity for forecasting technique development. In short, the wherewithal now exists for the development and validation of improved predictive models for sky-ground ratio and visible contrast transmittance over slant paths in the lower troposphere.

2.2 AFGL-TR-79-0257: Daytime Visibility, A Conceptual Review

The ability of a human observer to perform tasks involving visual search and the determination of visual ranges (*i.e.* visibilities), is a commonly recognized skill that is presently under increasing competition from a variety of sophisticated electro-optical systems. The performance of these E/O systems, in turn, is increasingly evaluated analytically through the medium of computer codes designed to specify not only the E/O systems characteristics, but also the characteristics of the optical medium in which the system is embedded. Thus for applications involving the evaluation airborne systems, modelling the optical properties of the atmosphere becomes of necessary and immediate importance. The conceptual loop is closed by virtue of the necessity for a determination of surface visibility as an initial input to most atmospheric models. Thus, as background to the general modelling task, it was deemed quite appropriate to review in this report the underlying concepts used in defining and determining visibility.

Several comments from this review report and its parallel publication, Johnson (1981b), are summarized and reproduced in the following paragraphs.

Visual Thresholds for Daylight Illumination (Sec. 2, AFGL-TR-79-0257)

The determination of a human observer's capability to discern barely perceptible changes in the apparent luminance difference between an object and its surrounding background (*i.e.* the luminance contrast threshold), has been a fruitful field for vision research for many years. An extensive experimental effort was initiated at the Tiffany Foundation in New York during the early years of World War II, the data for which were tabulated by Duntley (1946) and the experimental results for which were discussed by Blackwell (1946). An important point well illustrated by these data is that the contrast threshold for the daylight adapted human eye changes very little as a function of background luminance, but is a strong function of the angular subtense of the target and of the time spent looking at the target.

To illustrate this rather fundamental psychophysical relationship, we have generated the composite plots shown in Fig. 2-1. In this figure, the contrast values shown along the horizontal axis are defined by Eq. (1), and in each case have been adjusted from the experimental liminal values (*i.e.*, 50% prob. of detection) to values appropriate for confident sighting (99% confidence). The correction factors are from Taylor (1964). Equation (1) thus represents the most fundamental relationship involved in any visual search scenario.

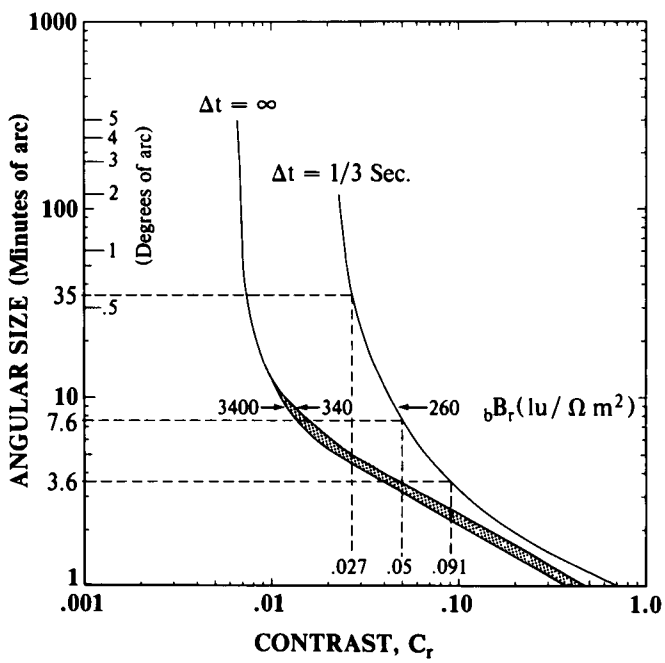

Fig. 2-1. Angular size as a function of contrast for a 99% probability (confidence) and a lack of knowledge of target position of ±4 deg. or more (Gordon, 1979). (Fig. 1 from AFGL-TR-79-0257).

$$C_r = \frac{{}_tB_r - {}_bB_r}{{}_bB_r} = \frac{{}_tB_r}{{}_bB_r} - 1 \,, \qquad (1)$$

where C_r represents the apparent contrast, at distance r, of the visual target t against its background b; ${}_tB_r$ represents the apparent luminance of the visual target as seen from distance r; and ${}_bB_r$ represents the apparent luminance of the background against which the target is viewed as seen from distance r.

In Fig. 2-1, the curves to the left, labeled $\Delta t = \infty$ are from the Tiffany data for long duration viewing, where the viewing times Δt were 24 s and longer. The curve to the right, labeled Δt = 1/3 s is from Taylor (1964). As one can note from these graphical displays, the Tiffany long duration data indicate via the slowly spreading shaded area, that large changes in the luminance of the daylight horizon background (*i.e.* 3400 to $340 lu\,\Omega^{-1}m^{-2}$) make little difference to the discernible threshold contrast C_r. However, as illustrated by the horizontal offset between the $\Delta t = \infty$ and the Δt = 1/3 s plots, the time used in viewing the object does have an appreciable influence on the contrast threshold, particularly for targets at the larger angular sizes.

These data also clearly illustrate the underlying rationale for the WMO (1971) recommendation: "In order that daytime visibility measurements should be representative, they should be made using objects subtending an angle of not less than 0.5 degrees at the observer's eye." The 0.5 deg angular size (*e.g.*, equivalent to the solar or lunar disc) and the commonly recommended threshold contrast of 0.025 are clearly related through the Taylor Δt = 1/3 s data.

Directional Scattering of Atmospheric Aerosols

(Sec. 3, Atmos. Environ. **15**, Johnson (1981b))

The measurement of two discrete values of atmospheric directional scattering function coincidently with the measurement of total volume scattering coefficient is a powerful capability that is built into the Visibility Laboratory integrating nephelometer. It is essential, if one is to describe the optical properties of an atmosphere, either for a specific contrast transmittance determination, or for a general purpose modelling application, that a reliable entry into the directional characteristics of those properties be available. The work of Barteneva (1960) has been heavily used by the Visibility Laboratory as this entry, but there have been continuous queries as to the complete generality one could assign to the Barteneva data (Johnson *et al.* 1979). Measurements made with our instrument have, I believe, answered that question beyond reasonable doubt.

Barteneva (1960) provides a catalog of proportional directional scattering functions $\sigma(\beta)/s$ for the photopic sensor based upon 624 measurements made during 1955-1958 at various locations in the U.S.S.R. and at sea. For each volume scattering function she gives a range of total volume scattering coefficients appropriate to that function. Median values of scattering coefficient were derived for each of the gradual scattering function classes, Nos. 1-10. This resultant catalog of gradual functions and their associated median scattering coefficients is appropriate for describing atmospheres characterized as very clear to heavy haze, Nos. 1-10 respectively.

It became apparent during the analysis of the measurements from the directional channels of Visibility Laboratory nephelometer that its data compared well to the Barteneva data. When its median scattering coefficient values and its gradual class $\sigma(\beta)/s$ curves were put into the form of their ratio to the Rayleigh (*i.e.*, molecular scattering, as was the nephelometer data), then there was excellent correlation. Two sets of these comparative data are illustrated in Figs. 2-2 and 2-3.

It is of significance to note that whereas the original Barteneva data represent photopic measurements at ground level, the Visibility Laboratory measurements include data from several separate bands within the visible spectrum and from within a broad range of altitudes.

In Figs. 2-2 and 2-3, the horizontal axis is Optical Scattering Ratio $Q(z)$ which is defined as the ratio of the total volume scattering coefficient $s(z)$ to the Rayleigh scattering coefficient, ${}_Rs(z)$ where z is the altitude designator:

$$Q(z) = \frac{s(z)}{{}_Rs(z)} \,. \qquad (8)$$

The vertical axis is Volume Scattering Function Ratio, $q(z)$ which is the ratio of the total directional scattering function at angle beta, $\sigma(z,\beta)$ to the Rayleigh scattering function at the same angle and altitude, ${}_R\sigma(z,\beta)$:

$$q(z) = \frac{\sigma(z,\beta)}{{}_R\sigma(z,\beta)} \qquad (9)$$

Figure 2-2 represents multi-spectral directional scattering function data measured during fourteen flights made in the vicinity of St. Louis, MO., during the Summer of 1971. In each case the measurements made at scattering angles of 30 and 150 are plotted as $q(z)$ against the coincidently measured values of total scattering coefficient converted to values of $Q(z)$. The solid lines are the equivalent data extracted from the Barteneva catalog. The correlation is good over the entire range of $Q(z)$.

Figure 2-3 represents additional multi-spectral data of the same sort as in Fig. 2-2, that were measured at ground level in conjunction with 19 flights made in western Europe during the Summer of 1978. Again, the correlation is strong over a broad range of $Q(z)$.

The excellent comparisons of both the in-flight and surface measurements with the Barteneva directional data as illustrated in Figs. 2-2 and 2-3 argue powerfully for accepting the general applicability of the Barteneva scattering function catalog. It is this experimental verification of general applicability that establishes the practicality of developing simple and reliable models of atmospheric directional scattering properties.

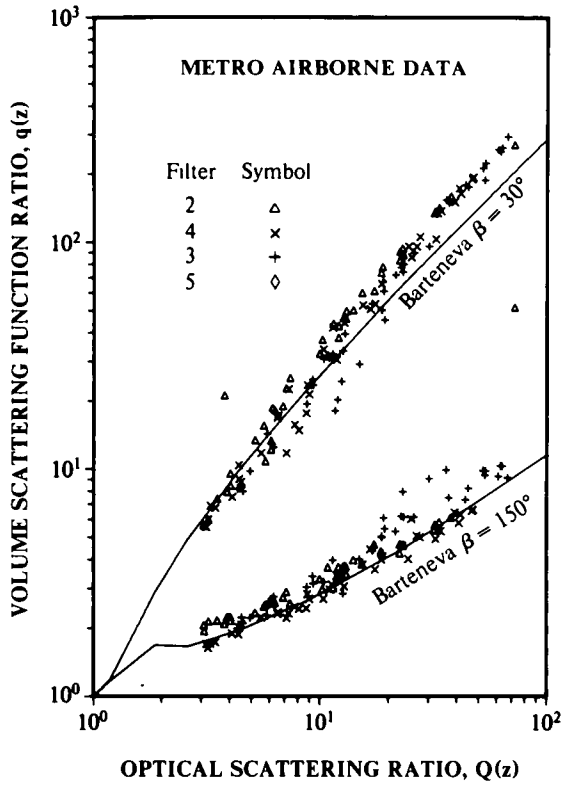

Fig. 2-2. Comparison of multi-spectral directional scattering ratios measured by Visibility Laboratory airborne nephelometer with the photopic ratios from Barteneva (1960). (Fig. 9 from sec. 3, Atmos. Environ. **15**, Johnson (1981b)).

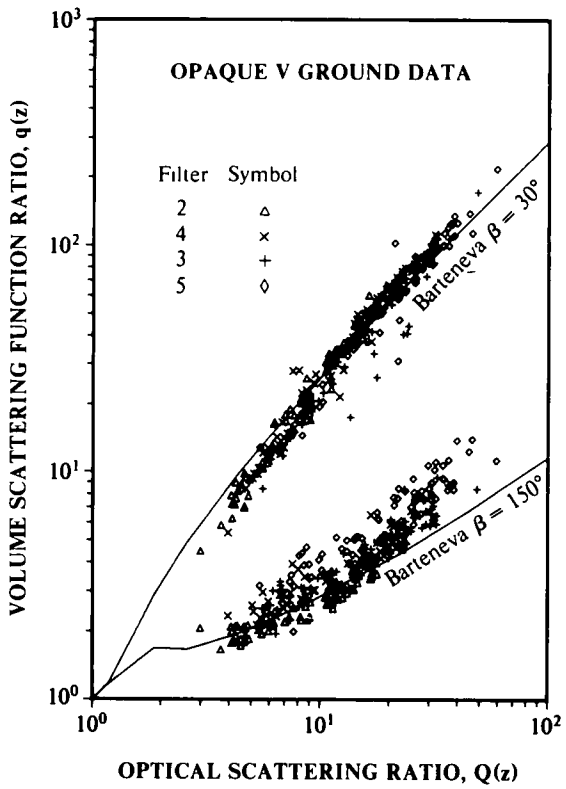

Fig. 2-3. Comparison of multi-spectral directional scattering ratios measured by Visibility Laboratory ground-based nephelometer with the photopic ratios from Barteneva (1960). (Fig. 10 from sec. 3, Atmos. Environ. **15**, Johnson (1981b)).

Conclusions

Although many early experimentalists established the viability of visual determinations of daytime contrast transmittance along horizontal paths of sight and related this determination to the concept of "visibility", there are equally well documented and sometimes not as fully understood associated caveats. However, within the boundaries established by these caveats, horizontal visibility determinations derived from instrumental measurements of atmospheric extinction coefficient are adequately relatable to visual observations.

The extension of these concepts to the more general case of contrast transmittance determinations along vertically inclined paths of sight implies knowledge of the vertical variability in atmospheric extinction coefficient and the directional scattering properties along the path. These data have been obtained through the use of a multi-channel nephelometer and indicate a strong correlation between the measured scattering coefficient and the aerosol directional scattering function.

The modelling implications of these data are indeed enticing. The evidence to date strongly supports the contention that with an adequate specification of total volume scattering coefficient $s(z)$ and its Rayleigh component, one can enter the Barteneva catalog or its parameterized equivalent, and obtain a truly representative expression of the directional scattering function $\sigma(z,\beta)$ for any spectral band within the visible spectrum. Thus, a reliable specification of the directional scattering properties of the atmospheric aerosol can be reasonably deduced from a measurement of the total volume scattering coefficient alone.

2.3 AFGL-TR-81-0198: An Operational Technique for Estimating Visible Spectrum Contrast Transmittance

The visual detection of distant objects is restricted by air molecule and aerosol particle scattering and to a lesser extent by atmospheric absorption. The complexity of multiple scattering and absorption processes and the inherent variability of the aerosol particle distribution and composition require effective simplifications in order that estimates of contrast transmittance through the atmosphere can be made rapidly and consistently.

A series of modelling approximations that relate optical scattering properties to meteorological variables are derived from experimental data and combined with available analytic approximations for radiative transfer calculations to develop an operational technique for the estimation of directional path radiance and directional slant-path contrast transmittance. The approach involves validation

of the individual elements of the procedure through reference to simultaneous optical and meteorological measurements gathered by the Visibility Laboratory (Johnson *et al.* 1979) over the past several years with a specially instrumented Air Force C-130 aircraft under sponsorship of the Air Force Geophysics Laboratory. The high resolution profile measurements were made in a wide range of metcorological and geographical conditions in the United States and western Europe.

The path contrast transmittance in the visible spectrum depends most critically upon the distribution of total volume scattering coefficient, both along the path and in the surrounding atmosphere. Accordingly, an attempt was made to condition the approximation procedures for the radiative transfer calculations and for all input parameters in a manner consistent with the existing capability to model and predict the scattering coefficient structure and behavior.

Sensitivity of Spectral Contrast Transmittance to Selected Changes in Physical Parameters (Sec. 6, AFGL-TR-81-0198)

Systematic model calculations were made to illustrate the effects of typical variations in physical parameters upon the slant path contrast transmittance and the corresponding range of object detection. For this purpose, a two-layer atmosphere was assumed, consisting of a primary haze layer of varying optical thickness and single scattering albedo, and an overlying upper troposphere-stratosphere layer of relatively clear air with a constant optical scattering ratio of 1.3 and a single scattering albedo of 0.97. The trial calculations were carried out for an assumed wavelength of 550 nm. The responses in contrast transmittance to parameter changes would be qualitatively similar for other visible wavelengths but would show systematic quantitative differences for the same aerosol loading in the haze layer because of the wavelength dependence of both the total optical depth and the single scattering phase function.

Results are shown for a range of haze layer depths, aerosol concentrations and absorption, and for selected values of surface reflectance and solar zenith angle. The parameters are varied individually while holding each of the other variables constant and equal to their values for the assumed reference atmospheres given in Appendix C of Hering (1981a), which are in general representative of clear sky conditions observed in the summer season in northern Germany. The first two sets of calculations, Sections 6.1 and 6.2, were based upon reference atmosphere "A". The vertical extent of the haze layer for this reference atmosphere was assumed to be 3 km except that a few comparative calculations were made also for an assumed haze layer top at 500m altitude while holding the overall optical thickness the same as for the 3 km case. The third set of trial results (Section 6.3) were based upon reference atmosphere "B" (Appendix C of Hering (1981a)), with the haze layer extending to 1.3 km and with a single scattering albedo of .83 and an optical scattering ratio of 16.

Object at the Earths's Surface and the Sensor at 6km. From Eq. (4), the contrast transmittance, $T_c = C_r/C_o$, of a downward path of sight to an object at the earth's surface is given by the product of the path radiance transmittance, T_r, and ratio of the inherent background radiance of the surrounding terrain and the apparent background radiance as measured at the sensor altitude, ${}_bL_o/{}_bL_r$. It follows that the contrast transmittance decreases with an increase in the optical thickness of the viewing path in concert with both a decrease in $T_r(z,\theta)$ and an increase in the path radiance, L_r^*, generated by the enhanced aerosol particle scattering. For the case with the object at the surface and the sensor at 6 km, the responses of T_c to changes in optical thickness and to changes in the cosine of the zenith viewing angle are shown in Fig. 2-4. Since we have assumed that the surface reflectance obeys Lambert's law, the asymmetry of T_c in the upsun and downsun viewing directions is small. Except for viewing angles near the horizon, the calculated T_c from the surface to 6 km decreases more or less in direct proportion to the increase in slant path distance.

For diagnostic purposes let us define an arbitrary target acquisition range (TAR) where the contrast transmittance reduces to 10 percent. Illustrated in Fig. 2-5 are the calculated changes in TAR that correspond to selected changes in the physical variables. Again we assume a target located at the earth's surface and a sensor altitude of 6 km. The calculations were made for an azimuth viewing angle of 180° (downsun). The calculated TAR for the reference atmosphere is 13.5 km. Comparing responses of the TAR to the departures of the individual

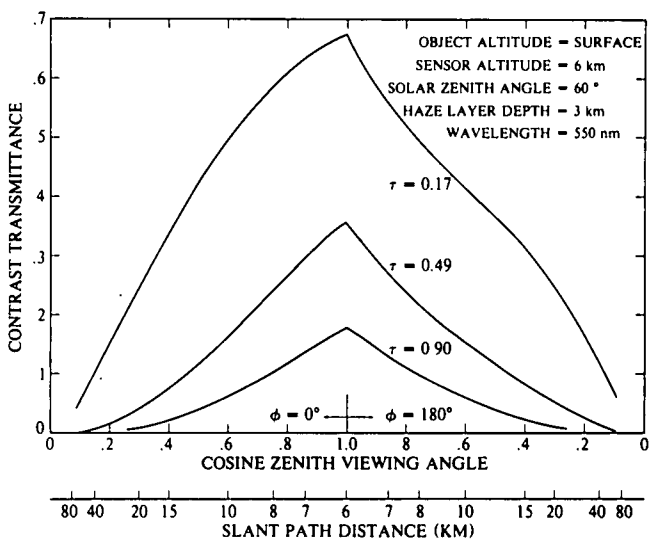

Fig. 2-4. Diagnostic calculations of contrast transmittance as a function of zenith viewing angle for a target viewed against a terrain background. Values of τ are total atmosphere optical depth. (Fig. 6-1 from AFGL-TR-81-0198).

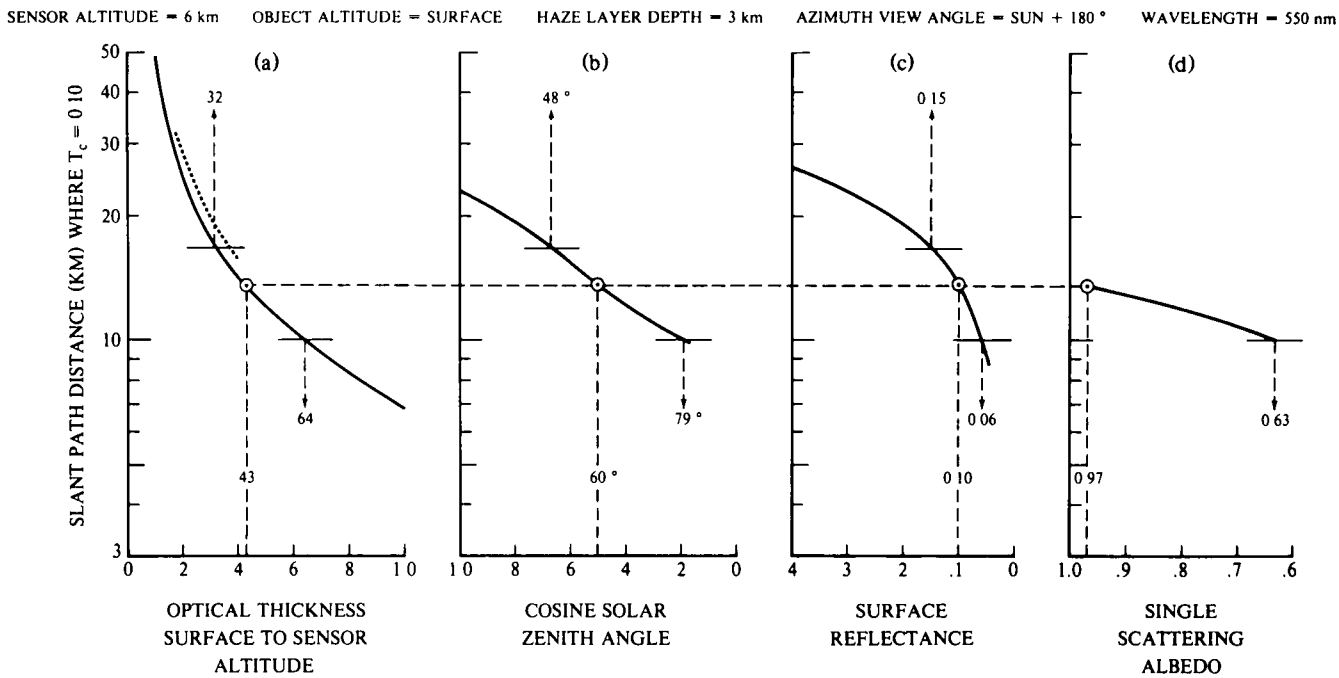

Fig. 2-5. Variations in target acquisition range (T_c = 0.10) associated with departures of selected parameters from the assumed reference atmosphere values. The horizontal dashed line denotes parameter values for this reference atmosphere. The horizontal bars identify a change of ±25 percent from the slant path distance where T_c = 0.10 for the reference atmosphere, *e.g.* 13.5 ±3.4 km. (Fig. 6-2 from AFGL-TR-81-0198).

parameters from their values given by the reference atmosphere, we note that a 25 percent increase in TAR is associated with about a 25 percent decrease in the optical thickness of the haze layer. On the other hand about a 50 percent increase in optical thickness is required for a 25 percent decrease in TAR. The dotted line shown in Fig. 2-5 for the relationship of TAR with optical thickness depicts the calculated TAR for an haze layer top at 0.5 km in lieu of the 3 km altitude assumed for the reference atmosphere. Notice that the TAR differs only by approximately 15 percent for a haze layer with the greatly reduced vertical extent but with increased extinction so as to yield the same optical thickness.

Figure 2-5b shows that changes in ln TAR are directly proportional to the changes in the cosine of the solar zenith angle. For example, a decrease in solar zenith angle of 12 degrees results in about a 25 percent increase in TAR for the reference atmosphere. Notice also (Fig. 2-5d) that a 25 percent decrease in TAR is associated with an increase in haze layer absorption from the small amount associated with clear remote atmospheres (single scattering albedo = 0.97) to the large amount corresponding to urban atmospheres (single scattering albedo = 0.63).

For objects viewed against a terrain background, the TAR has a significant direct dependence upon the surface reflectance. For example (Fig. 2-5c), the calculated TAR decreases by 25 percent as the surface reflectance changes from the value associated with a brown field (0.10) to a value representative of a grass field (0.06).

Object at the Surface and Sensor at 20 km
(Sec. 6.3, AFGL-TR-81-0198)

The third and last set of trial calculations differs from the previous two in that a different reference atmosphere (REF-B in Appendix C of Hering (1981a)) was assumed. The haze layer is more shallow, extending to 1.3 km, and the scattering ratio and single scattering albedo in the haze layer are 16 and 0.83 respectively. With the assumed sensor altitude of 20 km, the viewing path has a long segment through the relatively clear region in the lower stratosphere and upper troposphere. Yet another departure from the previous calculations is that the target at ground level is viewed in the upsun rather than the downsun direction.

The calculated slant range corresponding to 5 percent apparent contrast (contrast transmittance of 10 percent) for the reference atmosphere and for specific changes in the individual parameters of the atmosphere are shown in Fig. 2-6. We note, for example, that each of the following parametric changes in the reference atmosphere result in a decrease in the slant path distance corresponding to 5 percent contrast transmittance in the range of 19 to 25 percent:

a. 50 percent increase in haze layer depth

b. Factor of 5 increase in the aerosol scattering ratio in the upper troposphere

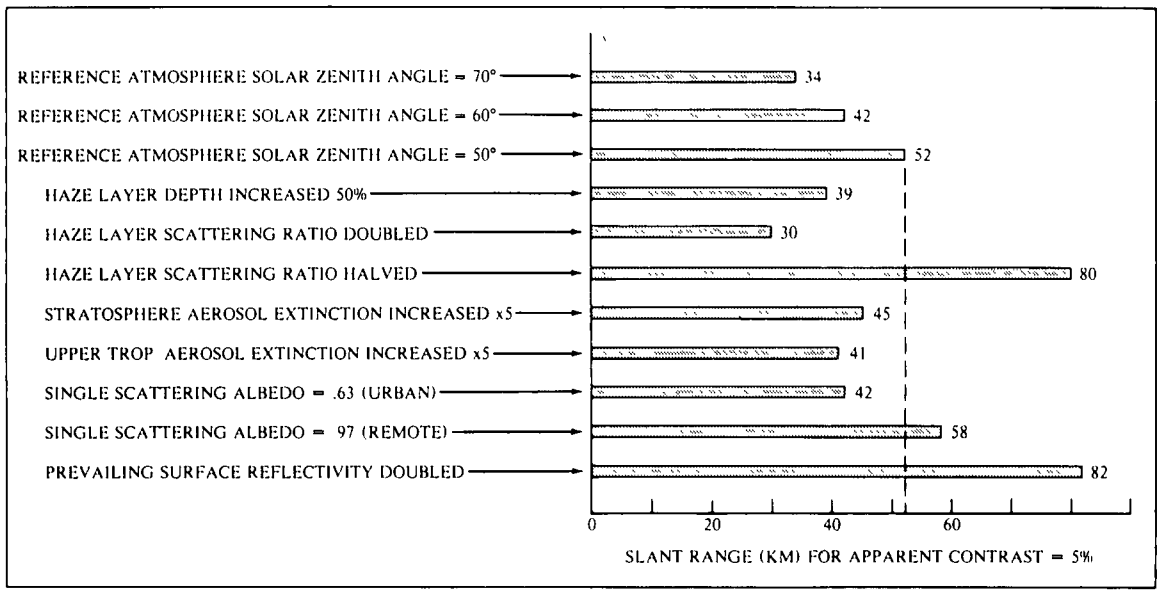

Fig. 2-6. Comparison of the slant range corresponding to apparent contrast of 5 percent for reference atmosphere (Ref. B, Appendix C) and selected changes in the reference atmosphere. (Fig. 6-2 from AFGL-TR-81-0198).

c. Increase in haze layer absorption corresponding to a change in single scattering albedo from .83 to .63

d. Increase in solar zenith angle from 50 to 60 deg

It should be emphasized that the results described in this section are specific only for the conditions imposed on the trial calculations. However, these examples provide some insight into the changes in image transmittance characteristics that are associated with typical changes in the environment.

Summary & Remarks

Simultaneous optical and meteorological measurements between ground level and 6 km altitude gathered by the Visibility Laboratory in recent years in the United States and Europe with an instrumented aircraft have provided the basis for the development of a technique for estimating atmospheric path radiance and directional contrast transmittance. The technique is relatively fast and easy to apply yet is designed to take full advantage of the present limited capability to observe and predict the relevant atmospheric variables. Various modelling approximations are introduced to simplify the calculations of radiative transfer and to help specify the vertical distribution of atmospheric attenuation coefficient and the single scattering phase function. Critical examinations of the assumptions and approximations were made through reference to the extensive series of airborne meteorological/optical measurements. Model input parameters are the number of atmospheric layers selected and the average optical scattering ratio and single scattering albedo for each layer, the solar zenith angle, the extra-terrestrial solar irradiance, a representative wavelength and the surface reflectance. The computer program calculates the sky and terrain radiance corresponding to any selected point and direction and the contrast transmittance for any slant atmospheric path.

The techniques developed during the course of the experimental optical measurement and analysis program can provide relatively fast and consistent estimates of optical atmospheric properties over any slant path, as a function of wavelength in the visible spectrum. To the extent that a climatological data base of conventional meteorological observations exists, the techniques in their present form can be used to estimate readily the frequency distributions of such quantities as spectral contrast transmittance, as a function of location and season.

Refinements in the modelling approximations are being made as validation tests and experiments continue. Results to date indicate that further parameterization of selected components of the model can be made which will improve computational efficiency and at the same time retain the capability to take advantage of all relevant observing and forecasting information. A realistic goal is to employ the computer model as part of a data acquisition and microprocessing system for real time estimates of image transmission properties. Additional experiments are planned to examine further the tradeoffs between the type, accuracy, frequency and density of optical/meteorological observations and the reliability of the estimates of spectral contrast transmittance.

2.4 AFGL-TR-81-0251: An Analysis of Infrared and Visible Atmospheric Extinction Measurements in Europe

There are a variety of optical infrared sensors in use today, whose performance is strongly influenced by the atmospheric infrared extinction Mie calculations based on model particle size distributions result in the following trends [Shettle and Fenn (1979)] When the atmospheric conditions range from clear to hazy, aerosol extinctions are generally smaller at infrared wavelengths than at visible wavelengths Except in very clear air, this will result in better optical propagation within the infrared "window" regions (about $3-5\mu m$ and $8-13\mu m$) than at visible wavelengths However, in the presence of large droplets of size about equal to the wavelength, such as may occur in mist and fog, the infrared aerosol extinction can become greater than the visible aerosol extinction, resulting in poorer optical propagation of infrared wavelengths

Goals of the Analysis

(Sec 1 1, AFGL-TR-81-0251)

This analysis of the OPAQUE data was directed toward two goals The first goal was to evaluate the variations in the measured data relative to model predictions In general, haziness and the associated optical changes, such as a decrease in the radiance transmittance, are caused by increases in the aerosol particle content of the atmosphere This aerosol includes droplets which may be composed of varying fractions of water, sea salt, soot, and so on, as well as solid particles such as dust Measurements have been made of the size distribution of these particles, their chemical content, and their indices of refraction Most models are based on Mie calculations whose inputs are the most likely aerosol particle size distributions and the most likely refractive index distributions as a function of wavelength Since measured aerosol characteristics in the atmosphere vary, it is to be expected that the transmittance also should vary The extensive OPAQUE data set, which clearly illustrates these typical radiance transmittance variations, should be valuable for evaluating how well the models predict them

The second goal of the analysis was to develop improved techniques for estimating the infrared transmittance based on more conventional measurements and observations Like the infrared transmittance, the visible transmittance is also influenced by the aerosols The meteorological quantities are also related to the aerosols For example, aerosol particle size is influenced by relative humidity, and aerosol content is influenced by airmass history Since the visible, meteorological, and infrared regimes affect or are affected by the aerosols, it might be possible to develop an adequate empirical model to relate the infrared radiance transmittance directly to the visible and meteorological quantities

Related Theoretical Studies

(Sec 2 2, AFGL-TR-81-0251)

There has been a great deal of work on the various theoretical aspects of predicting aerosol particle extinction Two rather well thought out works are those of Shettle and Fenn (1979) and Nilsson (1979) These papers discuss the most probable aerosol characteristics such as particle size, and show the resulting computed extinction characteristics Pinnick *et al* (1979) report similar calculations based on the measured drop size properties of fogs

In general, the results of these calculations may be summarized as follows If the relative particle size distribution and refractive index distribution of the aerosol remain constant, and only the number density changes, then the magnitude of the aerosol extinction coefficient will vary, but the spectral relationships will be fixed That is, the ratio of extinction coefficient at two given wavelengths will be a constant If relative particle size distribution or refractive index distribution are allowed to change, then the spectral relationships will change

The visible extinction should be more strongly affected by the sub-micron region of the particle size distribution, while the infrared extinction should be more strongly affected by the larger particles in the micron region of the particle size distribution [as may be inferred from figures in Nilsson (1979)] The terms accumulation and coarse modes [Whitby (1978)] refer to two peaks often observed at two size ranges in the particle size distribution Since these size ranges are partly influenced by independent processes, the two modes may not always be closely related [Fitch and Cress (1981) and Whitby (1978)] Thus one might expect some variation in the visible to infrared extinction relationship Jennings *et al* (1978) discuss the effect of refractive index variations on atmospheric extinction

One difficulty inherent in the aerosol extinction calculations is the difficulty in assigning reasonable particle size distributions The distributions respond to a number of environmental factors, both macroscopic and microscopic For example, Yue and Deepak (1980) discuss the effects of sedimentation rates on the drop size distribution in fogs

In spite of the uncertainties in particle size distribution and refractive index, models based on particle size distributions can be very useful Perhaps the most commonly used model of this sort is the LOWTRAN model LOWTRAN essentially uses four haze models and two fog models for the aerosol portion of the program The haze models are based on an assignment of the most likely particle size distribution and refractive index distribution for four conditions urban, rural, maritime, and tropospheric In the LOWTRAN 3B model, the relative particle size distribution and refractive index distribution are held constant within each model, and only the number density is allowed to vary Thus, for a given model, say rural, the ratio of extinction coefficient at two given wavelengths is a constant

In the LOWTRAN 5 model [Kneizys *et al* (1980)] the effect of relative humidity on relative particle size distribution and refractive index is included Thus the ratio of infrared to visible aerosol extinction coefficient is no longer a constant, but is a function of relative humidity The effect of relative humidity is much stronger in the

maritime model than in the urban or rural models The analysis in this report will include some discussion of how the measured infrared to visible ratios compare with the ratios inherent in the LOWTRAN models

Method to Sort Infrared Extinctions

(Sec 5 3, AFGL-TR-81-0251)

In view of these considerations (relationships between molecular, aerosol and water vapor extinction versus measurement uncertainties), it was most important to try to develop some mechanism for sorting out the incidence of high infrared extinctions (or the incidence of high infrared to visible extinction ratios) If the low infrared extinctions could be isolated by some criteria in a lower bin, they could be treated with a stochastic model The remaining data would go into an upper bin The upper bin would hopefully include all of the high infrared extinctions These extinctions would be high enough that their variations become more significant relative to the instrumental noise, and they would also be high enough relative to the molecular and water vapor extinctions that it would be more important to study their variations

The really high infrared aerosol extinctions are expected to occur when near condensation conditions result in suspended water droplets of size about equal to the wavelength or larger This condition is defined as mist or fog depending on whether the visibility is greater than 1 km, or less than or equal to 1 km [McIntosh (1963) and Proulx (1971)] In particular, McIntosh defines mist as "A state of atmospheric obscurity produced by suspended microscopic water droplets or wet hygroscopic particles The term is used for synoptic purposes when there is such obscurity and the associated visibility exceeds one km the corresponding relative humidity is greater than about 95 percent The particles contained in mist have diameters mainly of the order of a few tens of microns " Thus a reasonable approach is to define an upper bin which should include all of the mist and fog incidents

It should be noted that in the U S , the term mist is popularly used to describe drizzle, we are using the term not to mean drizzle, but as defined above Also it should be noted that it is common field practice to report this mist condition as thin fog, judging by the comments of local weather offices and sample weather reports from the U S and Europe [see Table 6-1 of Duntley *et al* (1973) and Table 6-3 of Johnson *et al* (1979)]

Thus in order to isolate the high infrared extinctions in an upper bin, a reasonable approach is to attempt to isolate those conditions with large suspended droplets, *i e* mist and fog For this data base, it was most effective to use two predictors to define the upper bin and the lower bin First, the visible extinction is required to be greater than 1 km^{-1} (visibility <3 km) for the data to be included in the upper bin (mist and fog bin) The S>1 km^{-1} cutoff was chosen because it is a reasonable threshold for mist, this is where the instrumental noise becomes less significant, and this is the threshold above which high IR aerosol extinctions begin to occur The additional requirement for the high bin data is that RH must be greater than or equal to about 94% (The cutoff used was log(1-RH/100) = -1 2 or RH ≈ 93 7%) This threshold limits the bin to near condensation cases The choice of 94% as opposed to 95% is required due to the uncertainty in the hygrometer This cutoff allows inclusion of the very high infrared extinctions observed at relative humidities above 94% (Fig 5-2) Those points not included in the upper bin, *i e* those with $S \leq 1$ km^{-1} **or** RH<94%, are included in the lower bin

Figure 2-7 illustrates the separation of data into the lower bin, consisting primarily of clear to haze conditions, and upper bin, consisting primarily of mist and fog Theoretically, one would expect this sorting mechanism to separate the bulk of the low infrared extinctions from the high infrared extinctions

Comparison of Measured and Model Mist and Fog Aerosol Extinctions

(Sec 6 8, AFGL-TR-81-0251)

The measured data in the upper bin may be compared with the LOWTRAN 5 model using the ratios of infrared to visible aerosol extinction α_{aer}/S The measured ratios, listed in Table 2 1, may be compared with the ratios inherent in the aerosol portion of the model The LOWTRAN 5 ratios for the 99% relative humidity haze models and the fog models are listed in Table 2 2 Figure 2-8 illustrates the model to measurement comparison

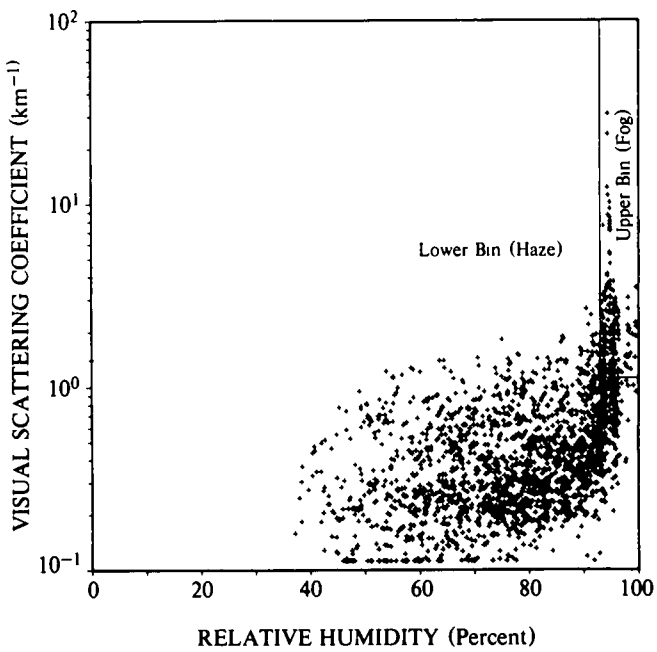

Fig. 2-7. Visible extinction and relative humidity thresholds for definition of the upper (mist) bin and the lower (haze) bin (Fig 5-6 from AFGL-TR-81-0251)

Table 2.1. Measured Ratios of Infrared to Visible Aerosol Extinction α_{aer}/S, Upper Bin (Mist).

Cum Freq (%)	Summer α_{aer}/S		Winter α_{aer}/S	
	3–5μm	8–12μm	3–5μm	8–12μm
98	1 15	1 02	70	90
95	87	82	42	53
80	16	21	099	093
50	060	061	053	027
30	040	037	037	016

Table 2.2. LOWTRAN 5 Ratios of Infrared to Visible Aerosol Extinction α_{aer}/S, Fog and 99% Relative Humidity Haze Models.

Model	Model α_{aer}/S	
	3–5μm	8–12μm
Rural 99%	17	11
Urban 99%	17	099
Mar 99%	92	43
Trop 99%	037	017
Rad Fog 1	1 22	68
Rad Fog 2	1 45	24
Adv Fog 1	1 08	1 23
Adv Fog 2	1.09	1 24

Comparing Tables 2.1 and 2.2, one can see that at least 50% of the measured ratios for each season fall lower than any of the model ratios except the tropospheric. In fact the 50% ratios for the high bin are lower than the rural, urban, or maritime ratios for any relative humidity. Thus many of the ratios are somewhat lower than predicted. The 80% cumulative frequency measured ratios from Table 2.1 compare well to the 99% RH values from Table 2.2. And the 95% or 98% cumulative frequency measured ratios compare well to the fog model ratios.

Thus in the upper bin, which is characterized by visual extinctions greater than 1 km^{-1} and relative humidities over 94%, some of the measured ratios are typically expected fog ratios, but many are typical haze ratios or lower.

One significant way in which these data differ from the LOWTRAN model is the manner in which these ratios in the upper bin vary. Based on LOWTRAN, one might expect to chose a model based on the recent airmass history or the current conditions. One would for example choose the urban 99% model if fog had not formed, or one of the fog models if fog had formed. If this information is lacking, the LOWTRAN 5 recommendation is to use 99% aerosol models for S of 2 to 4 km^{-1}, radiation fog for S of 4 to 10 km^{-1}, and advection fog for S>10 km^{-1}. From this model, one might expect the ratios to be reasonably constant for a fair time period. In fog, for example, one might expect to use ratios above 1 as long as the fog lasted. In contrast to this expectation, the OPAQUE data show that within a given episode of reduced visibility and high relative humidity, the infrared to visible ratio is quite variable, on a short time scale. Additionally, the

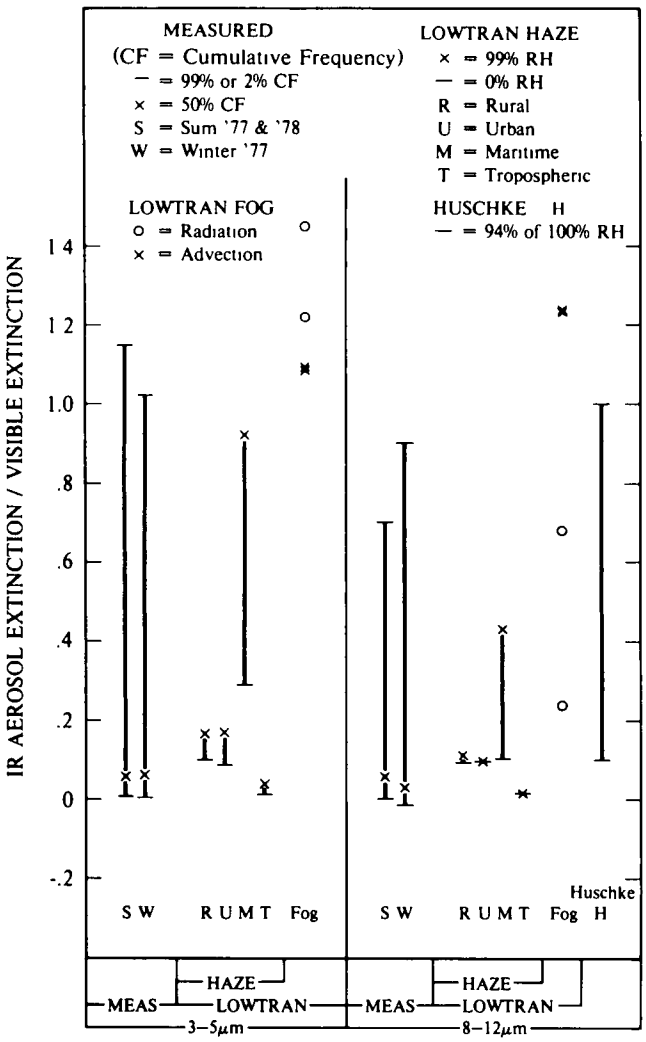

Fig. 2-8. Comparison of measured and model ratios of infrared aerosol extinction to visible extinction for upper bin (mist and fog). (Fig. 6-8 from AFGL-TR-81-0251).

high ratios are not distributed with visual extinction in the same way one might expect from the model. There are many high α_{aer}/S ratios in the $S \approx 1-2$ km^{-1} range, as well as low ratios at higher values of S. The variations in Table 2.1 do not appear to correspond to changes in conditions from non-fog to fog, but rather correspond to short term variations within the fog.

These results can explain one reason that experimentalists may obtain results significantly different from those predicted by LOWTRAN. Basically, LOWTRAN predicts one extinction for a given condition. These OPAQUE data show that the model extinction is a pretty good estimate of the median condition, but that the aerosol extinction varies significantly about that median as a result of short term variations in IR extinction, which may be associated with short term variations in particle size distribution.

The upper bin data may also be compared with the aerosol portion of the Huschke (1976) model. For the upper bin, the measured relative humidities are between 94% and 100%. This corresponds to a range of .1 to 1.0 in Huschke's 8-12μm infrared to visible ratio. As may be seen in Table 2.1, some of the observed 8-12μm ratios fall within this range, but most are lower Again, the character of the variations is somewhat different from the Huschke model. Even in cases where the relative humidity is constant for a number of hours, and we believe the air to be saturated, *i.e.* at about 100% relative humidity, the infrared to visible ratio is quite variable due to the short term variations discussed earlier. This model, as well as the LOWTRAN model, might be improved by using a distribution of expected ratios rather than using one expected ratio.

3. ADDITIONAL MODELLING CONCEPTS

In addition to, and as background for the development of the Hering model discussed in Section 2, substantial modelling effort has been devoted to an evaluation and extension of the Gordon model for a clear atmosphere which was first presented in Gordon (1969). This early model for calculating optical properties of the clear, cloud-free lower troposphere was based upon the concept of equilibrium radiance as introduced even earlier by Duntley (1948). Though there are more precise models for computations of atmospheric optical properties, such as those discussed in Chandrasekhar (1960) and, Collins and Wells (1965), the speed and simplicity of the Gordon model make it an attractive element in one's computational bag of tricks.

Whereas several elements of the Gordon model calculations have appeared in earlier reports associated with this experimental program, Duntley *et al.* (1975, 1978b), they have been somewhat fractionated and inconvenient to retrieve. Thus, it is appropriate in this final report to bring these several elements together into a more complete and informative format. The following paragraphs, therefore, discuss the use of the Gordon model in two contexts. The first compares atmospheric optical properties as calculated by the Gordon model with the equivalent properties derived for an idealized Rayleigh atmosphere, and with the properties of real atmospheres as defined by experimental measurements. The second extrapolates the model into a more general configuration based upon equilibrium reflectance and applies this form to the case of partly cloudy conditions.

3.1 The Gordon Clear Day Model Comparisons with Rayleigh and Turbid Atmospheres

The concept of equilibrium radiance is a natural consequence of the equation of transfer [Eq. (3.10), Duntley *et al.* (1957)]

$$dL(z,\theta,\phi)/dr = -\alpha(z)\ L(z,\theta,\phi) + L_{\bullet}(z,\theta,\phi)\ . \qquad (3.1)$$

This equation relates the incremental change in radiance $dL(z,\theta,\phi)$ at altitude z in direction zenith angle θ and azimuth ϕ, over the incremental path length dr to the attenuation coefficient $\alpha(z)$, the radiance $L(z,\theta,\phi)$ and the path function $L_{\bullet}(z,\theta,\phi)$. Equilibrium radiance $L_q(z,\theta,\phi)$ is defined as the radiance when dL equals zero, therefore, [Eq. (11), Duntley *et al.* (1957) and Eq. (40), Chandrasekhar (1960)]

$$L_q(z,\theta,\phi) = L_{\bullet}(z,\theta,\phi)/\alpha(z)\ . \qquad (3.2)$$

Thus it is equal to the Chandrasekhar source function $\mathcal{J}$.

The preceding equations are precise for monochromatic radiation. They are also, however, a reasonable engineering approximation for broad band sensors in the visible spectrum.

Review of Equilibrium Radiance Model

The equilibrium radiance model was based upon two assumptions: 1) equilibrium radiance for a given path of sight is constant with altitude, and 2) absorption is negligible.

When the equilibrium radiance for a given path of sight is constant (first assumption), the equation of transfer can be integrated with the result that the path radiance $L_r^{\bullet}(z,\theta,\phi)$ is a function of the equilibrium radiance and the radiance transmittance [Eq. (11), Gordon (1969)]

$$L_r^{\bullet}(z,\theta,\phi) = L_q(z,\theta,\phi)\ [1-T_r(z,\theta)]\ . \qquad (3.3)$$

The sky radiance is the path radiance from out of the atmosphere to the sensor

$$L_{\infty}^{\bullet}(z,\theta,\phi) = L_q(z,\theta,\phi)\ [1-T_{\infty}(z,\theta)]\ . \qquad (3.4)$$

The radiance transmittance is defined as

$$T_r(z,\theta) = \exp[-\int_o^r \alpha(z)dr]\ . \qquad (3.5)$$

Transmittance is expressed as a function of θ but not ϕ since the attenuation coefficient is assumed to be isotropic horizontally. The transmittance from space to sensor at zenith angle θ is function of the vertical transmittance and the relative optical airmass $m_{\infty}(z,\theta)/m_{\infty}(z,0)$

$$\ln[T_{\infty}(z,\theta)] = [m_{\infty}(z,\theta)/m_{\infty}(z,0)]\ln[T_{\infty}(z,0)]\ . \qquad (3.6)$$

When there is no absorption (second assumption) the attenuation coefficient is equal to the scattering coefficient $s(z)$.

Given the above two assumptions an equation was developed, [Eq. (41), Gordon (1969)] for evaluating the equilibrium radiance from a knowledge of the sun scalar

irradiance out of the atmosphere, the scalar albedo, the normalized volume scattering function $\sigma(z,\beta)/s(z)$, the radiance transmittance from space-to-sensor and the sun zenith angle. This early equation is repeated below using current notation as a reader convenience.

$$L_q(z,\theta,\phi) = \epsilon_s(z)\left\{\frac{\sigma(z,\beta)}{s(z)} + \frac{{}_sA}{4\pi} + \left[\frac{1+{}_sA}{4\pi}\right]\right.$$
$$\times\left[\int_{2\pi}\left[\frac{\sigma(z,\beta)}{s(z)} + \frac{{}_sA}{4\pi}\right][1-T_\infty(z,\theta)]d\Omega\ /\right.$$
$$\left.\left.1-\left[\frac{1+{}_sA}{4\pi}\right]\int_{2\pi}[1-T_\infty(z,\theta)]d\Omega\right]\right\} \qquad (41)$$

Aspects of Real Atmosphere Comparable to Model

As noted above, for the model, the path radiance and hence sky radiance is a function of equilibrium radiance and the radiance transmittance of the path, Eqs. (3.3) and (3.4). These equations are consistent with some aspects of the real atmosphere as described below.

(A.) Analytical Basis. In a cloud-free real atmosphere the horizon sky is a function of the equilibrium radiance and the space-to-earth radiance transmittance

$$L^*_\infty(z,90,\phi) = L_q(z,90,\phi)[1-T_\infty(z,90)]\ . \qquad (3.7)$$

This is directly comparable to Eq. (3.4).

When there is no absorption even more portions of the real sky conform to Eq. (3.4). It has been found that all parts of the sky at a scattering angle β of 55 degrees from the sun conform to Eq. (3.4),

$$L^*_\infty(z,\theta,55°\beta) = L_q(z,\theta,55°\beta)[1-{}_sT_\infty(z,\theta)]\ , \qquad (3.8)$$

where ${}_sT_\infty(z,\theta)$ is the transmittance due to scattering.

In addition, in the solar almucantar (all sky radiances at the zenith angle of the sun) for sun angles 70 to 80 degrees we have a similar equation

$$L_q(z,\theta_s,\beta) = L^*_\infty(z,\theta_s,\beta)/[1-{}_sT_\infty(z,\theta_s)]\ . \qquad (3.9)$$

Thus, some portions of the sky conform to Eq. (3.4) in the real atmosphere when there is no absorption (the second assumption of the equilibrium radiance model).

(B.) Sky Radiance. When cloud-free sky radiance measurements are graphed in the form of log sky radiance versus linear angle from sun β, the curves formed by the different almucantars (constant zenith angle sky radiances) are nearly parallel. An example of this is given in Figs. 3-1 and 3-2. These sky radiances were measured with airborne instruments during flights on 28 October and 3 November 1970, Duntley *et al.* (1972a). The sky radiances were measured with a filtered sensor having a mean wavelength of 478 nanometers and an effective passband of 19.9 nanometers.

Kushpil' and Petrova (1971) describe similar near parallel curves and note that the separation of the curves is related to the transmittance due to scattering. Cloud-free sky radiance may be used to compute equilibrium radiance by rearranging Eq. (3.4), thus,

$$L_q(z,\theta,\phi) = L^*_\infty(z,\theta,\phi)/[1-T_\infty(z,\theta)]\ . \qquad (3.10)$$

When the equilibrium radiances computed using Eq. (3.10) are graphed as a function of angle from sun on the same grid as Figs. 3-1 and 3-2, the separations disappear. Thus equilibrium radiance is primarily a function of angle from sun and not of zenith angle. Figures 3-3 and 3-4 depict the equilibrium radiances computed from the sky radiances in Figs. 3-1 and 3-2. The fractional standard deviation of the individual equilibrium radiances from the average as a function of β, is 0.16 for both Figs. 3-3 and 3-4.

Similar graphs were made for all the cloud-free sky radiance data from flights C-154 and C-155 (28 and 30 October 1970). Sky radiances were measured at altitudes of approximately 4350, 2200, and 650 meters with four filters. The filtered sensor had mean wavelengths of 478, 557, 664 and 765 nanometers with effective passbands of 19.9, 78.5, 30.2 and 50.4 nanometers respectively. The relative spectral response values for the four filtered sensors are graphed in Fig. 3-5. Except for two cases where the space-to-sensor transmittances were in error, the average fractional standard deviation of the individual equilibrium radiances from the average at each β was 0.21 with a range of 0.13 to 0.29.

Comparable graphs have been made for many ground-based measurements of sky radiance and for many airborne measurements both low and high altitude (0.5 to 6 kilometers). The sky radiance measurements were made with various filtered sensors in the visible spectrum, including the photopically filtered sensor. These filtered sensors range in mean wavelength from 459 to 765 nanometers. Examples using photopic measurements of sky luminance are given in Fig. 1 of Gordon (1969) and Figs. 2 and 3 of Gordon *et al.* (1973). The equilibrium radiances derived from cloud-free sky radiances using Eq. (3.10) when graphed as a function of angle from sun, always cluster as a fairly tight function of β, similar in shape to the volume scattering function $\sigma(z,\beta)$.

In the equilibrium radiance model, the equilibrium radiance is assumed to be solely a function of the scattering angle from the sun. Thus from Figs. 3-3 and 3-4 we can see that the real world to a reasonable approximation has sky radiances which are primarily a function of the scattering angle from the sun and the radiance transmittance due to scattering.

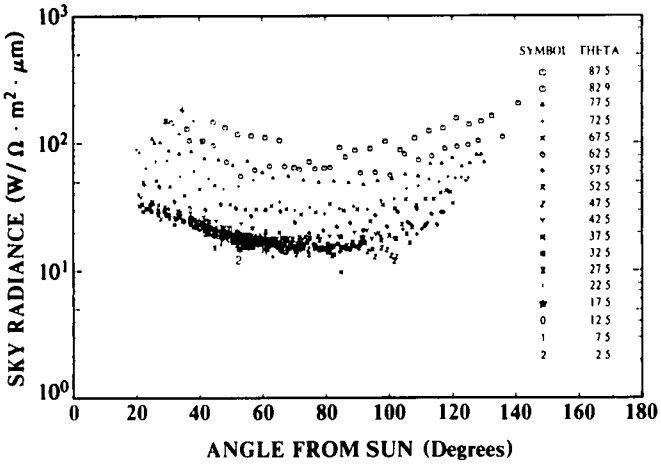

Fig. 3-1. Cloudless sky radiances as a function of angle from sun for flight C-154, 4.375 kilometer altitude above ground level.

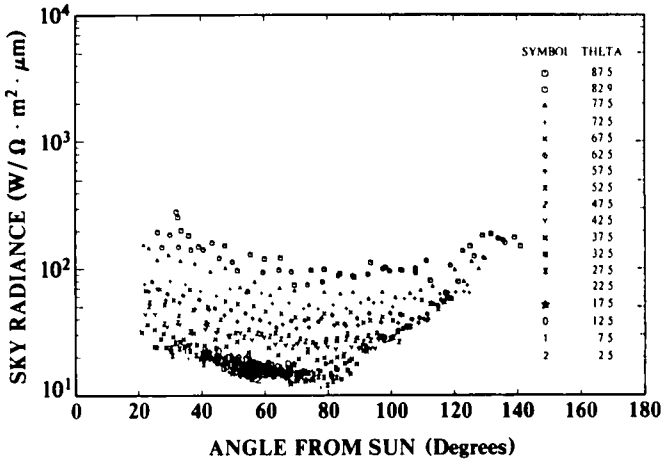

Fig. 3-2. Cloudless sky radiances as a function of angle from sun for flight C-157, 2.229 kilometer altitude above ground level.

The validation experiments of the method for obtaining earth-to-space path radiance from sky radiances measured at ground stations provide further evidence of the validity of Eqs. (3.4) and (3.10) for the real atmosphere.

(C.) Measuring Earth-to-Space Path Radiance from Ground Stations. The method of measuring contrast transmittance from ground stations has been completely described in Gordon *et al.* (1973). It uses sky radiance to obtain the equilibrium radiance at the appropriate scattering angle for the downward path of sight from earth-to-space. If θ is the zenith angle of the path of sight and θ' is the zenith angle of the sky radiance at the same scattering angle, the earth-to-space path radiance $L^*_\infty(\infty,\theta,\beta)$ is

$$L^*_\infty(\infty,\theta,\beta) = L^*_\infty(z,\theta',\beta)[1-T_\infty(\infty,\theta)]/[1-T_\infty(z,\theta')] \,. \quad (3.11)$$

This was derived by writing Eq. (3.10) in terms of θ and then θ' and then dividing the two equations and rearranging. Three experiments validated the method [Gordon *et al.* (1973)]. In addition the method was used during the Gemini program, Duntley *et al.* (1968), as part of a carefully controlled measurement of the visual capabilities of astronauts in earth orbit to discriminate test objects on the ground.

The method was found to be generally valid not only on cloud-free days but on days with some clouds as long as the path of sight and the sky radiance at θ' were cloud-free.

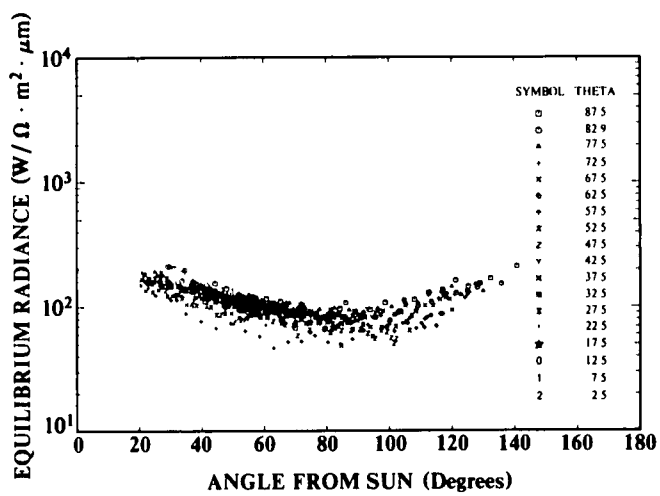

Fig. 3-3. Equilibrium radiance derived from sky radiances as a function of angle from sun for flight C-154, 4.375 kilometer altitude above ground level, filter 2.

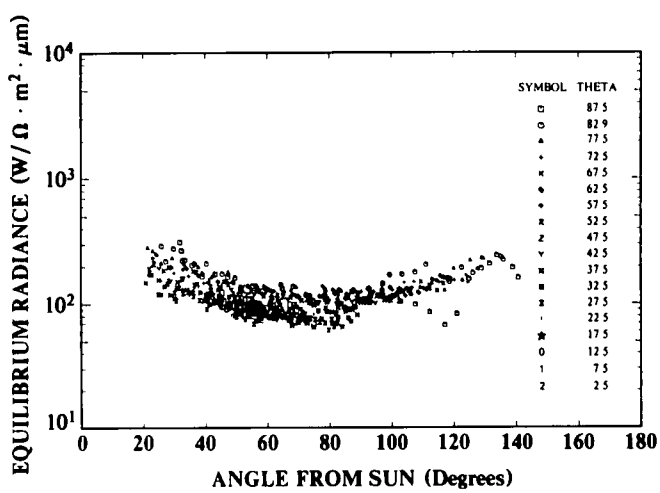

Fig. 3-4. Equilibrium radiance derived from sky radiances as a function of angle from sun for flight C-157, 2.229 kilometer altitude above ground level, filter 2.

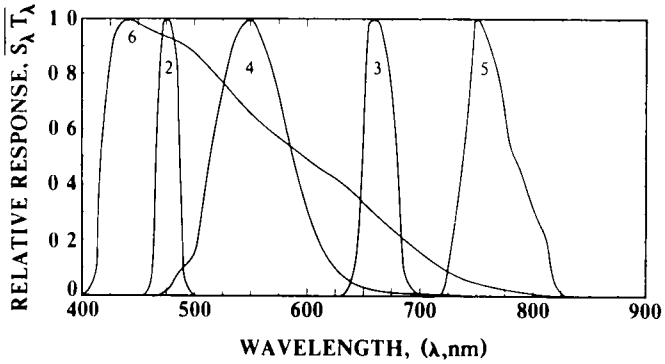

Fig 3-5 Standard spectral responses for airborne sensors Peak Wavelengths are 2 = 475nm Blue, 3 = 660nm Red, 4 = 550nm Photopic, 5 = 750nm N I R 6 = 440nm S-20

When the β for the path of sight is larger than all the scattering angles available in the upper hemisphere (this happens most often when the sun zenith angle is small) an approximation is used of the sky radiance at β=90 degrees This approximation was also used in the validation tests

Additional validation of Eqs (3 4) and (3 10) for the real atmosphere is implied by the validation study of the method of obtaining scattering transmittance from sky ratios

(D) Scattering Transmittance from Sky Ratios A method has been developed for obtaining the scattering transmittance from sky radiance ratios at equivalent angles from sun, Duntley *et al* (1972b and 1978b) The method stems from the suggested nomographic method of Kushpil' and Petrova (1971) for obtaining radiance transmittance from sky radiance ratios at equivalent scattering angles from the sun Again Eq (3 10) is divided by a similar equation for the angle θ' This time both θ and θ' are upward paths of sight at the same scattering angle,

$$L^*_\infty(z,\theta,\beta)/L^*_\infty(z,\theta',\beta) = [1-{}_sT_\infty(z,\theta)]/[1-{}_sT_\infty(z,\theta')] \quad (3\ 12)$$

Equation (3 12) can also be put in terms of the relative airmass and the vertical space-to-earth scattering transmittance

$$L^*_\infty(z,\theta,\beta)/L^*_\infty(z,\theta',\beta) = \frac{1-{}_sT_\infty(z,0)^{m_\infty(z\,\theta)/m_\infty(z\,0)}}{1-{}_sT_\infty(z,0)^{m_\infty(z\,\theta)/m_\infty(z\,0)}} \quad (3\ 13)$$

Although not solvable directly, Eq (3 13) can be solved for vertical transmittance by iterative means

An extensive body of solar transmissometer and sky scanner data collected during an early program at the Visibility Laboratory was used for validation study, Duntley *et al* (1978b) Both sky radiance and solar transmissometer data were available for approximately 100 cases with clear skies for each of four filters The filtered sensors had mean wavelengths of 459, 505, 560 and 661 nanometers respectively The relative spectral response values for the broadband filtered sensors used on the rooftop of the Visibility Laboratory are graphed in Fig 3-6

It was assumed that the total transmittance was the product of the scattering transmittance and transmittance due to ozone The ozone transmittances were based on the total ozone for the U S Standard Atmosphere (1976), and the spectral absorption values of Vigroux (1953) which are in good agreement with the Inn and Tanaka (1953) values

The ratios of the transmittance from sky radiance ratios times the ozone transmittance divided by the transmittance from the solar transmissometer ${}_sT_\infty(0,0)$ ${}_aT_\infty(0,0)/T_\infty(0,0)$ were averaged for each filter, this average of the ratios is given in Table 3 1 Column 5 The fractional standard deviation is given in Column 6

The best comparisons between the sky ratio times ozone transmittance and the solar transmissometer values (the best average transmittance ratio) should be for Filters 1 and 2 where the spectral responses are relatively unaffected by line or band absorption other than ozone The average transmittance ratio for Filters 1 and 2 is 0 98 with a fractional standard deviation of 0 05

On the other hand H_20 absorption bands start at 688 nanometers so that the Filter 4 solar transmissometer data may well be affected by water vapor in the atmosphere This possibly accounts for the relatively high transmittance ratio of 1 06 for Filter 4 mean wavelength 661 nanometers

This completes the review of the similarities between real atmosphere equations and the model Now we will compare the equilibrium radiance model results using Eq (41), Gordon (1969) to the Rayleigh atmosphere and the real atmosphere for the photopic sensor

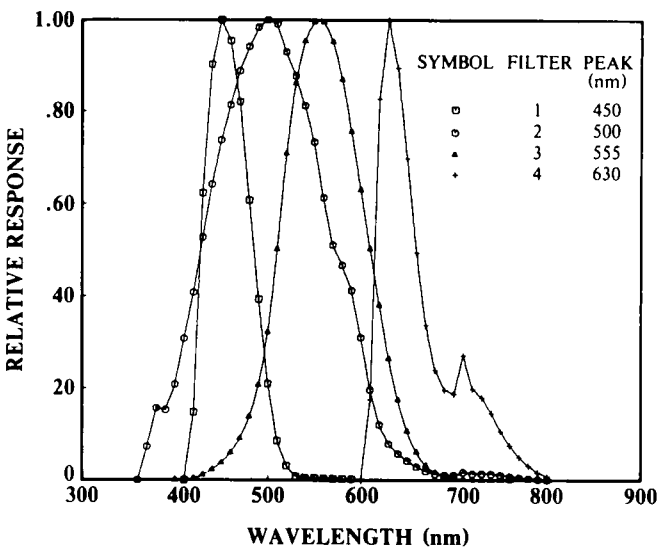

Fig. 3-6. Standard spectral responses for Visibility Laboratory rooftop sensors

Table 3.1. Scattering Transmittance from Sky Radiance Ratios Times Ozone Transmittance Divided by Total Transmittance from Solar Transmissometer for all Cloudless Data from January through September 1964 at Visibility Laboratory

Filter	Mean Wavelength nm	Effective Passband nm	Average Total Transmittance	Average $\frac{{}_{S}T_{\infty}(0\,0)\,{}_{a}T_{\infty}(0\,0)}{T_{\infty}(0\,0)}$	Fractional Standard Deviation	No of Cases	Ozone Transmittance
1	459	58 1	713	985	051	110	996
2	505	151 9	750	981	047	103	984
3	560	106 8	782	1 030	058	105	970
4	661	61 4	821	1 062	078	96	978

Model Calculations

(A.) Rayleigh Atmospheres. Equilibrium radiance model atmosphere calculations can be made for the Rayleigh atmosphere since the volume scattering function and radiance transmittance are well specified. The approximate equation for the normalized volume scattering function for Rayleigh scattering is

$$ {}_{R}\sigma(\beta)/{}_{R}s = 3(1+\cos^2\beta)/(16\pi) \; . \qquad (3.14) $$

The parenthetical modifier for altitude is not used since the normalized Rayleigh scattering is not a function of altitude.

Sky radiances or luminances have been computed for the photopic Rayleigh atmosphere by Coulson *et al.* (1960), Pyaskovskaya-Fesenkova (1979), and Tousey and Hulburt (1947). Comparison of the equilibrium radiance model was made to these other models in Duntley *et al.* (1975). The equilibrium radiance model computations were made with Eq. (41), Gordon (1969) using the same vertical radiance transmittance, solar irradiance out of the atmosphere, solar zenith angle, and albedo as for the other models. The results of the comparisons are depicted in Figs. 3-7, 3-8 and 3-9.

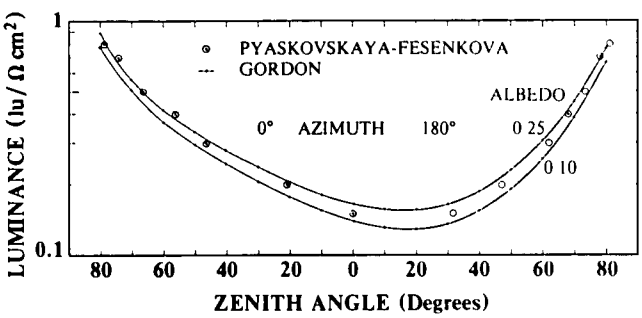

Fig. 3-8. Rayleigh sky luminances ($lu/\Omega cm^2$ or stilbs) for Pyaskovskaya-Fesenkova and Gordon using vertical earth-to-space beam transmittance of 0.861, a sun illuminance out of the atmosphere of 13 lu/cm^2, and a sun zenith angle of 60 degrees

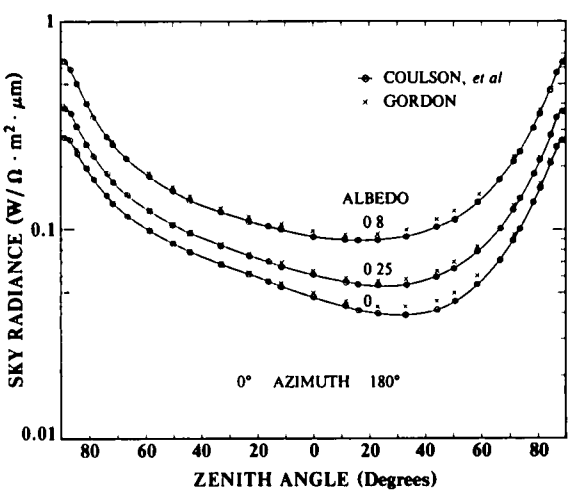

Fig. 3-7. Rayleigh sky Radiance for Coulson, *et al.* and Gordon using a vertical beam transmittance of 0.861, sun zenith angle of 36.8°, and a sun scalar irradiance at ground level of π.

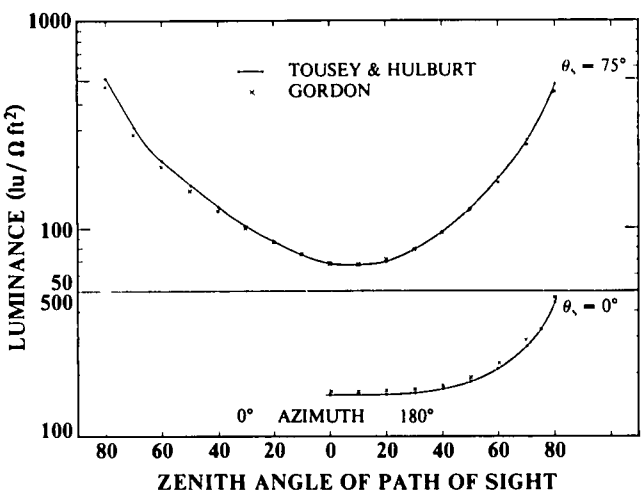

Fig. 3-9. Rayleigh sky luminance ($lu/\Omega ft^2$ at 10,000 feet) for Tousey and Hulburt (1947) and Gordon (1969) for sun illuminance out of the atmosphere of 13,600 $lu/\Omega ft^2$, ground-level scattering coefficient of 0.017 km^{-1}, and an albedo of 0.20.

The sky radiance values for Coulson *et al.* and the equilibrium radiance model for azimuths toward and away from the sun are graphed in Fig. 3-7. The comparison is best nearest the horizon in both azimuths. The values for the equilibrium radiance model near the zenith are slightly higher than for the Coulson model.

Pyaskovskaya-Fesenkova presented an isoluminance plot appropriate for albedos other than zero. The computations for the equilibrium radiance model were made using scalar albedos of 0.10 and 0.25. These are depicted as continuous curves in Fig. 3-8. The angular positions of the isoluminance values for the Pyaskovskaya-Fesenkova graph were estimated and are depicted in Fig. 3-8 as separate points. The curve for 0.25 albedo is close to the Pyaskovskaya-Fesenkova values near the horizon but higher near the zenith.

The solid lines in Fig. 3-9 represent the values given by Tousey and Hulburt. The values for the equilibrium radiance model compare well near the zenith and are slightly lower near the horizon for the sun at a zenith angle of 75 degrees. For the zero degree sun zenith angle, the equilibrium radiance model values are consistently a little higher than the Tousey and Hulburt values, comparing best at the zenith.

In general, the photopic Rayleigh sky radiance values from the equilibrium radiance model compare reasonably well to the values of Coulson *et al.* Pyaskovskaya-Fesenkova, and Tousey and Hulburt.

Since the model compares reasonably well to other models, the next step is to compare it to the real atmosphere.

(B.) Model Comparison to Measured Atmospheres. For comparison of the model to various Visibility Laboratory ground-based measurements, a value of 1.89E3 $W/m^2\mu m$ was used for the photopic solar irradiance out-of-the-atmosphere. This value is based on the spectral solar irradiance values of Johnson (1954) and the standard luminosity function.

Calculations for the equilibrium radiance model were made [Duntley *et al.* (1975)] for the photopic Rayleigh atmosphere. The Rayleigh normalized volume scattering function was obtained from Eq. (3.14). The photopic Rayleigh vertical space-to-earth radiance transmittance of 0.907 was based on the spectral total volume scattering coefficients from Eq. (14) of Penndorf (1957) and the sea level scale height for the U.S. Standard Atmosphere (1976).

Equilibrium radiance model calculations were made for the non-Rayleigh atmosphere [Duntley *et al.* (1978)] using the extensive catalog of photopic ground-level normalized volume scattering functions provided by Barteneva (1960). The 22 combinations of Barteneva scattering class functions and vertical space-to-earth radiance transmittances used for the model atmosphere computations are summarized in Table 3.2.

Downwelling Irradiance. The downwelling irradiance is defined as

$$E(z,d) = \int_{2\pi} L(z,\theta,\phi)\cos\theta d\Omega \ , \qquad (3.15)$$

Table 3.2. Transmittance and Scattering Function Specifications for Evaluation of Model Atmosphere Equations.

Earth-to-Space Vertical Transmittance	Barteneva Scattering Function Class No.								Total No. of Cases
0.9	2	3							2
0.8	2	3	4	5					4
0.7		3	4	5	5'	6			5
0.6		3	4	5	5'	6			5
0.5			4	5	5'	6	6'	7	6
Total No. of Cases	2	4	4	4	3	3	1	1	22

where the radiance array is for zenith angles 0 to 90 degrees including the sun or moon where appropriate.

Scalar albedo 0.10 is representative of cultivated fields. It is also an intermediate albedo for non-snow-covered terrains. We will use the model values for 0.1 scalar albedo to compare to the measured irradiances when albedo is unspecified.

For the model calculations, the range of downwelling irradiance due to changing scattering function for albedo 0.10 is small, being with ± 0.045 of the average for each sun zenith angle for each transmittance.

The average values from the model calculations of downwelling irradiance for scalar albedo 0.10 for each transmittance are graphed as a function of sun angle in Fig. 3-10a. The irradiance for the photopic Rayleigh atmosphere for 0.10 scalar albedo is given as a solid curve, as well as the irradiance from Brown (1952) for the average clear day. The Brown curve is similar to the average model values for 0.7 transmittance for sun zenith angles 0 to 70 degrees but is higher at sun zenith angles 80 and 85 degrees. A vertical transmittance value of 0.7 is commonly used as the average clear-day photopic transmittance therefore it is reasonable to assume the Brown values are representative of a transmittance of 0.7. Thus the equilibrium radiance model results for downwelling irradiances are reasonably consistent with the Brown average irradiances which are generally used as an irradiance standard for comparison.

Photopic downwelling irradiance for the portable instrument data for 1962 to 1967, Duntley *et al.* (1975), is graphed in Fig. 3-10b as a function of sun zenith angle. The irradiance data are designated by symbols indicating the radiance transmittance in 0.10-transmittance increments; *e.g.*, the symbol ⊙ indicates a transmittance of 0.85 ± 0.05 or values of transmittance from 0.800 to 0.899. These downwelling irradiances are all measured by an irradiometer. The two curves superimposed on the graph are the photopic Rayleigh atmosphere values for 1.0 albedo (conceived as an upper limit) and the average clear-day values of Brown.

The measured values of downwelling irradiance for the 1962 to 1967 period cluster about the average values of Brown and lie beneath the upper limiting values for the Rayleigh atmosphere. The measured irradiances show a

rough decrease as transmittance decreases similar to that shown in Fig. 3-10a for the average irradiances from the equilibrium radiance model.

The measured irradiances in Fig. 3-10b are for skies with an unobscured sun but with partially cloudy as well as clear skies. The model, however, represents a cloudless sky. Therefore for a more direct comparison, the data set was sorted to obtain zero cloud cover data within ± 0.02 of the transmittance and ± 2 degrees of the sun zenith angles used in the model computations. The bulk of these were for 0.8 transmittance. These are graphed in Fig. 3-11 along with similarly sorted data from the photopic irradiances measured with an irradiometer on the Visibility Laboratory rooftop during 1964, Duntley *et al.* (1978b).

When the 23 measured values in Fig. 3-11 are divided by the average values from the model (graphed as a curve in Fig. 3-11), the average ratio is 0.999 with a standard deviation of 0.14. This is excellent agreement.

Equilibrium Radiance. Four of the model evaluations of equilibrium radiance were for a space-to-earth transmittance of 0.8, a sun zenith angle of 70 degrees and a scalar albedo of 0.1. The Barteneva scattering functions used were her gradual classes 2, 3, 4 and 5. These values are graphed in Fig. 3-12 as solid curves. Barteneva's measurements of normalized volume scattering function were for ground level and for scattering angles from 16 to 164 degrees. Therefore we have limited the curves of equilibrium radiance to the scattering angles within the range of her measured values.

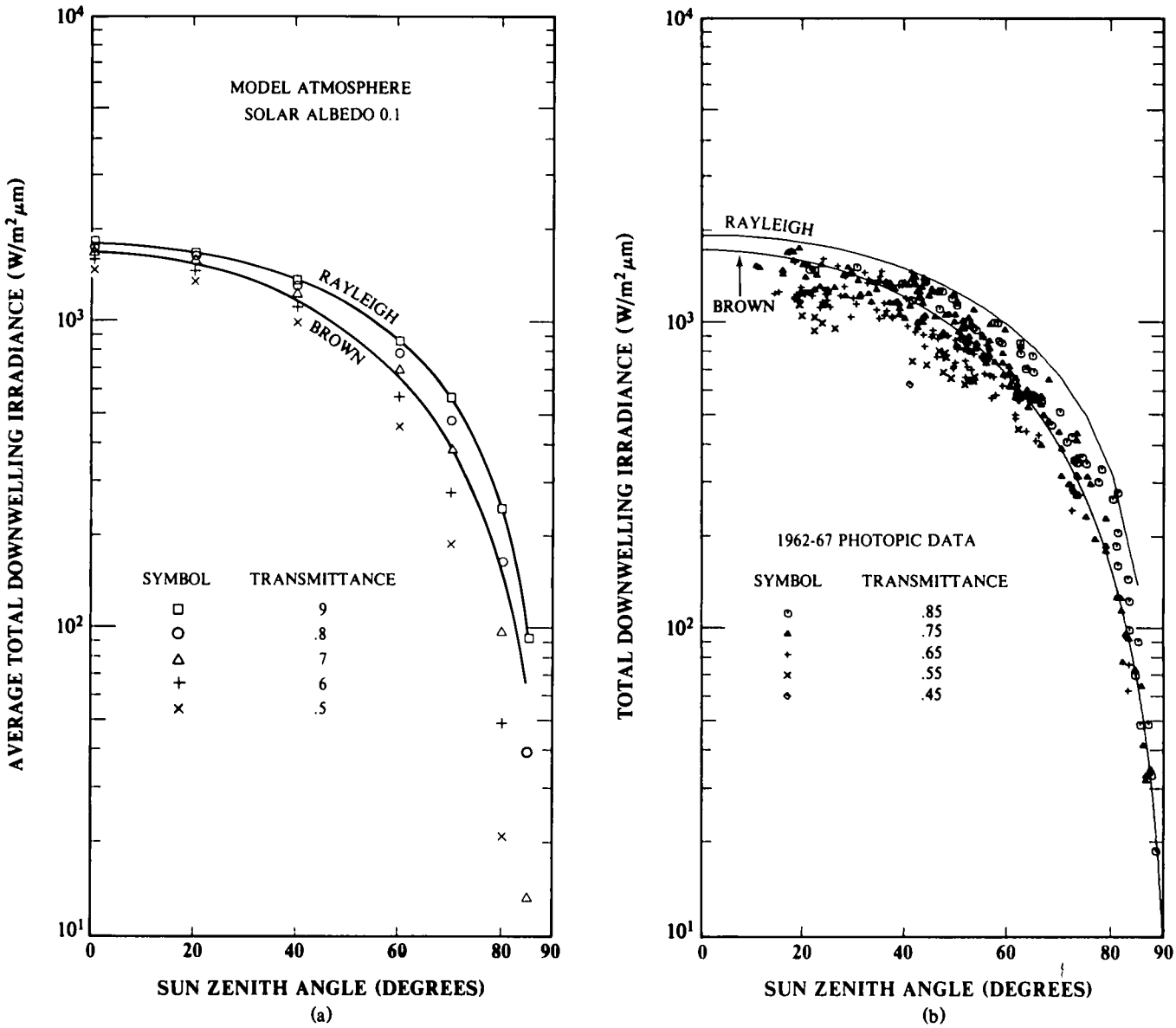

Fig. 3-10. Photopic downwelling irradiance data and equilibrium radiance model values compared to Brown.

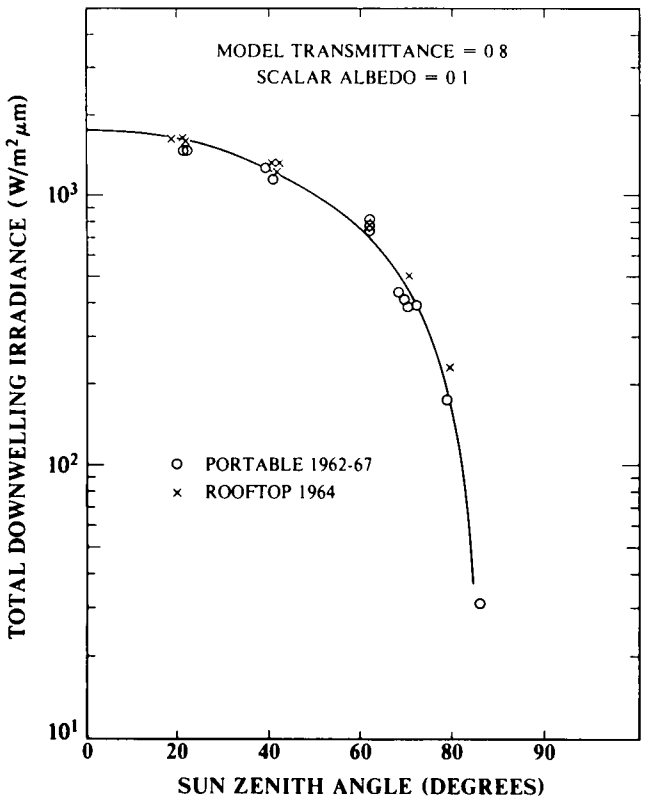

Fig. 3-11. Comparison of equilibrium radiance model to measured photopic irradiances for cloudless skies with transmittances 0.8 ±0.02 and sun zenith angles within ±2 degrees of model calculations.

The data bank of sky radiances and solar transmittances measured on the Visibility Laboratory rooftop in 1964, Duntley *et al.* (1978), contained approximately 100 cloud-free photopic measurements. Four of these were within ±0.02 of the transmittance 0.8 and within ±2 degrees of the sun zenith angle of 70 degrees. The equilibrium radiances derived from the sky radiances in the azimuths 0 and 180 degrees from the sun using Eq. (3.10) for these four cases are also graphed in Fig. 3-12. Although scalar albedo for these data sets is not available, an estimate of 0.1 is reasonable for the terrain surrounding the data site at the Visibility Laboratory.

The agreement between the curves for the model calculations and the equilibrium radiances based on the sky radiance and radiance transmittance measurements is quite good. Three of the four data sets compare quite closely to the model, with one data set slightly higher than the model at the larger scattering angles.

Similar graphs for seven other sun zenith angle transmittance combinations were drawn using altogether 26 data sets including those in Fig. 3-12. Most of the data sets (22) were for a transmittance of 0.8 ±.02, three sets were for 0.7 transmittance and one for 0.6. The only large discrepancy between data sets and model was for the single data set for the low transmittance of 0.6 where absorption may be a problem.

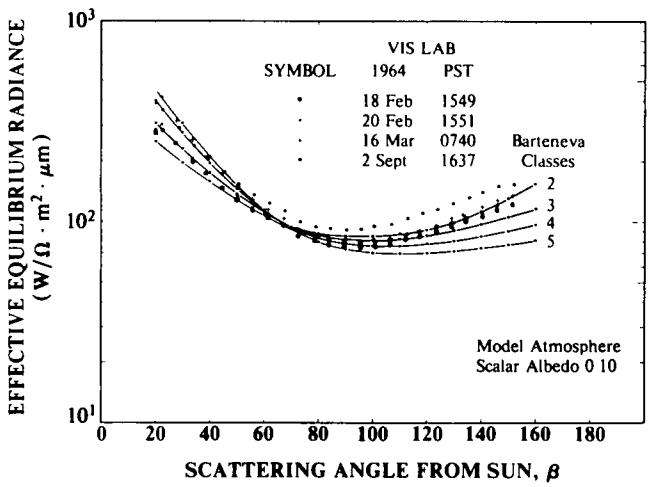

Fig. 3-12. Photopic equilibrium radiance derived from cloudless sky radiance data as a function of angle from sun for sun zenith angle 70 ±2 degrees and space-to-earth transmittance 0 80 ± 02, compared to model atmosphere calculations using Barteneva scattering functions

On the basis of these limited data sets several trends were noted. The comparison between data sets and model for the 0.8 and 0.7 transmittance indicated generally good agreement at intermediate sun zenith angles. The model was slightly high at the small sun zenith angle of 20 degrees and slightly low for the large sun zenith angle 80 degrees. When a fair number of data sets were available at one transmittance and sun zenith angle, the data sets sometimes showed more variability than the model. For instance for transmittance 0.8 and 80 degrees sun zenith angle, two of the data sets compared closely to the model and four data sets were higher than the model.

The comparison of model to data sets is sufficiently good to warrant further use of the model as a viable engineering approximation for cloudless days in the visible portion of the spectrum. The observed differences between some of the data sets and the model are sufficiently intriguing to warrant further study with a larger number of data sets.

Summary

An equilibrium radiance model of a clear (cloud-free) atmosphere for use in the visible region of the spectrum was presented by Gordon (1969). This model was based upon two assumptions: 1) the equilibrium radiance for a given path of sight does not change with altitude, and 2) absorption is negligible. Comparison of the model to three other models for the photopic Rayleigh atmosphere indicate good agreement. Good agreement is also indicated by comparisons of the model to the real atmosphere during cloud-free days for various broad-band measurements in the visible spectrum.

When equilibrium radiance is not constant for a path of sight, it is necessary to know the path function and attenuation coefficient values for each element of the path

from 0 to r in order to obtain the path radiance Assuming equilibrium radiance constant allows path radiance to be computed from the total path transmittance and the equilibrium radiance Thus assuming equilibrium radiance constant represents a tremendous, yet reasonable, simplification

3.2 A Preliminary Model Extension to Cloudy Day Conditions

During the last several years, the Visibility Laboratory has made measurements with both a path function meter and an integrating nephelometer on an instrumented aircraft, Duntley *et al* (1978a) A fall 1976 deployment in Europe contained flights during mostly cloudy or overcast conditions These data were used to compute the point function equilibrium radiance using Eq (3 16)

$$L_q(z,\theta,\phi) = L_*(z,\theta\,\phi)/s(z) \qquad (3\ 16)$$

The point function equilibrium radiance is equal to the path function divided by the attenuation coefficient or in the absence of strongly absorbing particles like smoke or multi-droplet reflecting surfaces such as clouds, the total volume scattering coefficient $s(z)$ Surprisingly even under these relatively turbid conditions, many of the equilibrium radiance profiles were relatively constant with altitude An example is given in Fig 3-13 for a flight with scattered to broken low clouds, clear high altitude Figure 3-13 contains the profiles of the path function and the volume scattering coefficient with altitude as well as the computed equilibrium radiance profile The three profiles of equilibrium radiance with altitude are for three filters having mean wavelengths of 478, 557 and 664 nanometers and effective passbands of 20, 78 and 30 nanometers respectively The relative spectral responses of the filtered sensors are given in Fig 3-5

If we restrict the data to the 33 profiles wherein 1) the path of sight of the path function meter is relatively constant with altitude and 2) none of the individual path segments are obviously in a cloud, 60 percent of the equilibrium radiance profiles have standard deviations from the mean of 25 percent or less This includes some overcast cases as well as scattered to broken clouds Sixty percent of the cloudy day cases is a sufficiently large portion of the cases to warrant considering the modelling implications for the cloudy case

For equilibrium radiance to be constant with altitude it must be assumed that the path of sight is either all sunlit or all in the cloud shadow in addition to the path segments being cloud-free

Sky-Ground Ratio Format for Contrast Transmittance

One of the most general forms of the contrast transmittance equation is

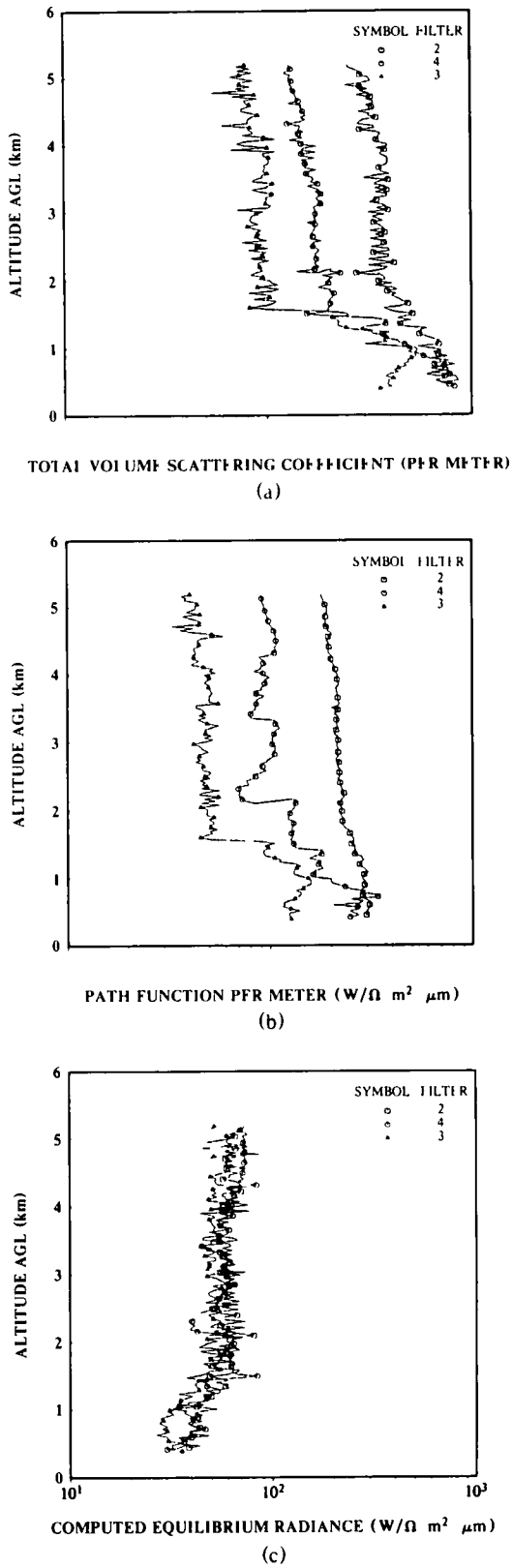

Fig. 3-13. Measured total volume scattering coefficient, path function, and computed equilibrium radiance as a function of altitude for flight C-401 Flight was near noon on 5 December 1976 in northwestern France with scattered cumulus and scattered thin cirrus

$$C_r(z,\theta,\phi)/C_o(z_t,\theta,\phi) =$$
$$\{1+L_r^*(z,\theta,\phi)/[{}_bL_o(z_t,\theta,\phi)\,T_r(z,\theta]\}^{-1}\,, \qquad (3.17)$$

where $C_r(z,\theta,\phi)$ is the apparent contrast of an object, $C_o(z_t,\theta,\phi)$ is the inherent contrast, and ${}_bL_o(z_t,\theta,\phi)$ is the inherent radiance of the background against which the object is seen. In the Gordon model, the path radiance is a function of the equilibrium radiance and the transmittance of the path. Substituting Eq. (3.3) into Eq. (3.17) and rearranging we get

$$C_r(z,\theta,\phi)/C_o(z_t,\theta,\phi) =$$
$$\{1+L_q(z,\theta,\phi)[T_r(z,\theta)^{-1}-1]/{}_bL_o(z_t,\theta,\phi)\}^{-1}\,. \qquad (3.18)$$

The equilibrium radiance divided by the inherent background radiance is the sky-ground ratio. The concept of sky-ground ratio was originally established by Duntley (1946 and 1948), repeated by Middleton (1952) and discussed at length by Duff (1972). This ratio is not a constant although it is often misused as such. It is preferable to determine the equilibrium radiance and the inherent background radiance separately since both vary with path of sight, but independently.

As noted in the references in the preceding paragraph, the non-cloud horizon radiance at θ',ϕ' is equal to the equilibrium radiance for the path of sight at θ,ϕ with the same scattering angle. However, for many situations the scattering angles associated with horizontal paths of sight will not coincide with those of downward inclined paths of sight. Also, there is often a problem of clouds on the horizon, precluding use of the horizon measurement to obtain equilibrium radiance.

When the space-to-sensor radiance transmittance $T_\infty(z,0)$ is known in addition to the path transmittance $T_r(z,\theta)$, the equilibrium radiance can be computed from cloud-free sky radiance other than the horizon radiance using Eq. (3.4). There will still be some downward paths of sight which have angles from sun greater than any available from sky radiances. In these instances, the sky radiance and hence equilibrium radiance at a scattering angle of 90 degrees can probably be used as a reasonable approximation. This approximation was found to be valid for the method of measuring earth-to-space contrast transmittance from ground stations Gordon *et al.* (1973) and is probably an equally valid engineering approximation for the shorter paths.

A Generalized Equation for Equilibrium Radiance

(A.) Partial Cloud, Sun Unobscured. In order to be able to use Eq. (3.4) we need to assume the non-cloud or blue sky portions of the upper hemisphere are completely sunlit. Therefore we will assume only the section of the sky surrounding the sun is cloud-free, as described by zenith angles $\theta_1' \rightarrow \theta_s \rightarrow \theta_2'$. Similarly the azimuth description of the cloud-free section is $\phi_1' \rightarrow \phi_s \rightarrow \phi_2'$. Having only one cloud-free portion of the sky near the sun is rather limiting but it does extend the model beyond the completely cloudless sky case.

The integral of the radiance field over 4π, is the total scalar irradiance $\epsilon(z)$

$$\epsilon(z) = \int_{4\pi} L(z,\theta',\phi')\,d\Omega\,. \qquad (3.19)$$

The scalar albedo is defined as the lower hemisphere or upwelling scalar irradiance $\epsilon(z,u)$ divided by the upper hemisphere or downwelling scalar irradiance $\epsilon(z,d)$

$${}_sA(z) = \epsilon(z,u)/\epsilon(z,d) = \frac{\int_0^{2\pi}\int_{\pi/2}^{\pi} L(z,\theta',\phi')\sin\theta'\,d\theta'\,d\phi'}{\int_0^{2\pi}\int_0^{\pi/2} L(z,\theta',\phi')\sin\theta'\,d\theta'\,d\phi'}\,. \qquad (3.20)$$

In general we will use the symbol A to designate an irradiance ratio.

Now let us assume that the downwelling scalar irradiance from the non-cloud or blue sky ${}_b\epsilon(z,d)$ is

$${}_b\epsilon(z,d) = \int_{\phi_1'}^{\phi_2'}\int_{\theta_1'}^{\theta_2'} L_q(z,\theta',\phi')[1-T_\infty(z,\theta')]\sin\theta'\,d\theta'\,d\phi'\,. \qquad (3.21)$$

The basic equation for the equilibrium radiance in terms of the sun scalar irradiance ${}_s\epsilon(z)$, the downwelling diffuse scalar irradiance ${}_d\epsilon(z,d)$ and the scalar albedo is [Eq. (26), Gordon (1969)]

$$L_q(z,\theta,\phi) = {}_s\epsilon(z)[\sigma(z,\beta)/s(z) + {}_sA(z)/4\pi] +$$
$${}_d\epsilon(z,d)[1+{}_sA(z)]/4\pi\,. \qquad (3.22)$$

The downwelling diffuse scalar irradiance in the cloudy case is the sum of the downwelling non-cloud or blue sky and the downwelling cloud scalar irradiance ${}_c\epsilon(z,d)$

$${}_d\epsilon(z,d) = {}_b\epsilon(z,d) + {}_c\epsilon(z,d)\,. \qquad (3.23)$$

Also the upwelling scalar irradiance can be expressed as

$$\epsilon(z,u) = {}_sA(z)\epsilon(z,d) = {}_sA(z)[{}_s\epsilon(z) +$$
$${}_b\epsilon(z,d) + {}_c\epsilon(z,d)]\,. \qquad (3.24)$$

At this point we will introduce a new concept.

(B.) Cloud Scalar Irradiance Ratio. Any reflectance has a limiting range of 0 to 1. What we need is a cloud reflectance in relation to the rest of the 4π radiance distribution. The cloud scalar irradiance can be defined as a cloud scalar irradiance ratio or reflectance ${}_{sc}A$ times the remainder of the 4π light distribution or scalar irradiances.

Thus

$$ {}_c\epsilon(z,d) = {}_{sc}A\,[{}_s\epsilon(z) + {}_b\epsilon(z,d) + \epsilon(z,u)] \qquad (3.25) $$

Now substituting Eq. (3.24) into Eq. (3.25) which is then substituted into Eq. (3.23), we get

$$ {}_c\epsilon(z,d) = \frac{{}_s\epsilon(z)\,{}_{sc}A(z)[1+{}_sA(z)]}{1-{}_{sc}A(z)\,{}_sA(z)} + {}_b\epsilon(z,d)\left[1+\frac{{}_{sc}A(z)[1+{}_sA(z)]}{1-{}_{sc}A(z)\,{}_sA(z)}\right] . \qquad (3.26) $$

Finally substituting Eq. (3.26) into Eq. (3.22) and collecting terms we have the general expression for the equilibrium radiance,

$$ L_q(z,\theta,\phi) = {}_s\epsilon(z)[\sigma(z,\beta)/s(z) + G] + {}_b\epsilon(z,d)\,B , \qquad (3.27) $$

where

$$ B = 1/(4\pi) + G , \qquad (3.28) $$

and

$$ G = {}_sA(z)/(4\pi) + {}_{sc}A(z)[1+{}_sA(z)]\,/\,\{4\pi[1-{}_{sc}A(z)\,{}_sA(z)]\} \qquad (3.29) $$

(C.) Series Expansion to Obtain Sky Scalar Irradiance. A first approximation for the blue sky scalar irradiance ${}_b\epsilon_1(z,d)$ is found by computing the blue sky radiance and hence the sky irradiance using the equilibrium radiance from the sun alone (the first term in Eq. (3.27) above),

$$ L_{q1}(z,\theta',\phi') = {}_s\epsilon(z)[\sigma(z,\beta')/s(z) + G] . \qquad (3.30) $$

The blue sky scalar irradiance from Eqs. (3.21) and (3.30) is

$$ {}_b\epsilon_1(z,d) = {}_s\epsilon(z)\int_{\phi_1'}^{\phi_2'}\int_{\theta_1'}^{\theta_2'}[\sigma(z,\beta')/s(z)+G]\,[1-T_\infty(z,\theta')]\sin\theta'\,d\theta'\,d\phi' . \qquad (3.31) $$

Equation (3.31) is directly analogous to Eq. (31) in Gordon (1969).

The second approximation for the blue sky downwelling scalar irradiance, ${}_b\epsilon_2(z,d)$ is found by computing the equilibrium radiance $L_{q2}(z,\theta',\phi')$ using ${}_b\epsilon_1(z,d)$ from Eq. (3.31) in Eq. (3.27)

$$ {}_b\epsilon_2(z,d) = \int\!\!\int L_{q2}(z,\theta',\phi')[1-T_\infty(z,\theta')]\sin\theta'\,d\theta'\,d\phi' . \qquad (3.32) $$

Then

$$ {}_b\epsilon_2(z,d) = {}_b\epsilon_1(z,d) + {}_b\epsilon_1(z,d)\,B\int\!\!\int [1-T_\infty(z,\theta')]\sin\theta'\,d\theta'\,d\phi' \qquad (3.33) $$

The third approximation for the blue sky downwelling scalar irradiance is found by computing the equilibrium radiance $L_{q3}(z,\theta',\phi')$ using ${}_b\epsilon_2(z,d)$ in Eq. (3.27),

$$ {}_b\epsilon_3(z,d) = \int\!\!\int L_{q3}(z,\theta',\phi')[1-T_\infty(z,\theta')]\sin\theta'\,d\theta'\,d\phi' , \qquad (3.34) $$

and

$$ {}_b\epsilon_3(z,d) = {}_b\epsilon_1(z,d) + {}_b\epsilon_1(z,d)\,B\int\!\!\int [1-T_\infty(z,\theta')]\sin\theta'\,d\theta'\,d\phi' + {}_b\epsilon_1(z,d)\,B^2\left\{\int\!\!\int [1-T_\infty(z,\theta')]\sin\theta'\,d\theta'\,d\phi'\right\}^2 \qquad (3.35) $$

Let

$$ X = \int_{\phi_1'}^{\phi_2'}\int_{\theta_1'}^{\theta_2'}[1-T_\infty(z,\theta')]\sin\theta'\,d\theta'\,d\phi' . \qquad (3.36) $$

Now Eq. (3.35) can be written

$$ {}_b\epsilon_3(z,d) = {}_b\epsilon_1(z,d)(1+BX+B^2X^2) . \qquad (3.37) $$

Therefore

$$ {}_b\epsilon_n(z,d) = {}_b\epsilon_1(z,d)(1+BX+B^2X^2+\ B^{n-1}\ X^{n-1}\ ) \qquad (3.38) $$

This series is easily evaluated thus

$$ {}_b\epsilon(z,d) = {}_b\epsilon_\infty(z,d) = {}_b\epsilon_1(z,d)/(1-BX) \qquad (3.39) $$

Substituting Eq. (3.31) and (3.39) into (3.27), we find

$$ L_q(z,\theta,\phi) = {}_s\epsilon(z)\,\{\sigma(z,\beta)/s(z) + G + B\int\!\!\int [\sigma(z,\beta')/s(z)+G]\,[1-T_\infty(z,\theta')]\sin\theta'\,d\theta'\,d\phi'/(1-BX)\} . \qquad (3.40) $$

The first term in the braces is the direct scattering from the sun. The second term is the portion of the upwelling earth and downwelling cloud scalar irradiance due to the sun. The third term is the non-cloud sky scalar irradiance and reflectance from the earth and cloud of the non-cloud skylight.

When the sky is clear of clouds, ${}_c\epsilon(z,d)=0$, ${}_{sc}A(z)=0$, $G = {}_sA(z)/4\pi$, and Eq. (3.40) becomes equivalent to Eq. (41) of Gordon (1969). Thus Eq. (3.40) is the general expression for equilibrium radiance.

The cloud scalar irradiance ratio has a theoretical range of 0 to 1 as does the scalar albedo of the earth. All reflectances, whether irradiance ratios or albedos or radiance reflectances have this theoretical range when there is no emittance. The cloud scalar irradiance ratio correlates with the descriptions of dark to white clouds.

Equation (3.40) is easily solveable by computer. A program developed earlier to handle the zero cloud cover case can be modified to handle the partially cloud case. An evaluation of the limiting cases using cloud scalar irradiance ratios of 0 and 1 should be of interest to the analyst doing parametric studies.

Equilibrium Reflectance

(A.) Development of Concept. From the concepts of reflectance and equilibrium radiance one can derive the concept of equilibrium reflectance.

The inherent reflectance of an object ${}_{t}R_{o}$ or a background ${}_{b}R_{o}$ is defined as (Gordon (1964), p. 558 or Boileau and Gordon (1966), p. 805)

$$ {}_{b}R_{o}(z_{t},\theta,\phi) = \pi\ {}_{b}L_{o}(z_{t},\theta,\phi)/E(z_{t},d)\ . \qquad (3.41) $$

Let us similarly define equilibrium reflectance as

$$ R_{q}(z,\theta,\phi) = \pi\ L_{q}(z,\theta,\phi)/E(z,d)\ . \qquad (3.42) $$

Now combining Eqs. (3.16) and (3.42) we have

$$ R_{q}(z,\theta,\phi) = \pi\ L_{*}(z,\theta,\phi)/[s(z)E(z,d)]\ , \qquad (3.43) $$

which is an expression for equilibrium reflectance in terms of measureable parameters.

(B.) Equilibrium Reflectance Data. During the same field trip as illustrated by Fig. 3-13, measurements of downwelling irradiance were made concurrently with the measurements of path function and total volume scattering coefficient. During analysis of the point function equilibrium radiance it was noticed that when the profile varied with altitude, it was often paralleled by variations in the values of downwelling irradiance. An excellent example of this is given in Fig. 3-14. The profile for the pseudo-photopic Filter 4 mean wavelength 557 nanometers was flown very near sundown. The sharp change in the radiance and irradiance data near three kilometers altitude is due to a time lapse during an interruption in the ascent of the aircraft.

When the equilibrium radiances are divided by the irradiances, the parallel variations are not present in the quotients. The equilibrium reflectance is the quotient times π. It follows that when equilibrium reflectance is used to specify the vertical character of the atmosphere in lieu of equilibrium radiance, then we are no longer restricted to a path of sight which is either all sunlit or all shadowed from the sun.

The computed profile of equilibrium reflectance for flight C-390 is shown in Fig. 3-15. The standard deviation from the average was 0.81 for the equilibrium radiance and 0.14 for the equilibrium reflectance for Filter 4 flight C-390. The equilibrium reflectance was then computed for all the profiles during this deployment.

Figure 3-16 summarizes the fractional standard deviations from the average for each filter for the measurements of total volume scattering coefficient, path function and irradiance as well as the calculated values of equilibrium radiance and reflectance. The variability with altitude of the equilibrium reflectance was generally less than the variability of the equilibrium radiance.

In a later field trip, Johnson and Gordon (1980), it was verified that the irradiometer had developed problems of internal moisture affecting the irradiance measurements during descents from high altitude. Examination of the irradiance profiles with altitude of the two filters (Filters 3 and 5) which were potentially affected indicate that probably only one profile contains questionable data of significance. The other profiles are either entirely at lower altitudes where the problem did not occur or have standard deviations for equilibrium reflectance of 0.25 or below. This does not appreciably change the overall analysis of the data in Fig. 3-16.

An overcast example is given in Figs. 3-17 and 3-18 for flight C-399. The measurement of path function using Filter 5 in Fig. 3-17 indicates most of the signal was at or below the minimum calibrateable value (MCV) where the signal to noise ratio is low and can not be considered reliable. The equilibrium radiance and reflectance were evaluated for Filter 5 for only a small segment of four profiles where the signal was clearly above the MCV.

Even in the cases where the equilibrium radiance standard deviation was 0.25 or less, the equilibrium reflectance profiles generally had still smaller standard deviations. This also is illustrated in Fig. 3-19 where the irradiance and equilibrium reflectance profiles for flight C-401 can be compared to the path function and equilibrium radiance profiles for the same flight in Fig. 3-13.

Of the 33 profiles cited earlier from this deployment, 80 percent of the equilibrium reflectance profiles have standard deviation from the mean of 25 percent or less as compared to 60 percent of the equilibrium radiance profiles. It is also probable that some of the remaining 20 percent of the profiles were less obviously contaminated by intrusion of cloud wisps into the path segments being measured.

(C.) Equation of Transfer in Reflectance Form. The equation of transfer which is applicable to all real atmospheres relates the change in radiance for a small incremental path length to the attenuation coefficient and path function. Substituting Eq. (3.2) into Eq. (3.1) and rearranging; we get

$$ \{1/[L(z,\theta,\phi)-L_{q}(z,\theta,\phi)]\}\ dL(z,\theta,\phi) = -\alpha(z)dr\ . \qquad (3.44) $$

Equilibrium reflectance was defined as a function of

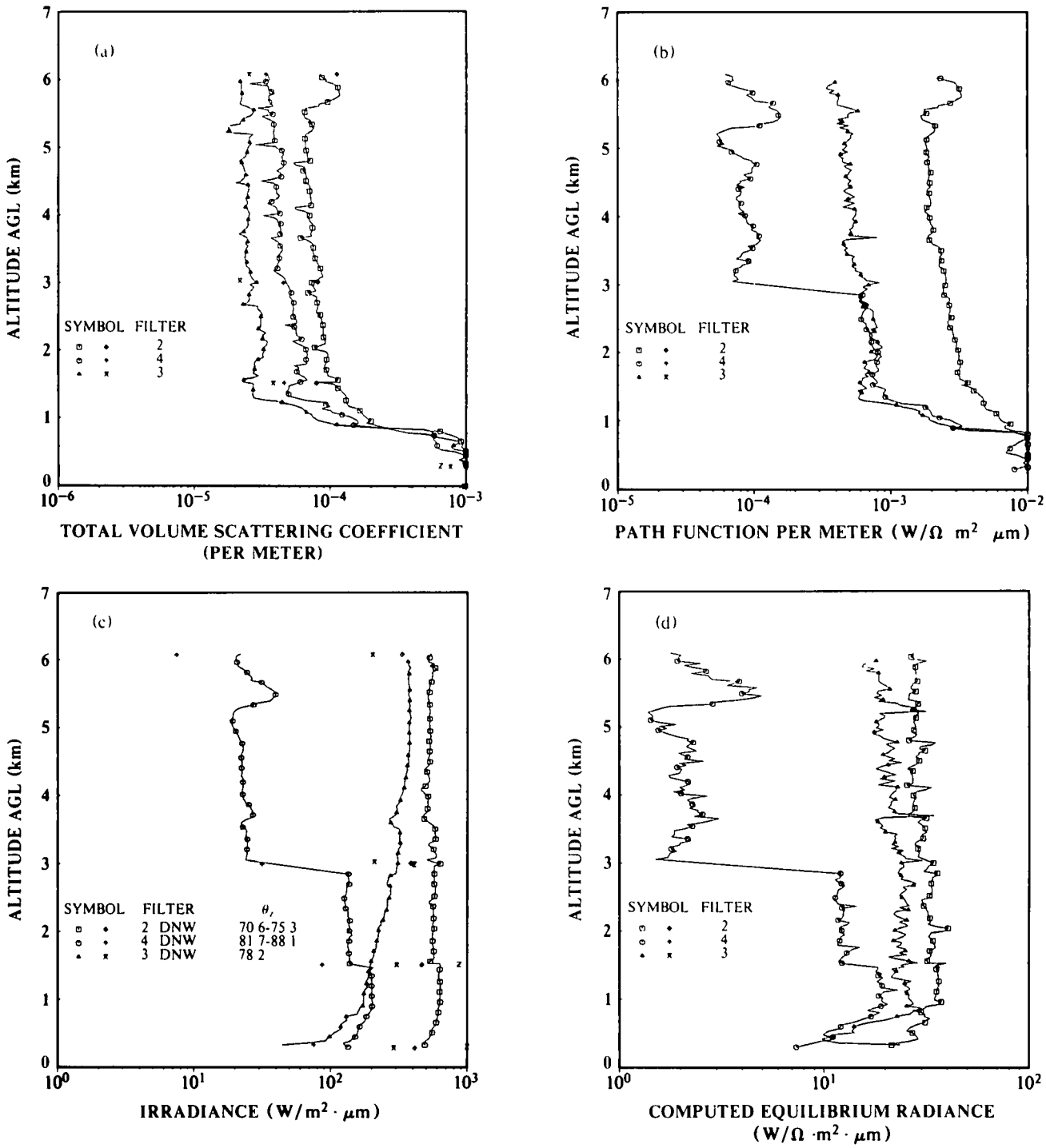

Fig. 3-14. Measured total volume scattering coefficient, path function, irradiance, and computed equilibrium radiance as a function of altitude for flight C-390 Flight was late afternoon on 25 October 1976 in Denmark with scattered changing to broken thin cirrus clouds

the downwelling irradiance in Eq. (3.42). Let us similarly define the effective reflectance $R(z,\theta,\phi)$ of any radiance $L(z,\theta,\phi)$ as

$$R(z,\theta,\phi) = \pi L(z,\theta,\phi)/E(z,d) \qquad (3.45)$$

If we multiply the numerator and denominator of the first term in Eq. (3.44) by $\pi/E(z,d)$, and use the relationships from Eqs. (3.42) and (3.45) we get the equation of transfer in reflectance form which is then expressed in integral form

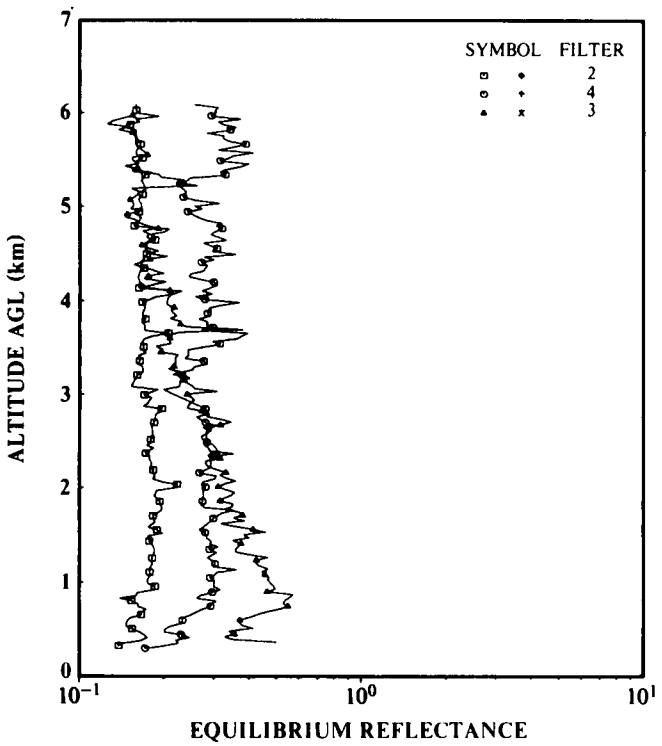

Fig. 3-15. Computed equilibrium reflectance as a function of altitude for flight C-390.

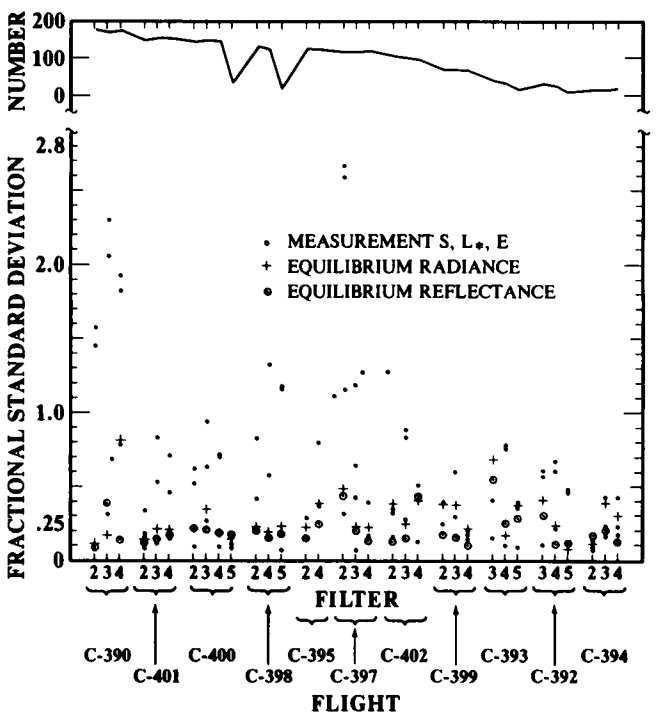

Fig. 3-16. Fractional standard deviations from the average for measurements • of total volume scattering coefficient, path function and downwelling irradiance, and for computed values of equilibrium radiance + and reflectance ⊙ for the flights during fall 1976.

$$\int_{R_o}^{R_t} \{1/[R(z,\theta,\phi)-R_q(z,\theta,\phi)]\}\, dR(z,\theta,\phi) = \int_{o}^{t} -\alpha(z)\,dr \ . \quad (3.46)$$

The reflectance is integrated between the limits of inherent reflectance $R_o(z_t,\theta,\phi)$ and apparent reflectance $R_r(z,\theta,\phi)$.

Equation (3.46) holds for all real atmospheres and monochromatic radiance. It is also a reasonable engineering approximation for broad band sensors in the visible spectrum.

As described above, we found that for many clear and cloudy situations, the point function equilibrium reflectance remains relatively constant with altitude. If we assume $R_q(z,\theta,\phi)$ equals $R_q(z_t,\theta,\phi)$, Eq. (3.46) can be integrated. The results of the integration are

$$\ln\{[R_r(z,\theta,\phi)-R_q(z_t,\theta,\phi)]/ [R_o(z_t,\theta,\phi)-R_q(z_t,\theta,\phi)]\}=\ln T_r(z,\theta) \ . \quad (3.47)$$

Rearranging we find

$$R_r(z,\theta,\phi) = R_o(z_t,\theta,\phi)\,T_r(z,\theta) + R_q(z_t,\theta,\phi)[1-T_r(z,\theta)] \ . \quad (3.48)$$

This is very similar in form to the model equation for obtaining the apparent radiance Eq. (10) Gordon (1969),

$$L_r(z,\theta,\phi) = L_o(z_t,\theta,\phi)\,T_r(z,\theta) + L_q(z,\theta,\phi)[1-T_r(z,\theta)] \ . \quad (3.49)$$

This equation relates the apparent radiance $L_r(z,\theta,\phi)$ at the sensor altitude z to the inherent radiance $L_o(z_t,\theta,\phi)$ at the target or object altitude z_t, the radiance transmittance and the equilibrium radiance.

In order to understand the relationship between Eqs. (3.48) and (3.49) better, let us now substitute Eq. (3.45) for the apparent reflectance in Eq. (3.49). Then rearranging, we have

$$L_r(z,\theta,\phi) = E(z,d)\{R_o(z_t,\theta,\phi)\,T_r(z,\theta) + R_q(z_t,\theta,\phi)[1-T_r(z,\theta)]\}/\pi \ . \quad (3.50)$$

Thus the path radiance term in Eq. (3.49) is different than the last term in Eq. (3.48) because the irradiance is not assumed constant with altitude, *i.e.*, $E(z,d)\neq E(z_t,d)$. It is a special case when $E(z,d)$ equals $E(z_t,d)$, then $L_q(z,\theta,\phi)$ equals $L_q(z_t,\theta,\phi)$ and $L_r^*(z,\theta,\phi)=L_q(z,\theta,\phi)[1-T_r(z,\theta)]$.

(D.) Sky-Ground Ratio, Reflectance Form. Contrast can be expressed in terms of reflectance as

$$C_o(z_t,\theta,\phi)=[{}_tR_o(z_t,\theta,\phi) - {}_bR_o(z_t,\theta,\phi)]/{}_bR_o(z_t,\theta,\phi) \ . \quad (3.51)$$

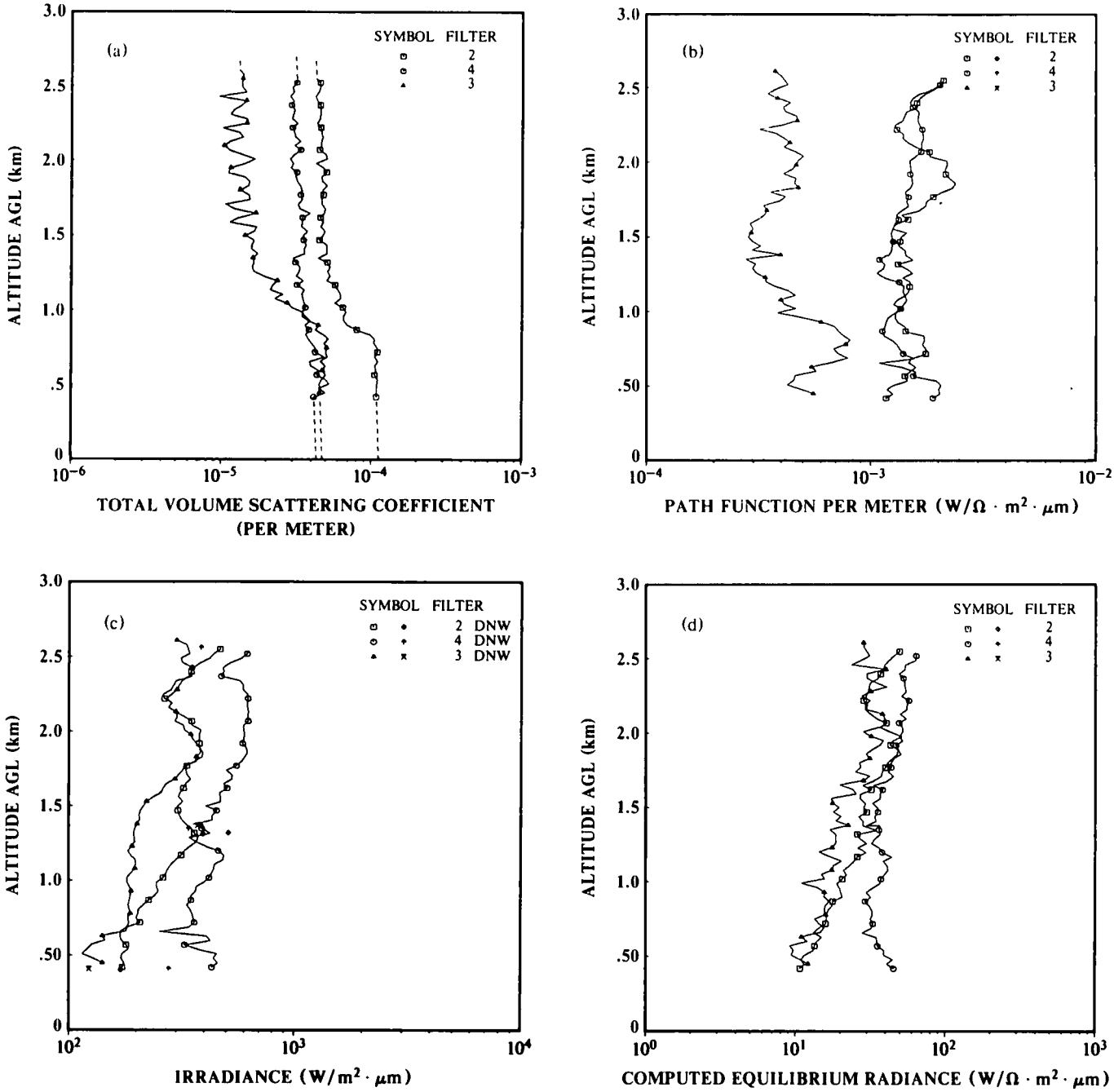

Fig. 3-17. Measured total volume scattering coefficient, path function, irradiance, and computed equilibrium radiance as a function of altitude for flight C-399.

Thus the contrast transmittance can be expressed as

$$\frac{C_r(z,\theta,\phi)}{C_o(z_t,\theta,\phi)} = \frac{[{}_tR_r(z,\theta,\phi) - {}_bR_r(z,\theta,\phi)]\ {}_bR_o(z_t,\theta,\phi)}{{}_bR_r(z,\theta,\phi)\ [{}_tR_o(z_t,\theta,\phi) - {}_bR_o(z_t,\theta,\phi)]} . \quad (3.52)$$

Now substituting in Eq. (3.48) for the apparent object and background reflectances, simplifying and rearranging we get

$$C_r(z,\theta,\phi)/C_o(z_t,\theta,\phi) = \{1+R_q(z_t,\theta,\phi)[T_r(z,\theta)^{-1}-1]/{}_bR_o(z_t,\theta,\phi)\}^{-1} . \quad (3.53)$$

The ratio $R_q(z_t,\theta,\phi)/{}_bR_o(z_t,\theta,\phi)$ is the sky-ground ratio in reflectance form. This ratio was expressed as a luminance ratio in Duntley (1948) and in radiance form in Eq. (3.18).

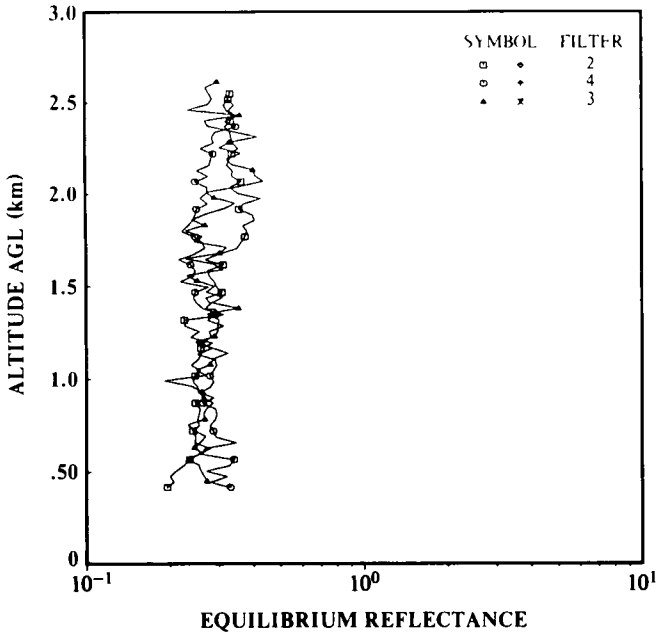

Fig. 3-18. Computed equilibrium reflectance as a function of altitude for flight C-399

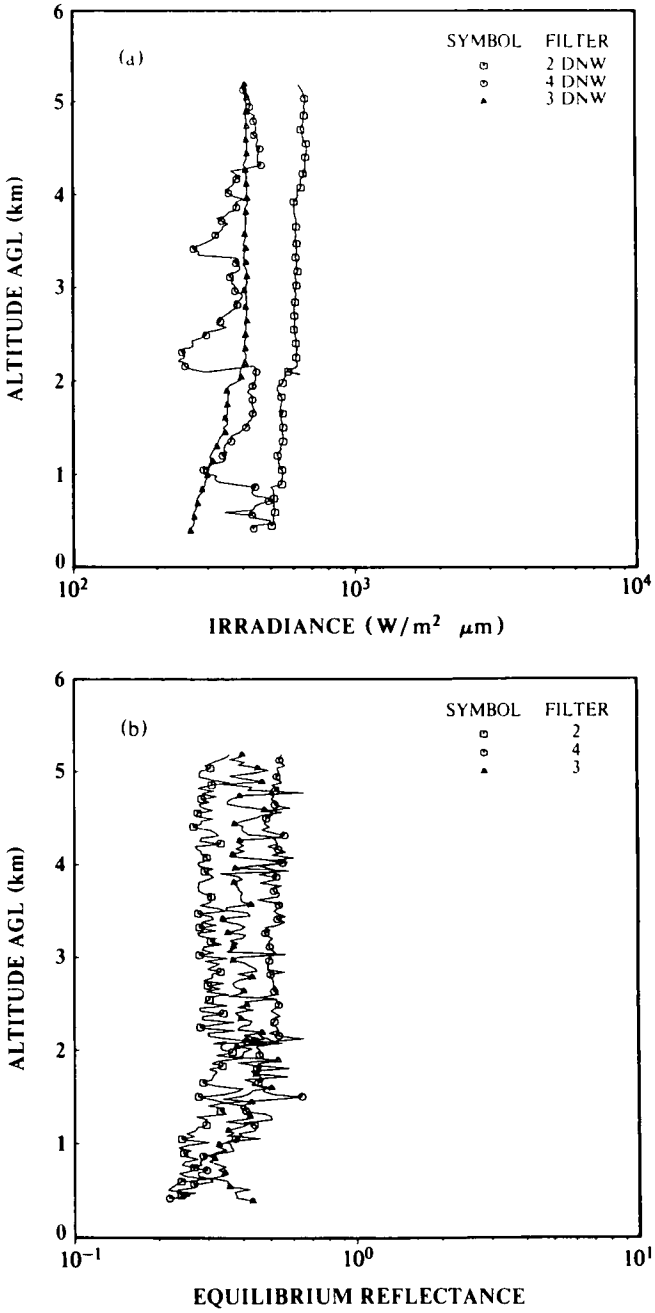

Fig. 3-19. Measured irradiance and computed equilibrium reflectance as a function of altitude for flight C-401

The inherent background reflectance must be based upon the downwelling irradiance at the object altitude. However, if the equilibrium reflectance is reasonably constant with altitude, it may be determined at any altitude in the path, including the observer altitude, as long as the equilibrium radiance and the irradiance from which it is determined, are at the same altitude and time. The effect of having the irradiance and the equilibrium radiance vary with altitude is factored out in the equilibrium reflectance and in the contrast ratio form of Eq. (3.53).

The ratio of the equilibrium reflectance divided by the background reflectance should not be used as a constant. Both the equilibrium reflectance and the background reflectance vary with path of sight but independently.

The background reflectance and the albedo are not usually equivalent. An object is generally not viewed against the average reflectance of the general terrain (albedo). The albedo not the background reflectance affects the equilibrium radiance as long as the background immediately surrounding the object against which the object is seen is small in size relative to the general terrain.

Equation (3.53) is the sky-ground ratio form of the contrast transmittance equation. It is perhaps the simplest form in which the contrast transmittance equation can be expressed and as such should be very useful for modelling and predictive purposes.

Summary

The equilibrium radiance model atmosphere for the visible spectrum has been expanded to include some aspects of the cloudy case thereby extending its usefulness.

Data indicate that equilibrium radiance for a given path of sight does not change with altitude up to altitudes of 6 kilometers for some partly cloudy days (60 percent of the cases for one field trip).

When equilibrium radiance is constant for a path of sight, path radiance can be computed from equilibrium radiance and the radiance transmittance of the path. Also,

the sky-ground radiance ratio form of the contrast transmittance equation may be used for many cloud-free paths of sight.

A general expression for equilibrium radiance has been derived that is appropriate for some partly cloudy cases as well as clear skies.

The equation of transfer was put into reflectance form and integrated. Thus the sky-ground ratio reflectance form of the contrast transmittance equation is derived. Data for the troposphere for the cloud-free path of sight support the derivation for a wide variety of real atmospheric conditions (80 percent of the cases during one field trip).

In order for equilibrium radiance to be constant for a path of sight, all path segments must be cloud-free and the entire path must be either sun unobscured or sun obscured. In order for equilibrium reflectance to be constant for a path of sight, all path segments must be cloud free but the path may be partially sunlit and partially shadowed from the sun. Thus the assumption of equilibrium reflectance constancy is much less restrictive and more generally useful than the assumption of equilibrium radiance constancy.

4. SUMMARY & RECOMMENDATIONS

This Final Report under contract F19628-78-C-0200 has addressed both the analysis of airborne and surface data collected in conjunction with the NATO Program OPAQUE, and the application of these analyses to the development of modelling concepts appropriate for the study and exploitation of the linking inter-relationships between the optical and meteorological states of the atmosphere. The Optical Data Analysis effort, task two under this two part research contract, has concentrated on the development of operationally useful modelling concepts related to the visible portions of the spectrum, and the analysis of the relationships existing at the surface between visible and infrared extinctions as a function of local relative humidity.

As recommended in Johnson *et al.* (1979), the data analysis portions of this contract task have used selected sub-sets of both the OPAQUE surface and profile data bases as starting points in the development of modelling concepts.

The airborne data base, containing primarily profile measurements of atmospheric volume scattering coefficients as illustrated in Johnson and Gordon (1980), and Johnson (1981b), and measurements of sky and terrain radiance distributions as illustrated in Johnson and Hering (1981b) has been only partially exploited in its potential. These data which describe the optical state of the atmosphere under a broad variety of meteorological circumstances have already provided the basis for the development of both the analytic Gordon models described in the preceding section, and the fast, operationally oriented Hering model summarized in Section 2 of this report, and described fully in Hering (1981a). It is recommended that further selective analysis of these airborne data be directed specifically to those sub-sets which describe the more turbid atmospheric conditions typified by cloudy, overcast days with incipient rain or drizzle episodes that are so far missing in most of the cases studied to date.

The OPAQUE surface data base, containing concurrent measurements of ground level extinction coefficients in both the visible and infrared regions of the spectrum, in conjunction with their concommitent meteorological and aerosol size distribution data, has also only partially been addressed. The recommendations contained in Johnson *et al.* (1979) for selective analysis of this extensive data set with particular attention to visible infrared relationships has resulted in the detailed evaluation and discussion contained in Shields (1981), portions of which also are summarized in Section 2. Comparison of these data with existing model predictions, primarily LOWTRAN 5, Kneizys *et al.* (1980) illustrated reasonable model performances on the average, but as one might suspect, substantial shortcomings in the prediction of the high frequency variations in extinction which occur under the more turbid conditions encountered during mist or fog episodes. Since it is during these turbid episodes when the visible-infrared relationships become erratic, that ones ability to reliably model the episode fails, it is important that additional work be done in this more difficult regime. As discussed in Shields (1981), it is understanding the conditions driving the time variances occurring during mist-fog episodes that may enable a more reliable modelling of these situations. It is recommended, therefore, that additional analysis of the OPAQUE surface data be directed toward those intervals identified as the "high bin" in Shields (1981) with particular attention to those data whose sample intervals were shorter than the hourly sample rate included in the standard data format described in Fenn (1978).

As discussed in most of the preceding reports associated with this research effort, the driving force behind the data analysis has been and continues to be the need for model development which will increase one's operational forecasting capability. That this modeling goal is being achieved as a result of these studies is illustrated by the discussion in Section 3 of the Gordon model and its extension to cloudy day conditions, and the development of the highly efficient Hering model described in Hering (1981ab). These model formats relate directly to one's ability to predict visible spectrum atmospheric optical properties from a variety of surface optical and/or meteorological measurements, observations or predictions. The extension of both of these modelling approaches into the arena of more turbid, non-uniform, and non-conservative atmospheres is underway and can be profitably accelerated. As our understanding of the inter-relationships between the direct and diffuse components of the atmospheres conservative and non-conservative flux fields is expanded through the exercise of these models, and as this understanding is impacted by additional studies of the visible infrared relationships as introduced in Shields (1981), then closing the modelling loop as first suggested in Fig.

1-3 becomes clearly a realizable goal. The link between the visible and infrared extinctions during turbid meteorological conditions is the one most in need of establishment. There is reason to believe, as established by an analysis of the directional scattering of atmospheric aerosols, mist and fogs, that this link might most readily be established by combining studies of the type illustrated by Shields (1981) with measurements of narrow angle forward scattering. The recommendation for further model development therefore is to continue the expansion of the existing model formats, both Gordon and Hering, to include the influences of the turbid atmosphere, and to accelerate the development of new model relationships defining the short term variances in visual and infrared extinctions, with the ultimate goal of combining these new and expanded model formats into the operational forecasting tool so urgently required.

5. ACKNOWLEDGEMENTS

This final report has been prepared for the Air Force Geophysics Laboratory under Contract No. F19628-78-C-0200. The authors wish to thank the members of the Visibility Laboratory technical staff for their assistance in preparing these data, and the members of the Atmospheric Optics Branch of the Air Force Geophysics Laboratory for their technical support and council.

We particularly thank Mr. Nils R. Persson, Jr., our senior computer specialist, Ms. Alicia G. Hill and Mr. John C. Brown, our specialists in computer assisted document preparation, for many diligent hours devoted to generating this final copy.

Two preceding reports, authored by Ms. Janet E. Shields and Mr. Wayne S. Hering, represent major contributions to the research reviewed in this Final Report. The authors are pleased to acknowledge these excellent technical contributions by their esteemed colleagues.

6. REFERENCES

Barteneva, O.D., "Scattering Functions of Light in the Atmospheric Boundary Layer", Bull. Acad. Sci. U.S.S.R., Geophysics Series, 1237-1244 (1960).

Blackwell, H.R., "Contrast Thresholds of the Human Eye", J. Opt. Soc. Am. **36**, 624-643 (1946).

Boileau, A.R., and J.I. Gordon, "Atmospheric Properties and Reflectances of Objects and Backgrounds for a Low Sun", Appl. Opt. **5**, 803-813 (1966).

Brown, D.R.E., *Natural Illumination Charts,* Report 374-1, Project Ns-714-100, Dept. of the Navy, Bureau of Ships, Washington, D.C. (1952).

Chandrasekhar, S., *Radiative Transfer,* (Dover Pub. Inc., New York, 1960).

Collins, D.G., and M.B. Wells, *Monte Carlo Codes for the Study of Light Transport in the Atmosphere,* Vols. I and II, (Radiation Research Association Inc., Fort Worth, Texas 1965).

Coulson, K.L., J.V.Dave, and Z. Sekara, *Tables Related to Radiation Emerging from a Planetary Atmosphere with Rayleigh Scattering,* (University of California Press, 1960).

Duff, E.A., "Atmospheric Contrast Transmission Application to the Visual Detection and Electro-Optical Lock-on Problem", Master of Science Thesis, School of Engineering Air University, USAF, Wright-Patterson AFB, Ohio (1972).

Duntley, S.Q., *Visibility Studies and Some Applications in the Field of Camouflage,* Summary Tech. Rept. Div. 16, NDRC, Vol. 2, NTIS No. AD 321 102, (Columbia Univ. Press, New York, 1946).

Duntley, S.Q., "Reduction of Contrast by the Atmosphere", J. Opt. Soc. Am. **38**, 179-191 (1948).

Duntley, S.Q., A.R. Boileau, and R.W. Preisendorfer, "Image Transmission by the Troposphere I", J. Opt. Soc. Am. **47**, 499-506 (1957).

Duntley, S.Q., R.W. Austin, J.L. Harris, and J.H. Taylor, "Experiments on Visual Acuity and the Visibility Markings on the Ground in Long Duration Earth-Orbital Space Flight", University of California, San Diego, Scripps Institution of Oceanography, Visibility Laboratory, SIO Ref. 68-6, also published as NASA-CR-1134, NASA, Washington, D.C. (1968).

Duntley, S.Q., R.W. Johnson, and J.I. Gordon, "Airborne and Ground-Based Measurements of Optical Atmospheric Properties in Central New Mexico", University of California, San Diego, Scripps Institution of Oceanography, Visibility Laboratory, SIO Ref. 72-71, AFCRL-72-0461, NTIS No. AD 751 936 (1972a).

Duntley, S.Q., R.W. Johnson, and J.I. Gordon, "Airborne Measurements of Optical Atmospheric Properties, Summary and Review", University of California, San Diego, Scripps Institution of Oceanography, Visibility Laboratory, SIO Ref. 72-82, AFCRL-72-0593, NTIS No. AD 754 898 (1972b).

Duntley, S.Q., R.W. Johnson, and J.I. Gordon, "Airborne Measurements of Optical Atmospheric Properties in Southern Illinois", University of California, San Diego, Scripps Institution of Oceanography, Visibility Laboratory, SIO Ref. 73-24, AFCRL-TR-73-0422, NTIS No. AD 774 597 (1973).

Duntley, S.Q., R.W. Johnson and J.I. Gordon, "Airborne Measurements of Optical Atmospheric Properties, Summary and Review II", University of California, San Diego, Scripps Institution of Oceanography, Visibility Laboratory, SIO Ref. 75-26, AFCRL-TR-75-0457, NTIS No. ADA 022 675 (1975).

Duntley, S.Q., R.W. Johnson, J.I. Gordon, "Airborne Measurements of Atmospheric Volume Scattering Coefficients in Northern Europe, Fall 1976", University of California, San Diego, Scripps Institution of Oceanography, Visibility Laboratory, SIO Ref. 78-3, AFGL-TR-77-0239, NTIS No. ADA 057 144 (1978a).

Duntley, S.Q., R.W. Johnson, J.I. Gordon, "Airborne Measurements of Optical Atmospheric Properties, Summary and Review III", University of California, San Diego, Scripps Institution of Oceanography, Visibility Laboratory, SIO Ref. 79-5, AFGL-TR-78-0286, NTIS No. ADA 073 121 (1978b).

Fenn, R.W., "OPAQUE, A Measurement Program on Optical Atmospheric Quantities in Europe, Vol. I, The NATO OPAQUE Program", Special Reports No. 211, AFGL-TR-78-0011 (1978).

Fenn, R.W., T.S. Cress, D. DeHart, R. Dirkman, J.D. Essex, K. Lichterberg, V.A. Marcello, J.E. Powers, E.P. Shettle, H. Soron, J. Sullivan, F.P. Suprin, R.B. Toolin, V.D. Turner, and F.E. Volz, "OPAQUE, A Measurement Program on Optical Atmospheric Quantities in Europe, Vol. II, The US/German OPAQUE Station near Meppen, Federal Republic of Germany", Special Reports No. 222, AFGL-TR-79-0068 (1979).

Fitch, B.W., and T.S. Cress, "Analysis of Aerosol Size Distributions Measured in the Lower Troposphere over Great Britain and Europe", in press, also as Sec. 3 of AFGL-TR-82-0049, "A Review of Measured Atmospheric Optical Properties and their Contemporary Aerosol Size Distributions" (1981).

Gordon, J.I., "Visibility III. Optical Properties of Objects and Backgrounds", Appl. Opt. **3**, 356-562 (1964).

Gordon, J.I., "Model for a Clear Atmosphere", J. Opt. Soc. Am. **59**, 14-18 (1969).

Gordon, J.I., J.L. Harris, and S.Q. Duntley, "Measuring Earth-to-Space Contrast Transmittance from Ground Stations", Appl. Opt. **12**, 1317-1324 (1973).

Gordon, J.I., "Daytime Visibility, A Conceptual Review", University of California, San Diego, Scripps Institution of Oceanography, Visibility Laboratory, SIO Ref. 80-1, AFGL-TR-79-0257 (1979).

Hering, W.S., "An Operational Technique for Estimating Visible Spectrum Contrast Transmittance", University of California, San Diego, Scripps Institution of Oceanography, Visibility Laboratory, SIO Ref. 82-1, AFGL-TR-81-0198 (1981a).

Hering, W.S., "Assessment of Operational Techniques for Estimating Visible Spectrum Contrast Transmittance", *SPIE Proceedings on Atmospheric Effects on System Performance,* Vol. 205, pp. 119-125 (1981b).

Hüschke, R.E., "Atmospheric Visual and Infrared Transmission Deduced from Surface Weather Observations: Weather and Warplanes VI", Report R-2016-PR, RAND, Santa Monica (1976).

Inn, E.C.Y., and Y. Tanaka, "Ozone Absorption", J. Opt. Soc. Am. **43**, 872 (1953).

Jennings, S.G., R.G. Pinnick, and H.J. Auverman, "Effects of Particulate Complex Refractive Index and Particle Size Distribution Variations on Atmospheric Extinction and Absorption for Visible through Middle IR Wavelengths", Appl. Opt. **17**, No. 24, 3922-3929 (1978).

Johnson, F.R., "The Solar Constant", J. Meteorol. **11**, 431-439 (1954).

Johnson, R.W., W.S. Hering, J.I. Gordon, B.W. Fitch, and J.S. Shields, "Preliminary Analysis & Modelling Based Upon Project OPAQUE Profile and Surface Data", University of California, San Diego, Scripps Institution of Oceanography, Visibility Laboratory, SIO Ref. 80-5, AFGL-TR-79-0285 (1979).

Johnson, R.W., and J.I. Gordon, "Airborne Measurements of Atmospheric Volume Scattering Coefficients in Northern Europe, Summer 1978", University of California, San Diego, Scripps Institution of Oceanography, Visibility Laboratory, SIO Ref. 80-20, AFGL-TR-80-0207, NTIS No. ADA 097 134 (1980).

Johnson, R.W. and W.S. Hering, "Measurements of Optical Atmospheric Quantities in Europe and Their Application to Modelling Visible Spectrum Contrast Transmittance", *Agard Proceedings on Special Topics in Optical Propagation,* AGARD-CP-300, pp. 14-1 to 14-12 (1981a).

Johnson, R.W., and W.S. Hering, "An Analysis of Natural Variations in Measured European Sky and Terrain Radiances", University of California, San Diego, Scripps Institution of Oceanography, Visibility Laboratory, SIO Ref. 82-6, AFGL-TR-81-0317 (1981b).

Johnson, R.W., "Spring and Fall Measurements of European Very Low Altitude Volume Scattering Coefficients", University of California, San Diego, Scripps Institution of Oceanography, Visibility Laboratory, SIO Ref. 81-33, AFGL-TR-81-0237, NTIS No. ADA 108 879 (1981a).

Johnson, R.W., "Daytime Visibility and Nephelometer Measurements Related to its Determination", Atmospheric Environment, **15**, 10/11, 1835 (1981b).

Johnson, R.W., "Airborne Measurements of European Sky and Terrain Radiances", University of California, San Diego, Scripps Institution of Oceanography, Visibility Laboratory, SIO Ref. 82-2, AFGL-TR-81-0275 (1981c).

Johnson, R.W. and B.W. Fitch, "A Review of Measured Atmospheric Optical Properties and Their Contemporary Aerosol Size Distributions", University of California, San Diego, Scripps Institution of Oceanography, Visibility Laboratory, SIO Ref. 82-22, AFGL-TR-82-0049 (1981).

Kneizys, F.X., E.P. Shettle, W.O. Gallery, J.H. Cherwynd, Jr., L.W. Abreu, J.E.A. Selby, R.W. Fenn and R.A. McClatchey, "Atmospheric Transmittance/Radiance Computer Code LOWTRAN5", AFGL-TR-80-0067 (1980).

Kushpil' V.I., and L.F. Petrova, "Determination of the Atmospheric Transmission from Sky Brightness Distribution", Opt. Tech. **38**, No. 4, 191-193 (1971).

Lumb, F.E., "The Influence of Cloud on Hourly Amounts of Total Solar Radiation at the Sea Surface", Quarterly Journal of the Royal Meteorological Society, **90**, 43-56 (1964).

McIntosh, D.H., *Meteorological Glossary* (Meteorological Office, Her Majesty's Stationary Office, London, 1963).

Middleton, W.E.K., *Vision Through the Atmosphere,* (University of Toronto Press, 1952), p. 72 and 127.

Nilsson, B., "Meteorological Influence on Aerosol Extinction in the 0.2-4.0μm Wavelength Range", Appl. Opt. **18**, No. 20, 3457-3473 (1979).

Penndorf, R., "Tables of the Refractive Index for Standard Air and the Rayleigh Scattering Coefficient for the Spectral Region Between 0.2 and 20.0 and Their Application to Atmosphere Optics", J.. Opt. Soc. Am. **47**, 176 (1957).

Pinnick, R.G., S.G. Jennings, P. Chýlek, and H.J. Auverman, "Verification of a Linear Relation Between IR Extinction, Absorption and Liquid Water Content of Fogs", Amer. Meteorological Soc., **36**, 1577-1586 (1979).

Proulx, G.J., *Standard Dictionary of Meteorological Sciences,* Scientific and Technical Division, Department of the Secretary of State, Ottawa, Canada, (McGill-Queen's University Press 1971).

Pyaskovskaya-Fesenkova, E.V., "Determining the Transmission Coefficient and Degree of Optical Stability of the Earth's Atmosphere", in *Atmospheric Optics,* Nikolai B. Divari, Ed., translated by S.B. Dresner, Consultants Bureau, (Plenum Publishing Corp., New York, 1979), p. 151.

Shettle, E. P., and R.W. Fenn, "Models for the Aerosols of the Lower Atmosphere and the Effects of Humidity Variations on their Optical Properties", AFGL-TR-79-0214, Air Force Geophysics Laboratory, Hanscom AFB, Massachusetts (1979).

Shields, J.S., "An Analysis of Infrared Visible Atmospheric Extinction Coefficient Measurements in Europe", University of California, San Diego, Scripps Institution of Oceanography, Visibility Laboratory, SIO Ref. 82-4, AFGL-TR-81-0251 (1981).

Taylor, J.H., "The Use of Visual Performance Data in Visibility Prediction", Appl. Opt. **3**, 562-569 (1964).

Tousey, R., and E.O. Hulburt, "Brightness and Polarization of the Daylight Sky at Various Altitudes Above Sea Level", J. Opt. Soc. Am. **37**, 78 (1947).

U.S. Standard Atmosphere, Superintendent of Documents, U.S. Government Printing Office, Washington, D.C. 20402 (1976).

Vigroux, E., "Etude Experimentale de L'Absorption de l'Ozone", Ann. de Phys. (Paris) (12) **8**, 742 (1953).

Whitby, K. T., "The Physical Characteristics of Sulfur Aerosols", Atmos. Env., **12**, 135-159 (1978).

World Meteorological Organization, "Guide to Meteorological Instrument and Observing Practices", Fourth Ed., Secretariat of the World Meteorological Organization, Geneva, Switzerland WMO-No. 8, TP. 3 (1971).

Yue, G.K., and A. Deepak, "Modeling of Growth, Evaporation and Sedimentation Effects of Transmission of Visible and IR Laser Beams in Artificial Fogs", Appl. Opt. **19**, No. 22, 3767-3929 (1980).

APPENDIX A

VISIBILITY LABORATORY CONTRACTS AND RELATED PUBLICATIONS

Previous Related Contracts:
F19628-73-C-0013, F19628-76-C-0004

PUBLICATIONS:

Duntley, S.Q., R.W. Johnson, J.I. Gordon, and A. R. Boileau, "Airborne Measurements of Optical Atmospheric Properties at Night", University of California, San Diego, Scripps Institution of Oceanography, Visibility Laboratory, SIO Ref. 70-7, AFCRL-70-0137, NTIS No. AD 870 734 (1970).

Duntley, S.Q., R.W. Johnson, and J.I. Gordon, "Airborne Measurements of Optical Atmospheric Properties in Southern Germany", University of California, San Diego, Scripps Institution of Oceanography, Visibility Laboratory, SIO Ref. 72-64, AFCRL-72-0255, NTIS No. AD 747 490 (1972a).

Duntley, S.Q., R.W. Johnson, and J.I. Gordon, "Airborne and Ground-Based Measurements of Optical Atmospheric Properties in Central New Mexico", University of California, San Diego, Scripps Institution of Oceanography, Visibility Laboratory, SIO Ref. 72-71, AFCRL-72-0461, NTIS No. AD 751 936 (1972b).

Duntley, S.Q., R.W. Johnson, and J.I. Gordon, "Airborne Measurements of Optical Atmospheric Properties, Summary and Review", University of California, San Diego, Scripps Institution of Oceanography, Visibility Laboratory, SIO Ref. 72-82, AFCRL-72-0593, NTIS No. AD 754 898 (1972c).

Duntley, S.Q., R.W. Johnson, and J.I. Gordon, "Airborne Measurements of Optical Atmospheric Properties in Southern Illinois", University of California, San Diego, Scripps Institution of Oceanography, Visibility Laboratory, SIO Ref. 73-24, AFCRL-TR-73-0422, NTIS No. AD 774 597 (1973).

Duntley, S.Q., R.W. Johnson, and J.I. Gordon, "Airborne and Ground-Based Measurements of Optical Atmospheric Properties in Southern Illinois", University of California, San Diego, Scripps Institution of Oceanography, Visibility Laboratory, SIO Ref. 74-25, AFCRL-TR-74-0298, NTIS No. ADA 013 164 (1974).

Duntley, S.Q., R.W. Johnson, and J.I. Gordon, "Airborne Measurements of Optical Atmospheric Properties in Western Washington", University of California, San Diego, Scripps Institution of Oceanography, Visibility Laboratory, SIO Ref. 75-24, AFCRL-TR-75-0414, NTIS No. ADA 026 036 (1975a).

Duntley, S.Q., R.W. Johnson, and J.I. Gordon, "Airborne Measurements of Optical Atmospheric Properties, Summary and Review II", University of California, San Diego, Scripps Institution of Oceanography, Visibility Laboratory, SIO Ref. 75-26, AFCRL-TR-75-0457, NTIS No. ADA 022 675 (1975b).

Duntley, S.Q., R.W. Johnson, and J.I. Gordon, "Airborne Measurements of Optical Atmospheric Properties in Northern Germany", University of California, San Diego, Scripps Institution of Oceanography, Visibility Laboratory, SIO Ref. 76-17, AFGL-TR-76-0188, NTIS No. ADA 035 571 (1976).

Duntley, S.Q., R.W. Johnson, and J.I. Gordon, "Airborne Measurements of Atmospheric Volume Scattering Coefficients in Northern Europe, Spring 1976", University of California, San Diego, Scripps Institution of Oceanography, Visibility Laboratory, SIO Ref. 77-8, AFGL-TR-77-0078, NTIS No. ADA 046 290 (1977).

Duntley, S.Q., R.W. Johnson, and J.I. Gordon, "Airborne Measurements of Atmospheric Volume Scattering Coefficients in Northern Europe, Fall 1976", University of California, San Diego, Scripps Institution of Oceanography, Visibility Laboratory, SIO Ref. 78-3, AFGL-TR-77-0239, NTIS No. ADA 057 144 (1978a).

Duntley, S.Q., R.W. Johnson, and J.I. Gordon, "Airborne Measurements of Atmospheric Volume Scattering Coefficients in Northern Europe, Summer 1977", University of California, San Diego, Scripps Institution of Oceanography, Visibility Laboratory, SIO Ref. 78-28, AFGL-TR-78-0168, NTIS No. ADA 068 611 (1978b).

Duntley, S.Q., R.W. Johnson, and J.I. Gordon, "Airborne Measurements of Optical Atmospheric Properties, Summary and Review III", University of California, San Diego, Scripps Institution of Oceanography, Visibility Laboratory, SIO Ref. 79-5, AFGL-TR-78-0286, NTIS No. ADA 073 121 (1978c).

Fitch, B.W. and T.S. Cress, "Measurements of Aerosol Size Distribution in the Lower Troposphere over Northern Europe", University of California, San Diego, Scripps Institution of Oceanography, Visibility Laboratory, SIO Ref. 81-18, AFGL-TR-80-0192, NTIS No. ADA 104 272 (1981). Also J.Appl.Met. **20**, No. 10, 1119-1128.

Gordon, J.I., "Model for a Clear Atmosphere", J. Opt. Soc. Am. **59**, 14-18 (1969).

Gordon, J.I., J. L. Harris, Sr., and S.Q. Duntley, "Measuring Earth-to-Space Contrast Transmittance from Ground Stations", Appl. Opt. **12**, 1317-1324 (1973).

Gordon, J.I., C. F. Edgerton, and S.Q. Duntley, "Signal-Light Nomogram", J. Opt. Soc. Am. **65**, 111-118 (1975).

Gordon, J.I., "Daytime Visibility, A Conceptual Review", University of California, San Diego, Scripps Institution of Oceanography, Visibility Laboratory, SIO Ref. 80-1, AFGL-TR-79-0257, NTIS No. ADA 085 451 (1979).

Hering, W. S., "An Operational Technique for Estimating Visible Spectrum Contrast Transmittance", University of California, San Diego, Scripps Institution of Oceanography, Visibility Laboratory, SIO Ref. 82-1, AFGL-TR-81-0198 (1981a).

Hering, W.S., "Assessment of Operational Techniques for Estimating Visible Spectrum Contrast Transmittance", *SPIE Proceedings on Atmospheric Effects on System Performance,* Vol. 205, pp. 119-125 (1981b).

Johnson, R.W., and J.I. Gordon, "Airborne Measurements of Atmospheric Volume Scattering Coefficients in Northern Europe, Winter 1978", University of California, San Diego, Scripps Institution of Oceanography, Visibility Laboratory, SIO Ref. 79-25, AFGL-TR-79-0159, NTIS No. ADA 082 044 (1979).

Johnson, R.W., W. S. Hering, J.I. Gordon, B. W. Fitch, and J.S. Shields, "Preliminary Analysis & Modelling Based Upon Project OPAQUE Profile and Surface Data", University of California, San Diego, Scripps Institution of Oceanography, Visibility Laboratory, SIO Ref. 80-5, AFGL-TR-79-0285, NTIS ADB 052 172L (1979).

Johnson, R.W., "Airborne Measurements of European Atmospheric Scattering Coefficients", *SPIE Proceedings on Atmospheric Effects on Radiative Transfer,* **195**, 31-38 (1979).

Johnson, R.W. and J.I. Gordon, "Airborne Measurements of Atmospheric Volume Scattering Coefficients in Northern Europe, Summer 1978", University of California, San Diego, Scripps Institution of Oceanography, Visibility Laboratory, SIO Ref. 80-20, AFGL-TR-80-0207, NTIS No. ADA 097 134 (1980).

Johnson, R.W. and W.S. Hering, "Measurements of Optical Atmospheric Quantities in Europe and Their Application to Modelling Visible Spectrum Contrast Transmittance", *AGARD Proceedings on Special Topics in Optical Propagation,* AGARD-CP-300, pp. 14-1 to 14-12 (1981a).

Johnson, R.W. and W. S. Hering, "An Analysis of Natural Variations in Measured European Sky and Terrain Radiances", University of California, San Diego, Scripps Institution of Oceanography, Visibility Laboratory, SIO Ref. 82-6, AFGL-TR-81-0317 (1981b).

Johnson, R.W., "Winter and Summer Measurements of European Very Low Altitude Volume Scattering Coefficients," University of California, San Diego, Scripps Institution of Oceanography, SIO Ref. 81-26, AFGL-TR-81-0154, NTIS No. ADA 106 363 (1981a).

Johnson, R.W., "Spring and Fall Measurements of European Very Low Altitude Volume Scattering Coefficients", University of California, San Diego, Scripps Institution of Oceanography, Visibility Laboratory, SIO Ref. 81-33, AFGL-TR-81-0237, NTIS No. ADA 108 879 (1981b).

Johnson, R.W., "Daytime Visibility and Nephelometer Measurements Related to its Determination", Atmospheric Environment, **15**, 10/11, 1835 (1981c).

Johnson, R.W., "Airborne Measurements of European Sky and Terrain Radiances", University of California, San Diego, Scripps Institution of Oceanography, Visibility Laboratory, SIO Ref. 82-2, AFGL-TR-81-0275 (1981d).

Johnson, R.W. and B.W. Fitch, "A Review of Measured Atmospheric Optical Properties and Their Contemporary Aerosol Size Distributions", University of California, San Diego, Scripps Institution of Oceanography, Visibility Laboratory, SIO Ref. 82-22, AFGL-TR-82-0049 (1981).

Shields, J.S., "An Analysis of Infrared and Visible Atmospheric Extinction Coefficient Measurements in Europe", University of California, San Diego, Scripps Institution of Oceanography, Visibility Laboratory, SIO Ref. 82-4, AFGL-TR-81-0251 (1981).

A Reprint from the

PROCEEDINGS

Of SPIE-The International Society for Optical Engineering

Volume 305

Atmospheric Effects on Electro-Optical, Infrared, and Millimeter Wave Systems Performance

August 27-28, 1981
San Diego, California

Assessment of operational techniques for estimating visible spectrum contrast transmittance

Wayne S. Hering
University of California, San Diego
Scripps Institution of Oceanography, Visibility Laboratory, La Jolla, California 92093

Assessment of operational techniques for estimating visible spectrum contrast transmittance

Wayne S. Hering
University of California, San Diego
Scripps Institution of Oceanography, Visibility Laboratory
La Jolla, California 92093

Abstract

Approximate solutions appropriate for real time calculations of directional path radiance and atmospheric contrast transmittance were developed and tested using an extensive data base gathered with a specially instrumented aircraft. The high-resolution, simultaneous optical and meteorological measurements were made in a broad range of environmental conditions and diverse geographical areas in the United States and western Europe. Modelling techniques based upon these data yield computationally fast and consistent results of reasonable accuracy. The effects of the natural variations in environmental physical parameters upon the calculations of spectral contrast transmittance are examined through systematic application of the modelling techniques. Comparative analyses are made of the changes in the visible spectrum contrast transmittance associated with typical changes in some of the relevant parameters such as the depth and density of the low-level haze layer, aerosol absorption, surface spectral reflectance, solar zenith angle and viewing path.

Introduction

The degredation of visible image contrast along a viewing path of increasing length is governed by (1) the attenuation of the inherent background and object radiances by air molecule and aerosol particle scattering and absorption, and (2) the generation of path radiance by molecular and aerosol scattering of ambient light into the path of sight. Direct measurements of radiance and aerosol concentration profiles for selected path segments cannot be made simply and inexpensively. Thus, operational estimates of contrast transmittance must be derived from model calculations that are based upon estimated variables, including the distribution of aerosol particles and their directional scattering and absorption properties. In this paper, we present the results of a systematic series of calculations designed to help identify the relative effects of the changes or uncertainties in relevant physical parameters upon the contrast transmittance of hazy, cloud free paths of sight.

Model for the calculation of contrast transmittance

The equation for apparent spectral radiance of the background b at altitude z and range r in the direction defined by zenith angle θ and azimuth angle ϕ is[1]:

$$ {}_bL_r(z,\theta,\phi) = T_r(z,\theta)\ {}_bL_o(z_t,\theta,\phi) + L_r^*(z,\theta,\phi) \tag{1} $$

where ${}_bL_o$ is the inherent background radiance at target altitude z_t, T_r is path transmittance, and L_r^* is the spectral path radiance generated by the scattering of light reaching the path from all directions.

The spectral contrast transmittance is given[1] directly by the product of ratio of the inherent and apparent (${}_bL_r$) background radiances and the path transmittance as follows,

$$ C_r(z,\theta,\phi)/C_o(z_t,\theta,\phi) = T_r(z,\theta)\,{}_bL_o(z_t,\theta,\phi)/{}_bL_r(z,\theta,\phi) \tag{2} $$

where $C_r = ({}_tL_r - {}_bL_r)/{}_bL_r$ is the apparent target contrast at path length r and $C_o(z_t,\theta,\phi) = ({}_tL_o - {}_bL_o)/{}_bL_o$ is the inherent target contrast at altitude z_t.

A computationally fast technique for the calculation of atmospheric path radiance and contrast transmittance was developed[2,3] through analysis of an extensive series of optical/meteorological measurements gathered by the Visibility Laboratory with an instrumented aircraft deployed in the United States and Europe. Model input parameters are the number of atmospheric layers, the average optical scattering ratio and single scattering albedo for each layer, solar zenith angle, representative wavelength, extra-terrestrial solar irradiance and surface reflectance. The computer code calculates the path radiance and contrast transmittance for any selected slant path.

Modelling approximations include the representation of the vertical profile of total volume scattering coefficient, $s(z,\lambda)$ by the profile of optical scattering ratio, $Q(z,\lambda) = s(z,\lambda)/s_R(z,\lambda)$ where s_R is the Rayleigh scattering coefficient, thus normalizing with respect to wavelength and pressure altitude. Under conditions of complete mixing within a given atmospheric layer, $Q(z,\lambda)$ would be constant in the layer. The aircraft measurements reveal large variability in $Q(z)$ depending upon the aerosol particle source strength and the nature of the convective and turbulent mixing processes. The model computer code will accept specification of as many layers as warranted by available observations. However, a prominent feature of most aircraft measured profiles[4] in the daytime, following the dispersion of surface ground based temperature inversions, is the strong tendency for good mixing with constant $Q(z)$ in the primary haze layer and again in the overlying troposphere. So that a simple 2-layer troposphere model assuming a constant $Q(z)$ in each layer provides a good first approximation of the scattering ratio profile on a majority of sunny days over inland areas.

Another special element of the model calculations involves the specification of the single scattering phase function for each layer To the extent that the detailed information about the phase function is known for a given layer, it can be incorporated directly into the model determinations But in the absence of such detailed information, an approximation for the phase function is used that was developed and tested using the experimental data base The phase functions are represented by two-term Henyey-Greenstein functions (see Kattawar[5], 1975), whose coefficients in turn are approximated by continuous functions[3] of the Mie scattering ratio, $Q(z)-1$, for each layer The functions are bounded by the theoretical Rayleigh phase function for a clear atmosphere and a phase function representative of clouds or fog for very large $Q(z)$

The series of airborne measurements served to validate individual model components as well as to test the overall model performance characteristics Shown for example in Fig 1 are profiles of total volume scattering coefficient measured near Meppen, Germany for three spectral bands 2 - a narrow band blue filter centered near 475 nm, 3 - a narrow band red filter centered near 660 nm, and 4 - a broad band photopic filter centered near 550 nm The relatively abrupt transition in scattering coefficient between the primary haze layer and the relatively clear air aloft that is evident in all 3 profiles is a typical feature of the daytime soundings measured over continental United States and Europe

Calculations of the sky and terrain radiance distributions based upon the measured scattering coefficient profile for this flight are shown in Figs 2 and 3 in comparison with the radiance distributions measured by the instrumented aircraft The agreement shown between calculated and observed radiance values is representative in general of model performance This midday flight was made under conditions of isolated patches of middle clouds and scattered thin cirrus Moderate haze extended to 1 3 km and the surface visibility was near 15 km The solar zenith angle averaged about 44 degrees The $\theta > 90°$ segments of the observed radiance distribution looking downward from an altitude of 200m, shown in Fig 2, reflect significant fluctuations that are caused by changes in the inherent reflectance of the underlying surface which varied from dark woods to open fields As shown in Fig 3, the influence of the surface reflectance variations on the radiance is greatly smoothed by the effects of the intervening atmosphere as measured from an altitude of 6 km by the scanning radiometer, which has a 5-degree field of view The measured directional radiance values at 6 km for viewing angles near the sun were subject to significant stray light error and are not shown in the comparison A prominent characteristic of the radiance distribution at 6 km is the bright horizon sky radiance which in this case had equivalent brightness in the upsun ($\phi = 0°$) and downsun ($\phi = 180°$) azimuth directions

Sensitivity of spectral contrast transmittance to selected changes in physical parameters

A systematic series of model calculations were made to illustrate the effects of typical variations in physical parameters upon the slant path transmittance and the corresponding range of object detection For this purpose, a two-layer atmosphere was assumed, consisting of a primary haze layer of varying optical depth and absorption, and an overlying upper troposphere-stratosphere layer of relatively clear air with a constant optical scattering ratio of 1 3 and a single scattering albedo of 0 97 The trial calculations were carried out for an assumed wavelength of 550 nm The responses in contrast transmittance to parameter changes would be similar for other visible wavelengths but would vary systematically for the same aerosol loading in the haze layer due primarily to the wavelength dependence of both the total optical depth and the single scattering phase function

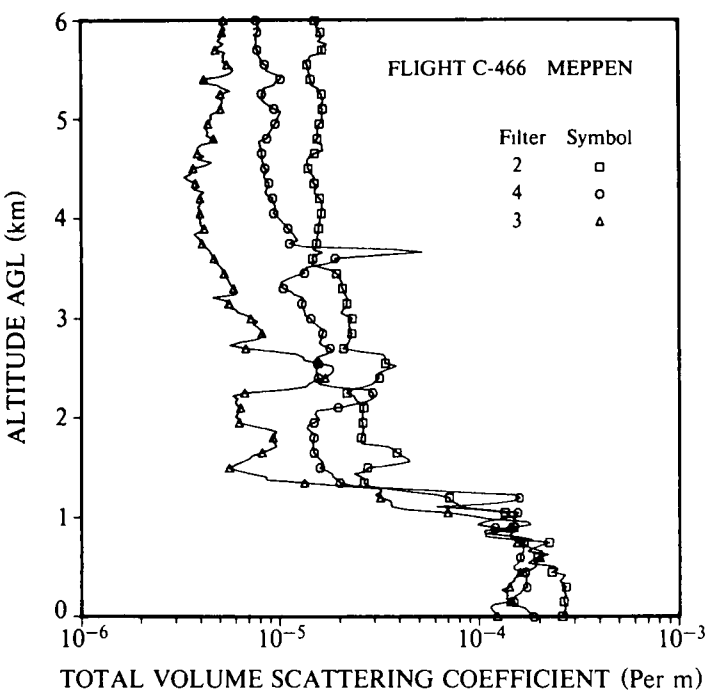

Figure 1 Measured profiles of total volume scattering coefficient, where 2 is the narrow band blue filter (475 nm), 3 is the narrow band red (660 nm), and 4 is the broad band photopic (550 nm) Aircraft measurements were made over Meppen, Germany, 15 August 1978

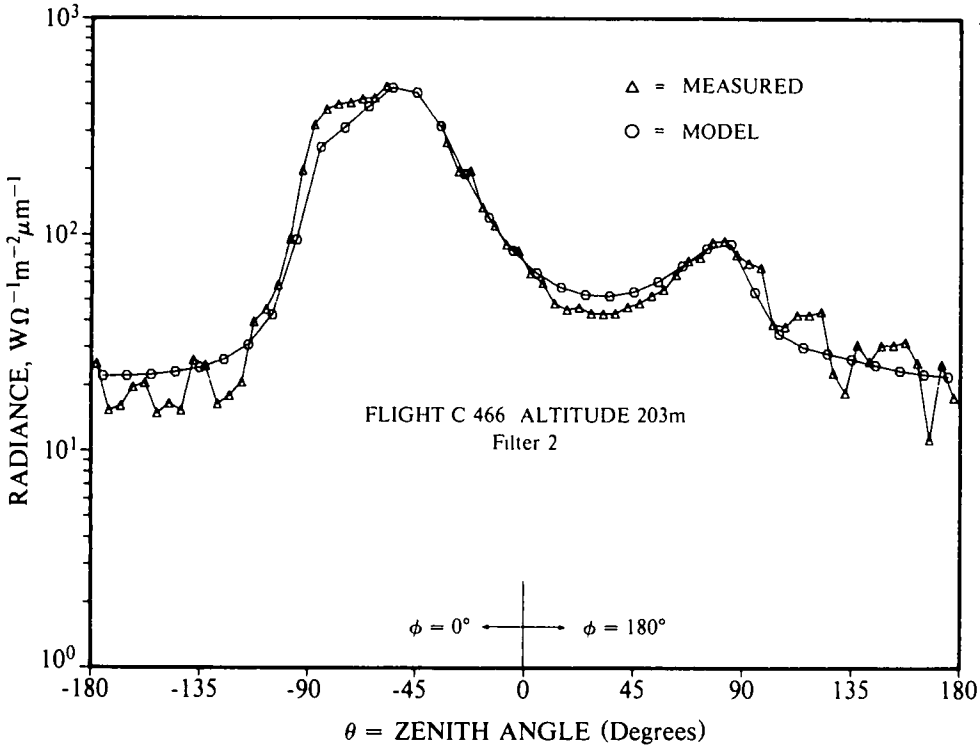

Figure 2 Comparison of measured and calculated sky and terrain radiance distributions at 200 m

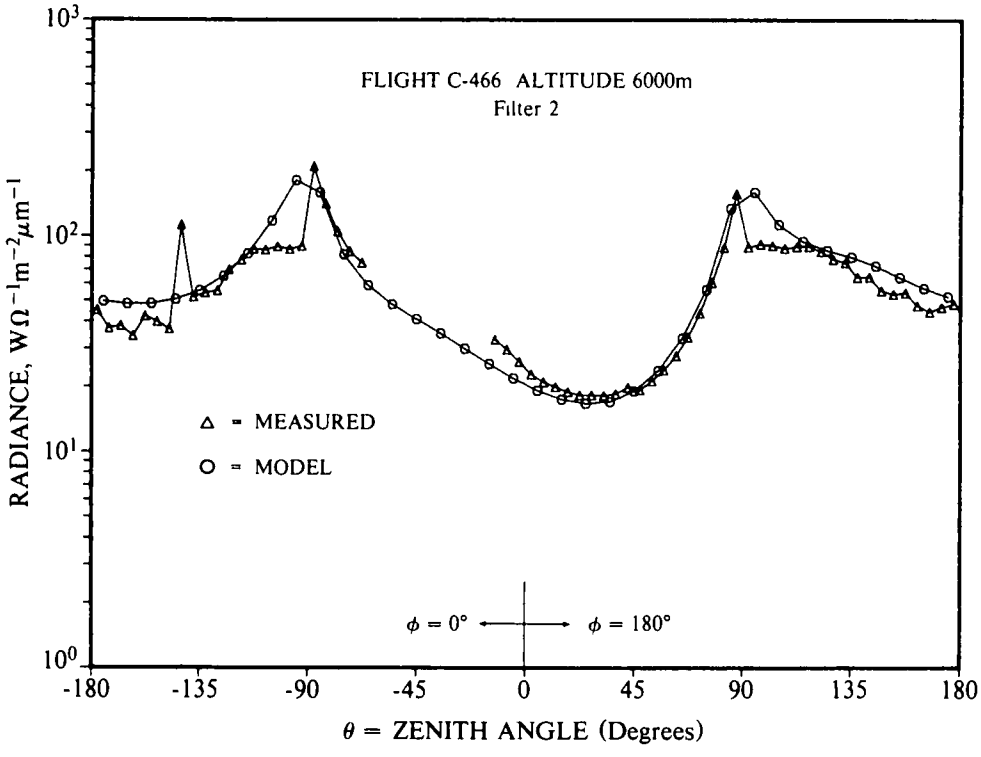

Figure 3 Comparison of measured and calculated sky and terrain radiance distributions at 6000 m

Results are shown for a range of haze layer depth, aerosol concentration and absorption, and for selected values of surface reflectance and solar zenith angle The parameters are varied individually while holding each of the other variables constant and equal to their values for an assumed reference atmosphere as follows, solar zenith angle = 60°, surface reflectance = 0 10, single scattering albedo = 0 97, and optical scattering ratio in the haze layer = 13 which corresponds to a horizontal surface equivalent visibility of about 20 km assuming a threshold contrast of 5 percent The vertical extent of the haze layer for the reference atmosphere was assumed to be 3 km except that a few comparative calculations were made also for an assumed haze layer top at 500m altitude while holding the overall optical thickness the same as for the 3 km case

Object at the earth's surface and the sensor at 6 km

From Eq (2), we observe that the contrast transmittance, $T_c = C_r/C_o$, of a viewing path extending downward from the sensor to an object at the earth's surface is given by the product of the path beam transmittance, T_r, and ratio of the inherent background radiance of the surrounding surface and the apparent background radiance as measured at the sensor, ${}_bL_o/{}_bL_r$ It follows that the contrast transmittance decreases with an increase in the extinction optical thickness of the viewing path in concert with both a decrease in $T_r(z,\theta)$ and an increase in the path radiance contribution, L_r^*, to ${}_bL_r$ (see Eq 1) The responses of T_c, for the case with the object at the surface and the sensor at 6 km, to changes in optical depth, τ, and to changes in the cosine of the zenith viewing angle are shown in Fig 4 Since we have assumed that the surface reflectance obeys Lambert's law, the asymmetry of T_c in the upsun and downsun viewing directions is small and is caused only by the directional changes in the direct solar backscattering component of the path radiance, L_r^* Except for viewing angles near the horizon, the calculated T_c from the surface to 6 km decreases more or less in direct proportion to the increase in slant path distance

For diagnostic purposes let us define a target acquisition range (TAR) where the contrast transmittance reduces to 10 percent Illustrated in Fig 5 are the calculated changes in TAR that correspond to selected changes in the physical variables Again we assume a target located at the earth's surface and a sensor altitude of 6 km The calculations were made for an azimuth viewing angle of 180° The calculated TAR for the reference atmosphere is 13 5 km Comparing responses of the TAR to the departures of the individual parameters from their values given by the reference atmosphere, we note that a 25 percent increase in TAR is associated with about a 25 percent decrease in the optical thickness of the haze layer On the other hand about a 50 percent increase in optical thickness is required for a 25 percent decrease in TAR The dotted line shown in Fig 5 for the relationship of TAR with optical thickness depicts the calculated TAR for an haze layer top at 0 5 km in lieu of the 3 km altitude assumed for the reference atmosphere Notice that the TAR differs only by approximately 15 percent for a haze layer with the greatly reduced vertical extent but with increased extinction so as to yield the same optical thickness

With regard to other parameters, the results show that changes in ln TAR are directly proportional to the changes in the cosine of the solar zenith angle For example, in rough measure the change in solar zenith angle during a one-hour period in the midmorning or afternoon in middle latitudes will result in about a 25 percent change in TAR for the reference atmosphere Notice also that a 25 percent decrease in TAR results from an increase in haze layer absorption from the small amount associated with clear remote atmospheres (single scattering albedo = 0 97) to the large amount corresponding to urban atmospheres (single scattering albedo = 0 63)

For objects viewed against a terrain background, the TAR has a significant direct dependence upon the surface reflectance For example, the calculated TAR decreases by 25 percent as the surface reflectance changes from the value associated with a brown field (0 10) to a value representative of a grass field (0 06)

Object at 6 km and the sensor at ground level

Diagnostic model calculations of T_c and TAR for an object at 6 km when viewed against a sky background from the earth's surface are shown in Fig 6 and 7 The reference atmosphere and selected changes to the reference atmosphere are the same as for the sensitivity analysis described in the preceding paragraphs In contrast with downward paths of sight, the calculated contrast transmittance of upward paths have large asymmetry in the upsun and downsun directions because of the enhanced path radiance generated by the increased scattering of sunlight at forward scattering angles As shown in Fig 6, the calculated T_c reduces to less than 10 percent for an azimuth viewing direction directly upsun when the total optical depth is 0 5 or larger In the downsun direction ($\phi = 180°$), T_c has only a modest variation with zenith viewing angle for angles less than about 70°

A strong dependence of target acquisition range in the downsun direction upon the optical thickness of the haze layer is evident in the results shown in Fig 7 A change in thickness of only 10 percent, holding other parameters of the reference atmosphere constant, results in about a 25 percent change in TAR A marked sensitivity of the TAR to changes in solar zenith angle is also found The observed decrease in TAR with an increase in solar altitude stems from the associated increase in the path radiance component of apparent background radiance In comparison with the results shown in Fig 5, the TAR for objects viewed against a sky background illustrated in Fig 7 show significantly less response to changes in the single scattering albedo of the haze layer and changes in surface reflectance

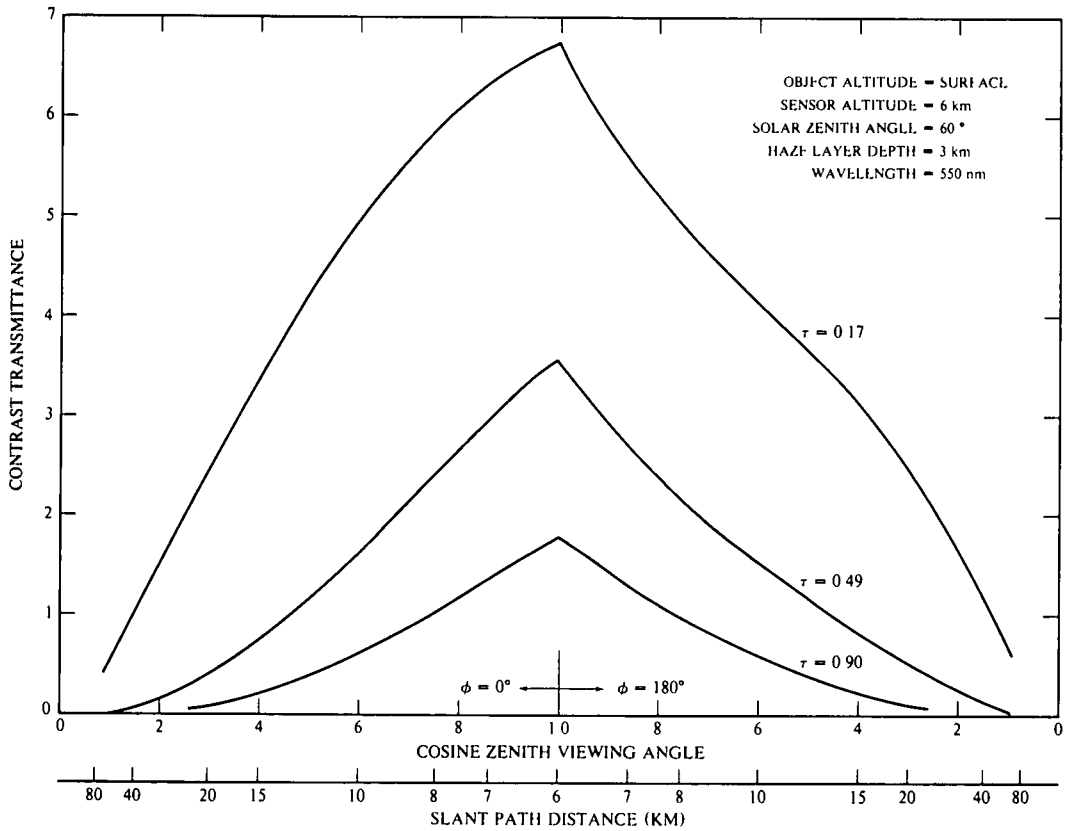

Figure 4. Diagnostic calculations of contrast transmittance as a function of zenith viewing angle for a target viewed against a terrain background. Values of τ refer to total atmosphere optical depth.

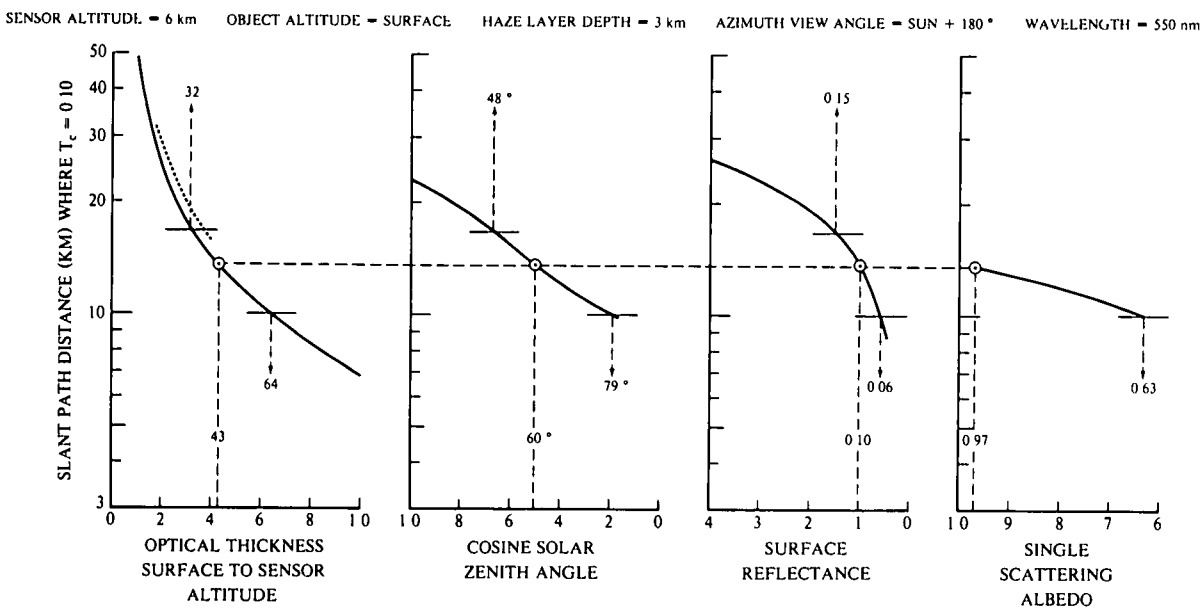

Figure 5. Variations in target acquisition range ($T_c = 0.10$) associated with departures of selected parameters from the assumed reference atmosphere values. The horizontal dashed line denotes parameter values for this reference atmosphere. The horizontal bars identify values of parameters corresponding to a change of ±25 percent from the slant path distance where $T_c = 0.10$ for the reference atmosphere, *i.e.* 13.5 ± 3.4 km.

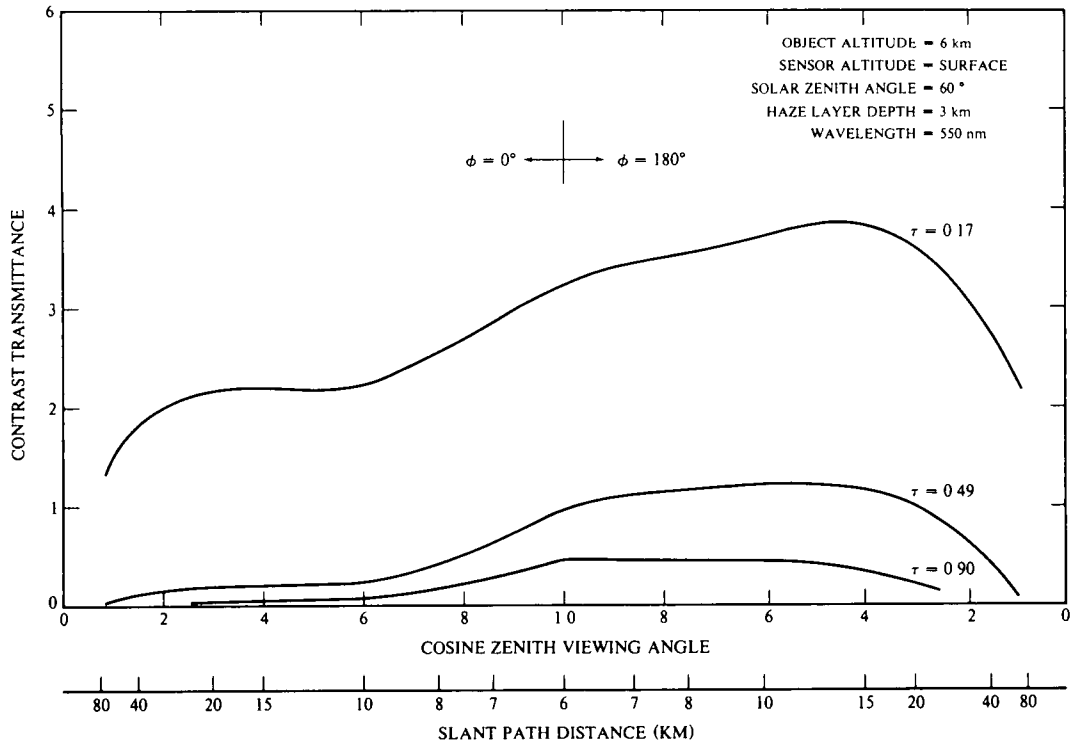

Figure 6. Same as figure 4 except for a target viewed against a sky background.

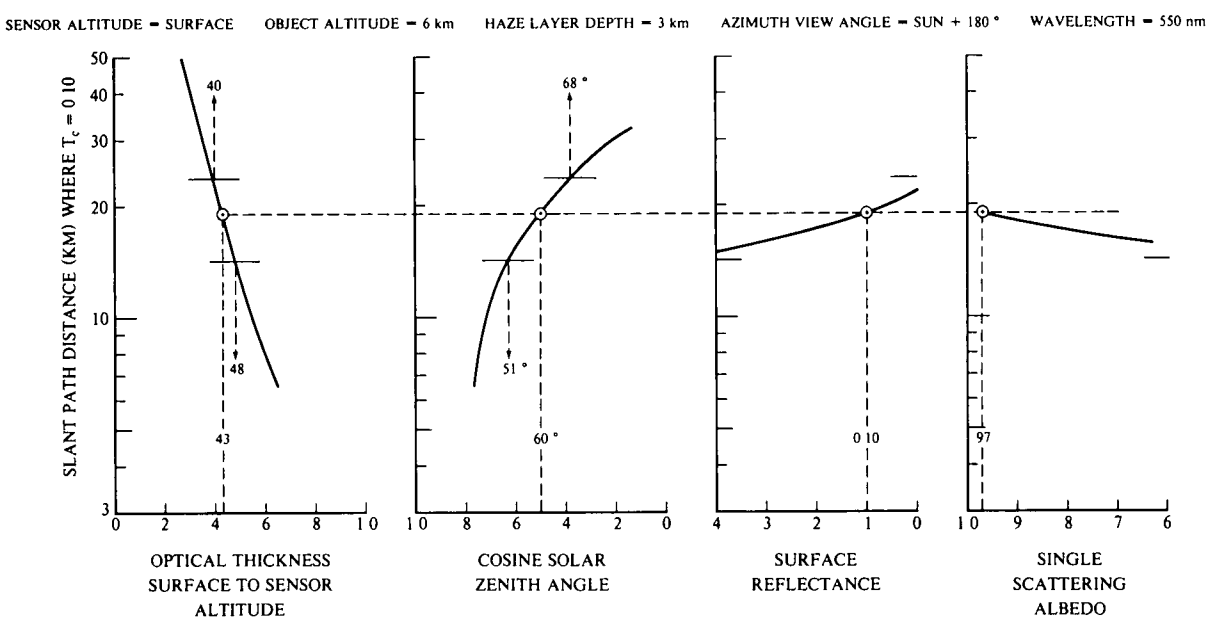

Figure 7. Same as figure 5 except for a target viewed against a sky background.

Acknowledgements

This work was supported by the Air Force Geophysics Laboratory under Contract F19628-78-C-0200 The author wishes to thank Richard W Johnson of the Visibility Laboratory for the encouragement and many helpful discussions on the diagnostic studies and Nils Persson of the Visibility Laboratory for his excellent assistance in performing the computer simulations

References

1 Duntley, S Q , A R Boileau, and R W Preisendorfer, "Image Transmission by the Troposphere I," J Opt Soc Amer , 47, 499-506 1957

2 Johnson, R W and W S Hering, "Measurements of Optical Atmospheric Quantities in Europe and their Application to Modelling Visible Spectrum Contrast Transmittance," Proceedings of 29th Symposium of the AGARD Electromagnetic Wave Propagation Panel, Monterey, CA, April 1981

3 Hering, W S , "An Operational Technique for Estimating Visible Spectrum Contrast Transmittance," to be published as Scripps Institution of Oceanography Scientific Report prepared for the Air Force Geophysics Laboratory 1981

4 Johnson, R W , W S Hering, J I Gordon, B W Fitch and J E Shields, "Preliminary Analysis and Modelling Based Upon Project OPAQUE Profile and Surface Data," University of California, San Diego, Scripps Institution of Oceanography; Visibility Laboratory, SIO Ref 80-5, AFGL-TR-79-0285 NTIS, ADB 052 172L 1979

5 Kattawar, G W , "A Three-Parameter Analytic Phase Function for Multiple Scattering Calculations," J Quant Spectrosc Radiant Transfer, 15, 839-849 1975

AGARD

ADVISORY GROUP FOR AEROSPACE RESEARCH & DEVELOPMENT

7 RUE ANCELLE 92200 NEUILLY SUR SEINE FRANCE

Paper Reprinted from
Conference Proceedings No. 300

SPECIAL TOPICS IN OPTICAL PROPAGATION

Papers and Discussions presented at the 28th Meeting of the Electromagnetic Wave Propagation Panel held in Monterey, California, USA, 6–10 April 1981.

NORTH ATLANTIC TREATY ORGANIZATION

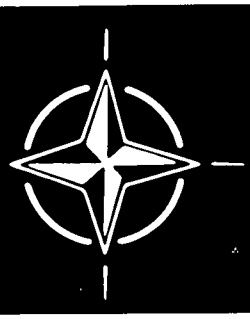

MEASUREMENTS OF OPTICAL ATMOSPHERIC QUANTITIES IN EUROPE AND THEIR APPLICATION TO MODELLING VISIBLE SPECTRUM CONTRAST TRANSMITTANCE

Richard W. Johnson and Wayne S. Hering
University of California, San Diego
Scripps Institution of Oceanography
Visibility Laboratory

ABSTRACT

An 80 flight series of simultaneous optical and meteorological measurements between ground level and an altitude of 6 km has been gathered by the Visibility Laboratory under the sponsorship of the Air Force Geophysics Laboratory. These flights were conducted as an independent but related adjunct to the NATO Program OPAQUE. Data flights were conducted over several European sites during each of five separate two month periods selected to be representative of each of the four temporal seasons.

Illustrative data representing altitude profiles of visible spectrum scattering characteristics are presented, as are the simultaneous measurements of ambient and dewpoint temperatures. In addition to these profile data, several contemporaneous sets of multi-spectral directional volume scattering function measurements at scattering angles of 30 and 150 degrees are presented. The use of these data as a basis for the development of a technique for estimating atmospheric path radiance and contrast transmittance is discussed.

A computer model for the estimation of these atmospheric properties that is relatively fast and easy to apply is described with examples of its performance. The model input parameters are wavelength, extra-terrestrial solar irradiance, solar zenith angle, the number of atmospheric layers selected and their altitude limits, the average optical scattering ratio and the single scattering albedo for each layer, and the terrain reflectance. Using a modelling approximation that relates the directional distribution of single scattering to the total volume extinction coefficient, and using the delta-Eddington method for calculating the diffuse radiative fluxes, the model predicts the directional path radiance and contrast transmittance of any slant atmospheric path as a function of wavelength.

1. INTRODUCTION

In the increasingly sophisticated world of electro-optical detection, search, and guidance, the requirement for establishing and predicting atmospheric influences on system performance continues to be a primary operational necessity. It is in this general context that the techniques discussed in this paper can most usefully be addressed. Thus, though the instrument development and data collection portions of this experimental program have been complete for some time, the analysis of the data is continuing, and the application of these analytic results is both timely and specifically germane to the problems of E/O performance within the lower troposphere.

The Visibility Laboratory has for a good number of years conducted an airborne measurement program in cooperation with, and under the sponsorship of the United States Air Force Geophysics Laboratory. For the past several years the program has been conducted as an independent but cooperative effort, Johnson, et al. (1979), in conjunction with the NATO program OPAQUE (Optical Atmospheric Quantities in Europe), Fenn (1978).

In the remainder of this note we will discuss briefly the measurement program, its resulting data base, and in more detail, the application of these data to the task of modelling tropospheric visible spectrum contrast transmittance.

2. AIRBORNE INSTRUMENTATION

The nephelometer system, designed and built at the Visibility Laboratory, Duntley, et al. (1977) provides measurements of both the total and directional volume scattering properties of its captured aerosol in four discrete spectral bands, as illustrated in Fig. 1. The measurements of total volume scattering coefficient are produced by optical integration over all scattering angles between 5° and 172° which are then corrected for potential truncation losses via the systems simultaneous directional scattering measurements. The measurements of directional volume scattering function are made at scattering angles of 30° (i.e. forward scatter) and 150° (i.e. backscatter). These narrow angle directional measurements provide the forward to backscattering ratios which are used to more thoroughly characterize the sample aerosol.

Upper and lower hemisphere scanning radiometers were designed for the measurement of sky and terrain radiance distributions. They operate in the same spectral bands as the nephelometer system, and provide 4π radiance maps processed to yield an average (5^{o} field of view) radiance value for each 6^{o} in azimuth and each 5^{o} in zenith angle. These automatic scanner systems were initially described in Duntley, et al. (1970) and since were equipped with remotely controlled neutral density filters to enhance their near sun measurement capabilities.

3. AIRBORNE MEASUREMENTS

Although there were nearly ninety data missions flown by the instrumented C-130 during the OPAQUE episode, as illustrated in Fig. 2 and Table 1, the general thrust of these data must be considered in the case study context rather than in the broader climatological context associated with the host nation's far more extensive set of surface measurements. Johnson, et al. (1979). Nonetheless, there are sufficient airborne measurements to clearly establish the essential aerosol scattering characteristics required for modelling those tropospheric optical properties most influencing slant path contrast transmittances. Selected samples of these data which have been used as validation data throughout the model development process are illustrated in Figs. 3 through 7 and discussed briefly in the following paragraphs.

3.1. Meteorological Properties

Measurements of atmospheric pressure, temperature and dewpoint temperature were made throughout each data mission in both the fixed altitude and ascent/descent flight modes. These data are illustrated in Figs. 3 and 4 which have been reproduced from Johnson and Gordon (1980). In each of these plots, the data represent four separate ascents or descents. Each profile is coded with a symbol that links it with its simultaneous optical data set. (see Fig. 1). There is good temporal stability within the temperature regime during the data interval as is indicated by the generally good reproducibility among the four separate profiles shown in Fig. 3. Additionally, and as will become apparent more importantly, one can see from the overlayed 1200z RAOB data that the vertical structure of the temperature profiles can be readily identified from either the fine structured aircraft data, or the more coarsely defined RAOB data.

In Fig. 4, relative humidity, as computed from the measured values of ambient and dewpoint temperature, has been plotted in the same format as used to display the temperature data. Whereas these derived values exhibit a significantly higher degree of temporal variability, the general reproduction of major structural characteristics, i.e. layers and trends, is maintained. It is immediately apparent however, from an examination of the RAOB data in Fig. 4, that major structural artifacts in derived properties can be missed if one uses measurements reported at inappropriate altitude increments. For example, note the strong moist layer in the Soesterberg data which is completely undetected in the RAOB profile. An immediate recommendation then for enhancing the utility of this type data for model development and/or tactical decision input would be to provide the basic RAOB data at standardized and relatively fine altitude increments similar to those inherent in aircraft soundings.

3.2. Optical Properties

The variation in scattering coefficient as a function of altitude is one of the essential requirements for accurate computations of slant path tropospheric contrast transmittance, and thus must be reliably modelled if one presumes to develop predictive capabilities. Profile measurements such as those illustrated in Fig. 5 can provide the data base required for this model development within the visible spectrum, and conceivably provide the necessary insights for extrapolation to longer optical wavelengths. The profile characteristics requiring specific attention are the number and depth of well defined and reasonably well mixed aerosol layers, the most representative value of scattering coefficient within each layer, and the directional scattering properties of the aerosol within each layer. The data in Fig. 5 identify the first two characteristics. In each case there are two well defined layers with the boundary at about 1200-1500 meters. The average value of scattering coefficient within each layer can be readily established subsequent to upper altitude stray light corrections based upon directional scattering and sky radiance measurements.

There is strong evidence that the specification of the directional scattering properties within each aerosol layer can be reasonably deduced from a knowledge of the total volume scattering coefficient alone. Johnson, et al. (1979) and Johnson (1981). An example of the data supporting this contention is illustrated in Fig. 6 from Johnson and Gordon (1980). In these data, directional scattering function measurements made by the Visibility Laboratory ground based nephelometer system are compared with similar data from Barteneva (1960). Whereas the Barteneva data represent over 600 sets of directional scattering measurements using photopic spectral response, the Visibility Laboratory data

represent measurements made in all four of the responses defined in Fig. 1.

The data shown in Fig. 6 have been normalized to reflect only aerosol scattering characteristics by using a ratio display format. Thus the vertical axis, Volume Scattering Function Ratio, represents the ratio of the volume scattering function $\sigma(z,\beta)$ to the Rayleigh (i.e. molecular) volume scattering function ${}_R\sigma(z,\beta)$ at the same scattering angle β i.e. $\mathcal{Q}(z) = \sigma(z,\beta)/{}_R\sigma(z\,\beta)$ where z is the altitude parameter Likewise, the horizontal axis, Optical Scattering Ratio, represents the ratio of the total volume scattering coefficient s(z)) to the Rayleigh volume scattering coefficient ${}_Rs(z)$ i.e. $Q(z) = s(z)/{}_Rs(z)$ These data and their airborne equivalents specifically support the contention that one can develop a parameterization that will adequately represent the directional scattering properties of an atmospheric aerosol once the optical scattering ratio Q(z) is specified, a fundamental simplification in any modelling attempt.

Our second major data set appropriate to the determination of tropospheric slant path contrast transmittances contains simultaneous measurements of sky and terrain radiances as determined from each of several different flight altitudes In Fig. 7, the apparent radiances throughout the combined upper and lower hemispheres which surrounded the aircraft during flight C-466 are defined in one graph. Each of the four individually coded plots represents the observed radiance along a vertical sweep from the zenith through the horizon to the nadir and is at a fixed and constant azimuth from the sun

The multi-spectral data typified by those illustrated in Fig. 7 provide a complete magnitude specification of the directional radiance field surrounding the aircraft. Thus they represent the net effects of the solar irradiance upon the total atmosphere within which the aircraft is implanted, including the influence of the underlying terrain. It is these data then, that allow one to close the modelling loop, in that they represent an essential intermediate step that a model must duplicate if it is to proceed to the subsequent determination of slant path contrast transmittance

4 EXPRESSIONS FOR PATH RADIANCE AND CONTRAST TRANSMITTANCE

The analytic expressions relating the fundamental equation of radiative transfer to the apparent spectral radiance of a distant target, and the apparent contrast of that target as observed against its background are well developed by Duntley, et al. (1957). Those most directly related to the development of the modelling concepts discussed herein are summarized below.

The apparent spectral radiance of a target t at a range r, as measured from an altitude z in a direction defined by zenith angle θ and azimuth angle ϕ is

$$ {}_tL_r(z\,\theta\,\phi) = T_r(z,\theta\,\phi)\,{}_tL_o(z,\,\theta\,\phi) + L_r^*(z\,\theta\,\phi) \qquad (1) $$

where ${}_tL_o$ is the inherent spectral radiance of the target, T_r is the spectral transmittance of the path, and L_r^* is the directional path radiance.

As discussed in Duntley, et al (1957), the directional path radiance is derived from the integration along the path of sight of the directional path function $L_\cdot(z,\theta,\phi)$ which is defined as the point function component of path radiance generated by the scattering of light reaching that point from all points within its surrounding field.

The expression for the path function is

$$ L_\cdot(z\,\theta\,\phi) = {}_\epsilon(z)\sigma(z\,\beta_s) + \int_{4\pi} L(z\,\theta\,\phi')\sigma(z\,\beta')\,d\Omega \qquad (2) $$

where $\sigma(z,\beta)$ is the directional volume scattering function at a scattering angle β, and ${}_\epsilon(z)$ is the solar scalar irradiance at altitude z.

The development from these fundamentals to expressions for the inherent and apparent spectral contrasts C_r and C_o of a target t against its background b is straight forward and results in the directional contrast transmittance along the path r as given by

$$ C_r(z,\theta,\phi)/C_o(z,\theta,\phi) = T_r(z\,\theta,\phi)\,{}_bL_o(z,\theta,\phi)/{}_bL_r(z,\theta,\phi) \qquad (3) $$

As emphasized by Duntley, et al. (1957), Eq. (3) does not involve restrictive assumptions and defines the law of contrast reduction in its most general form. It should be noted that Eq. (3) is expressed in terms of inherent and apparent background radiances ${}_bL_o$ and ${}_bL_r$, and is thus independent of target characteristics.

5. MODEL FOR ESTIMATING SLANT-PATH CONTRAST TRANSMITTANCE

The inherent variability of atmospheric structure and behavior and the complexities of radiative transfer processes require effective simplifying assumptions in order that estimates of contrast transmittance along any slant path in the atmosphere can be made rapidly and consistently. In pursuit of this objective, a series of modelling approximations relating optical properties to meteorological variables were derived from the broad experimental data base generated by airborne and surface measurement program. These relationships were combined with available analytic approximations for radiative transfer calculations to develop an operational technique for the estimation of directional path radiance and contrast transmittance. A detailed description of the model development and validation are presented in a report now being prepared for publication. A brief summary of the technique and several examples of model performance are given in the following paragraphs.

The calculation of the slant-path contrast transmittance with Eq. (3) requires consistent estimates of interrelated physical parameters. These include (a) the vertical profile of total volume scattering coefficient, $s(z)$, (b) the vertical profile of the phase function for single scattering, $[\sigma(z,\beta)/s(z)] = P(z,\beta)$, and (c) vertical profile of single scattering albedo, $\omega(z) = s(z)/\alpha(z)$, where $\alpha(z)$ is the total volume attenuation coefficient. It should be emphasized that the contrast transmittance along any slant path depends primarily upon the extinction coefficient distribution both along the path and in the surrounding atmosphere. Accordingly, an attempt was made to condition the approximation procedures for all parameters on the existing capability to model and predict the extinction coefficient structure and behavior from conventional meteorological measurements and observations.

5.1. Estimates of the scattering ratio profile

For profile modelling purposes, it is important to consider a conservative measure of scattering coefficient that in the absence of local sources or sinks does not change appreciably following the air motion. The photopic scattering mixing ratio, $Q(z)$, is such a parameter. As the vertical mixing within an identifiable atmospheric layer becomes more complete, $Q(z)$ becomes more constant with height within the layer. The optical scattering ratio is defined $Q(z) = s(z)/s_R(z)$, where $s_R(z)$ is the total volume coefficient for Rayleigh scattering at altitude z.

Profiles of $Q(z)$ derived from the extensive series of airborne optical measurements made by the Visibility Laboratory, reveal large variability depending upon the aerosol source strength and the nature of the convective and turbulent mixing processes. The problem is to model the essential characteristics of the $Q(z)$ profiles in a way that recognizes the operational observing and forecasting limitations yet takes maximum advantage of existing capabilities. A prominent feature of the daytime aircraft soundings of optical scattering is the marked tendency for $Q(z)$ to remain essentially constant with height in the troposphere above the haze layer and also within the low-level haze layer. The difference in $Q(z)$ between adjacent tropospheric layers is typically much larger than the vertical variability within each layer. It should be emphasized that the assumption of constant scattering ratio with height does not hold well for ground-based stable layers with little vertical mixing such as those associated with the nocturnal formation of fog. The computer code developed for this modelling effort has provision for up to 20 atmospheric layers for use in complex situations when detailed information about the extinction coefficient profile is available. However, for application to problems of contrast transmittance in hazy atmospheres in the daytime following the dispersion of any surface inversion existing at sunrise, it is reasonable to employ a model consisting of a stratospheric layer and two or three tropospheric layers of constant optical scattering ratio. Thus, the forecasting problem is reduced to the prediction of the altitude limits of the atmospheric layers and the scattering ratio within each layer.

5.2. Specification of the phase function for single scattering

The asymmetry of the phase function for single particle scattering depends in a complex way on the size distribution and refractive index of the aerosols present in the atmosphere and the wavelength of incident light. The prominent feature of aerosol scattering is that as the particle size increases with respect to the wavelength, the amount of energy scattered in directions close to that of the incident radiation increases markedly causing larger asymmetry in the phase function. Since the total volume scattering coefficient varies approximately as the square or cube of the particle radius depending upon the size parameter, we might expect that the scattering coefficient or scattering ratio, $Q(z)$, might provide, through analytic representation, a good first approximation for the single scattering phase function. Experimental evidence shows this to be true.

The approach used herein for model development was first to represent the single scattering phase function for Mie scattering $P_M(z,\beta)$ by two term Henyey-Greenstein functions (Kattawar, 1975) as follows,

$$P_M(\beta,g_1,g_2,c) = c\,P_1(\beta,g_1) + (1-c)P_2(\beta,g_2)\,, \tag{4}$$

and

$$P(\beta,g) = (1-g^2)/\,[\,4\pi(1-2g\cos\beta+g^2)^{3/2}\,]\,, \tag{5}$$

where the asymmetry factor, g, is given by

$$g = \frac{1}{2}\int_0^{\pi} P(\beta)\cos\beta\sin\beta d\beta \tag{6}$$

The phase function for single scattering has the normalized form,

$$\int_{4\pi} P(z,\theta,\phi)d\Omega = 1 \tag{7}$$

In turn, each of the Henyey-Greenstein parameters, $g_1(z)$, $g_2(z)$ and $c(z)$ were approximated as continuous functions of the Mie scattering ratio, $Q(z)-1$. The relationships between the phase function for combined aerosol and molecular scattering and the scattering ratio are bounded by the Rayleigh phase function $(Q=1, g=0)$ for a clear atmosphere and by a phase function representative of dense clouds or fog for very large $Q(z)$. Combined analysis of the asymmetry parameters (g_1,g_2,c) as derived from a least-squares fit of the Henyey-Greenstein functions to the average phase functions measured by Barteneva (1960) and to the phase functions derived from Mie calculations using typical aerosol distributions in haze and fog led to a consistent set of empirical equations expressing the asymmetry parameters as a function of the logarithm of the Mie scattering ratio, $(Q-1)$.

Independent evidence of the general applicability of the model estimates of $P(\beta)$ with respect to wavelength and altitude is given by a comparative study of directional scattering functions that were measured by the Visibility Laboratory airborne nephelometer and the Barteneva (1960) phase function measurements (see Section 3 and Fig. 6). In addition to the measurement of total volume scattering coefficient, the integrating nephelometer measured, separately, the directional scattering function at nominal scattering angles of 30° and 150° in four wavelength bands centered near 475, 550, 660, and 750 nm. The analysis by Johnson, et al. (1979) of the airborne data gathered by the Visibility Laboratory in Europe and the United States over all seasons indicates that the derived relationship between the phase functions scattering ratio holds well over all visible wavelengths and over all altitudes up to the highest levels sampled by the instrumented aircraft (usually near 6 km). Figures 8 and 9 show a comparison of phase functions as calculated from the model, calculated from Mie theory, and measured by Barteneva.

To the extent that more accuracy is desired and more complete information is available to define $P(z,\beta)$, the overall computer code for calculating path radiance and contrast transmittance was made general in that it will accept as input for each atmospheric layer any specified $P(z,\beta)$. However, in the absence of information other than an estimate of $Q(z)$, calculation of $P(z,\beta)$ from the system of model equations is recommended for haze only atmospheres. Important details typical of phase functions for fog conditions such as the prominent minimum near $\beta = 100°$ and the secondary maximum near 140° (see Fig. 9) are smoothed out by the representation with Henyey-Greenstein functions. It should be emphasized that important additional evidence of the applicability of the model for estimating $P(z)$ from $Q(z)$ will be obtained as we employ the technique more extensively for the specification of the sky and terrain radiances as measured in various deployments of the instrumented aircraft. Sample comparisons of measured and computed radiances are given in the following section.

5.3. Calculation of the path radiance component due to scattering of diffuse irradiance

As given by the first term on the right hand side of Eq. (2), the component of the directional path function produced by the scattering of direct solar irradiance incident on the path is calculated from estimates of the single scattering phase function determined by the technique described in the previous paragraphs. The second term on the right hand side of Eq. (2) is the component of path function resulting from the scattering of diffuse irradiance reaching the path from the surrounding sky and terrain. As in the case of the direct solar component, the directional dependence of the diffuse background contribution to the path radiance must be considered. Precise numerical

calculation of the radiance distribution resulting from the complex multiple scattering processes requires large amounts of computer time. For this reason, great emphasis has been placed upon the development of rapid approximate methods for radiation transfer calculations (Meador and Weaver, 1980). The appropriate choice of computational method from among the variety of available methods depends upon the results desired for the application at hand.

While it is important to retain complete directionality for calculation of the path radiance component due to single scattering of direct solar irradiance, approximate two stream methods often can be used effectively for fast calculation of the component due to scattering of diffuse irradiance provided that the asymmetric influence of the prominent forward scatter peak is managed adequately. The delta-Eddington approximation introduced by Joseph, Wiscombe and Weinman (1976) satisfies the requirement. It differs from the standard Eddington approximation, which assumes a simple cosine dependence of the single scattering phase function, in that it approximates the phase function by a truncated forward scatter peak and a two-term phase function expansion,

$$P_d(\beta) = 2f' \delta(1 - \cos\beta) + (1 - f')(1 + 3g'\cos\beta) , \tag{8}$$

where f' is the fractional scattering represented by the forward peak and g' is the asymmetry factor of the truncated phase function. In effect, the delta-Eddington approximation transforms most of the scattered radiation in the solar aureole into the direct solar flux component, and assumes that

$$f'(z) = g^2(z) \tag{9}$$

As an integral part of the technique for estimating directional contrast transmittance, the approximate diffuse radiance, $[L_D(z) + L_{D'}(z)\cos\theta]$, calculated by the Eddington computer code (Shettle and Weinman, 1979), as modified by the delta-Eddington approximation, is used directly to obtain the second term on the right hand side of Eq. (2); so that this component of the path function generated by the scattering of diffuse irradiance is given by

$$\int_{4\pi} L(z\,\theta',\phi')\,\sigma(z,\beta')d\Omega = L_D(z) + \frac{2}{3} L_{D'}(z)\cos\theta \tag{10}$$

5.4. Calculation of directional path radiance and contrast transmittance

With the procedures for estimating the direct and diffuse components described above, the directional path radiance L_r^* can be calculated from Eqs. (2) and (3) by finite summation over successive atmospheric layers using the trapezoidal rule. The computer code for calculation of directional path radiance and contrast transmittance along any slant path in accordance with Eqs. (1) through (8) requires the following input:

1) a representative wavelength λ that is commensurate with the spectral response of the sensor in μm
2) the solar irradiance $E_s(\infty)$ at the upper limit of the atmosphere in $w/m^2\mu m$ corresponding to spectral response of the sensor
3) the number of atmospheric layers n and the altitude z_n of the base of each layer in km
4) the average optical scattering ratio $Q(z)$ for each atmospheric layer
5) the average single scattering albedo $\omega(z)$ for each atmospheric layer
6) the average surface reflectance $R(\theta,\phi)$ and the reflectance of the immediate background of the viewed object if significantly different than the albedo of the general background
7) the object and observer altitudes in km and the viewing angle with respect to the sun, β, and zenith, θ, in degrees
8) the solar zenith angle θ_s in degrees.

6. RESULTS OF MODEL CALCULATIONS

Model calculations based upon the extensive data gathered by the airborne measurement program make possible a close analysis of the dependence of optical properties on meteorological conditions. Comparative analyses of observed data with the model calculations are being used to improve techniques for the prediction of image transmission properties from conventional meteorological observations. Some examples of

trial model calculations are illustrated in the following paragraphs.

Comparisons of the sky and terrain radiance distribution measured by the scanning radiometers and the model calculations of the radiance distribution from the observed input parameters are shown in Figs. 10 and 11 for the flight made on 15 August 1978 in northwestern Germany near Meppen. A 3-layer atmosphere was assumed for model calculations with the top of the haze layer at 1.3 km (see scattering coefficient profile in Fig. 5) and a tropopause height of 10 km. The observed features of the radiance distribution are typical of rural clear sky conditions observed in western Europe in the summer months. At the observation altitude deep within the haze layer at 200m, the sky radiance in the upsun direction, $\phi = 0°$, is substantially larger than the view angle away from the sun, $\phi = 180°$. However, the disparity in sky radiances in the upsun and downsun directions is much smaller looking upward from an altitude well above the haze layer near 6 km. The rather large fluctuations in measured radiance looking downward from the low altitude of 200m are caused by differences in the reflectivity of various terrain pattern features such as the green and brown fields and small wooded areas.

For the same experimental flight, Fig. 12 shows the contrast transmittance distribution for downward view angles from an observation level of 6 km and target altitude of 0.2 km that were calculated from the radiance distribution given by both the aircraft measurements and the model calculations. Looking overhead, Fig. 13 shows the apparent contrast as a function of zenith angle for an object at 20 km viewed from 0.2 km as calculated from the observed and model sky radiance distributions.

The model calculations can be used to assess quantitatively the changes in contrast transmittance associated with incremental changes in the individual environmental factors governing image transmission in the atmosphere. For purposes of illustration, the reference atmosphere as described in Table 2 was derived from the measurements made on 15 August 1978 near Meppen, Germany (see Fig. 5). As discussed above, the meteorological conditions observed on this flight are representative of clear sky conditions for this geographical area and time of the year. An optical scattering ratio of 16 for the haze layer converts to a horizontal visual range of about 16 km at the surface assuming an inherent target contrast of -1, no absorption and an apparent contrast threshold for detection of 5 percent. The single scattering albedo of 0.83 assumed for the haze layer is commensurate with measurements in rural areas in the United States by Weiss, et al. (1980).

For a specified azimuth angle, the slant range between the sensor and target altitudes where the apparent contrast of the target and background reduces to a fixed threshold value can be determined from systematic model calculations for successive zenith view angles. Calculation of the slant range corresponding to 5 percent apparent contrast for the reference atmosphere specified in Table 2 and for a series of individual incremental changes in various atmospheric variables are illustrated in Fig. 14. It should be emphasized that the indicated changes in slant range as a function of changes in the input variables are specific only for the variations about the given set of conditions, i.e. observation level at 20 km, target at surface, target reflectivity of 50 percent, azimuth view angle of zero with respect to the sun, and atmospheric structure as given by the reference atmosphere. However, the results illustrated here do provide insight into the relative impact of the parameter changes on contrast transmittance. Using approximate interpolation methods under the same prescribed conditions, we have calculated the changes in individual parameters which produce a family of equivalent effects. Thus, Table 3 illustrates those changes in conditions, any one of which will result in a corresponding 20% decrease in apparent contrast.

7. SUMMARY

The computer model developed during the course of the experimental optical measurement and analysis program can provide relatively fast and consistent estimates of optical atmospheric properties over any slant path as a function of wavelength in the visible spectrum. To the extent that a climatological data base of conventional meteorological observations exists, the technique in its present form can be used to estimate readily the frequency distributions of such quantities as spectral contrast transmittance as a function of location and season.

Refinements in the model are being made as validation tests and experiments continue. Early results indicate that further parameterization of selected components of the model can be made which will improve computational efficiency and at the same time retain the capability to take advantage of any and all relevant observational and forecast information. A realistic goal is to employ the computer model as part of a data acquisition and microprocessing system for real time estimates of image transmission properties. Future experiments are planned to examine the tradeoffs between the type, accuracy, frequency and density of optical/meteorological observations and the reliability of the estimates of spectral contrast transmittance.

8. ACKNOWLEDGEMENTS

The studies conducted prior to and during the preparation of this paper have involved the talents and skills of many persons associated with both the Air Force Geophysics Laboratory and the University of California, Visibility Laboratory. The authors gratefully acknowledge these contributions, and in particular would like to thank Dr. Robert Fenn and Mr. Eric Shettle of the Geophysics Laboratory and Ms. Jacqueline I. Gordon of the Visibility Laboratory for many constructive discussions, comments and suggestions.

This effort has been supported by the Air Force Geophysics Laboratory under Contract No. F19628-78-C-0200.

9. REFERENCES

Barteneva, O. D. (1960), "Scattering Functions of Light in the Atmospheric Boundary Layer," Bull. Acad. Sci. U.S.S.R., Geophysics Series, 1237-1244.

Duntley, S. Q., A. R. Boileau, and R. W. Preisendorfer (1957), "Image Transmission by the Troposphere I", J. Opt. Soc. Amer., 47, 499-506.

Duntley, S. Q., R. W. Johnson, J. I. Gordon, and A. R. Boileau (1970), "Airborne Measurements of Optical Atmospheric Properties at Night," University of California, San Diego, Scripps Institution of Oceanography, Visibility Laboratory, SIO Ref. 70-7, AFCRL-70-0137. NTIS, Ad 870 734.

Duntley, S. Q., R. W. Johnson, and J. I. Gordon (1977), "Airborne Measurements of Atmospheric Volume Scattering Coefficients in Northern Europe, Spring 1976," University of California, San Diego, Scripps Institution of Oceanography, Visibility Laboratory, SIO Ref. 77-8, AFGL-TR-77-0078. NTIS, ADA 046 290.

Duntley, S. Q., R. W. Johnson, and J. I. Gordon (1978a), "Airborne Measurements of Optical Atmospheric Properties, Summary and Review III," University of California, San Diego, Scripps Institution of Oceanography, Visibility Laboratory, SIO Ref. 79-5, AFGL-TR-78-0286. NTIS, ADA 073 121.

Duntley, S. Q., R. W. Johnson, and J. I. Gordon (1978b), "Airborne Measurements of Atmospheric Volume Scattering Coefficients in Northern Europe, Fall 1976," University of California, San Diego, Scripps Institution of Oceanography, Visibility Laboratory, SIO Ref. 78-3, AFGL-TR-77-0239. NTIS, ADA 057 144.

Fenn, R. W. (1978), "OPAQUE - A Measurement Program on Optical Atmospheric Properties in Europe, Vol. I. The NATO OPAQUE Program," Special Reports No. 211, AFGL-TR-78-0011.

Johnson, R. W. and J. I. Gordon (1980), "Airborne Measurements of Atmospheric Volume Scattering Coefficients in Northern Europe, Summer 1978," University of California, San Diego, Scripps Institution of Oceanography, Visibility Laboratory, SIO Ref. 80-20, AFGL-TR-80-0207.

Johnson, R. W., W. S. Hering, J. I. Gordon, B. W. Fitch and J. E. Shields (1979), "Preliminary Analysis and Modelling Based Upon Project OPAQUE Profile and Surface Data," University of California, San Diego, Scripps Institution of Oceanography, Visibility Laboratory, SIO Ref. 80-5, AFGL-TR-79-0285. NTIS, ADB 052 172L.

Johnson, R. W. (1981), "Daytime Visibility and Nephelometer Measurements Related to its Determination," Paper presented at Environmental Protection Agency Symposium on Plumes and Visibility, Grand Canyon, Arizona, Nov. 1980. Accepted for publication, ATMOSPHERIC ENVIRONMENT, Dec. 1980.

Joseph, J. H., W. J. Wiscombe, and J. A. Weinman (1976), "The delta-Eddington Approximation for Radiative Flux Transfer", Atmos. Sci., 33, 2452-2459.

Kattawar, G. W. (1975), "A Three-Parameter Analytic Phase Function for Multiple Scattering Calculations", J. Quant. Spectrosc. Radiant. Transfer, 15, 839-849.

Meador, W. E., and W. R. Weaver (1980), "Two Stream Approximations to Radiative Transfer in Planetary Atmospheres: A Unified Description of Existing Methods and a New Improvement", J. Atmos. Sci., 37, 630-643.

Shettle, E. P., and J. A. Weinman (1970), "The Transfer of Solar Irradiance Through Inhomogeneous Turbid Atmospheres Evaluated by Eddington's Approximation", J. Atmos. Sci., 27, 1048-1055.

Weiss, R. E., R. J. Chankan, A. P. Waggoner, N. Sadler, and J. Ognen (1980), "An Assessment of Light Absorption by Aerosol Particles in Urban, Rural and Remote Troposphere and Stratospheric Air", 1980 International Radiation Symposium Extended Abstracts, International Association of Meteorology and Atmospheric Physics, IUGG, 178-180.

Fig 2 Typical OPAQUE Flight Tracks

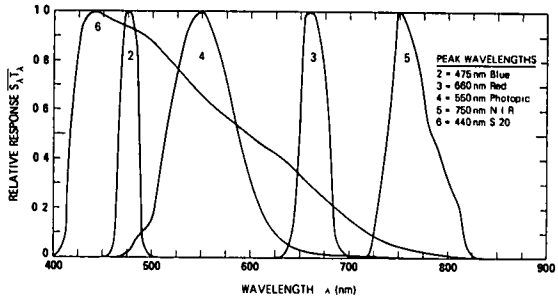

Fig 1 Standard Spectral Responses

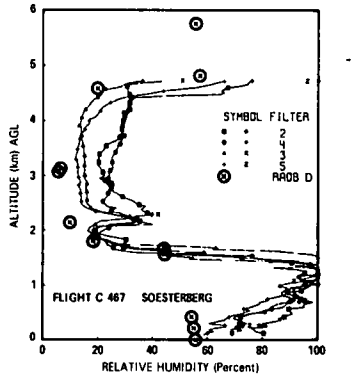

Fig 4 Relative Humidity Profiles Flight C-467

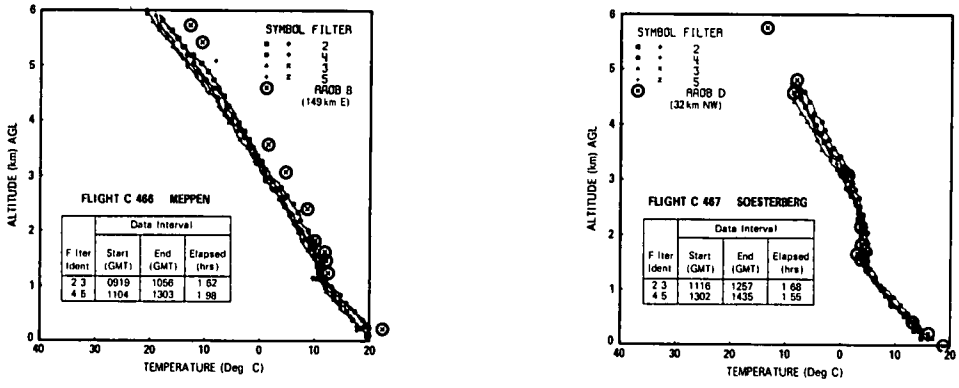

Fig 3 Temperature Profiles, Flights C-466 & C-467

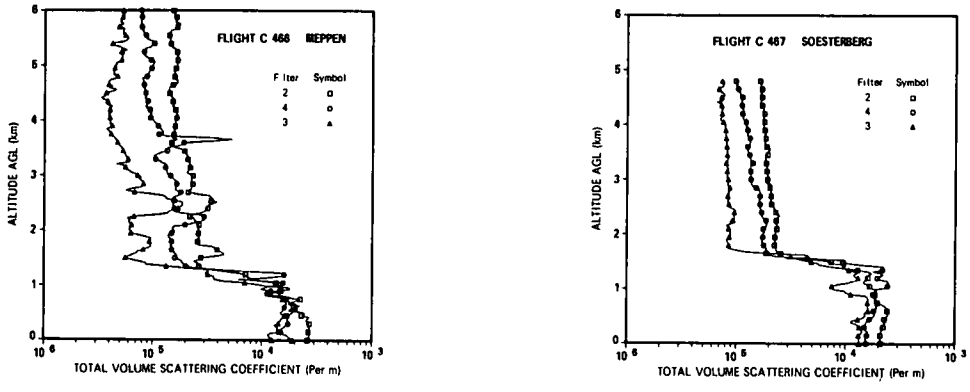

Fig 5 Total Volume Scattering Coefficient Profiles, Flights C-466 & C-467

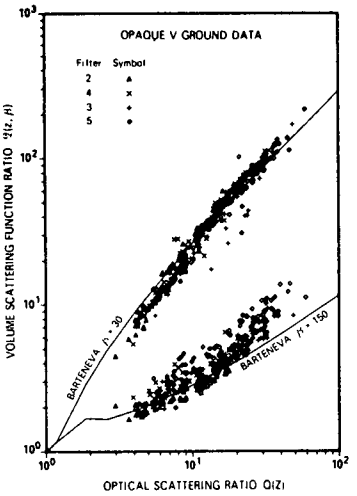

Fig. 6 Multi-Spectral Directional Scattering Measurements.

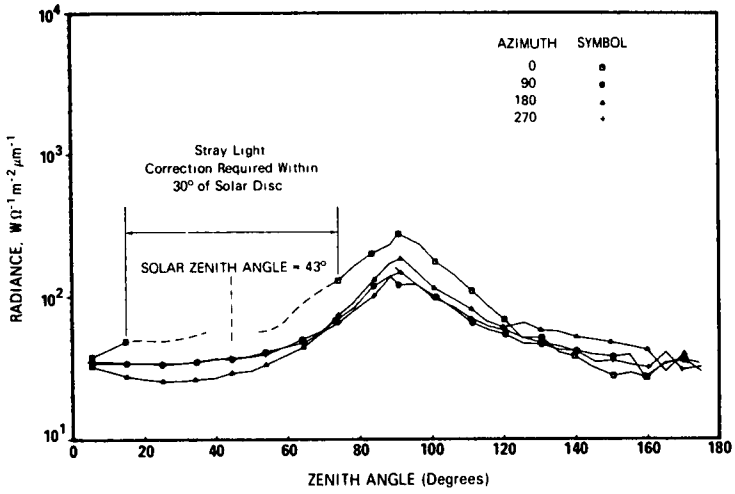

Fig. 7 Measured Sky and Terrain Radiance Distributions for Flight C-466, filter 2, 2953m AGL.

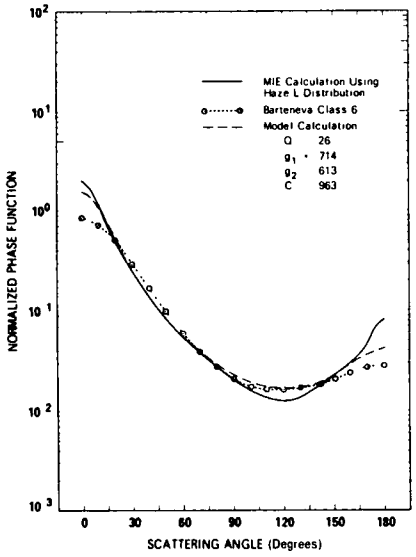

Fig. 8. Single scattering phase functions (a) calculated from Mie theory by Kattawar (1975) using Diermendjian (1969) Haze L distribution with a refractive index of 1.55-0.0i; (b) observed by Barteneva (1960) (class 6); and (c) calculated for scattering ratio of 26.

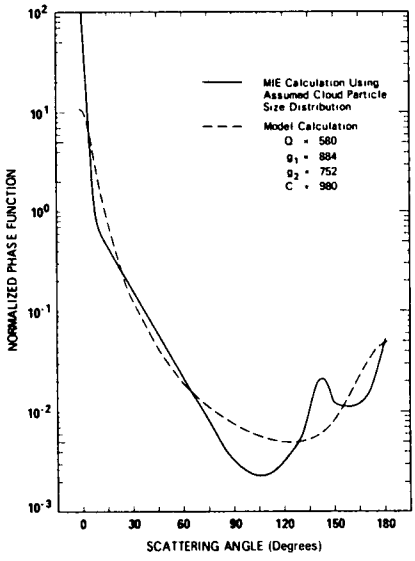

Fig. 9. Single scattering phase functions (a) calculated from Mie theory by Kattawar (1975) for cloud drop distribution $n = kr^{6}e^{-1.5r}$ and refractive index of 1.33-0.0i, and (b) calculated for scattering ratio of 580.

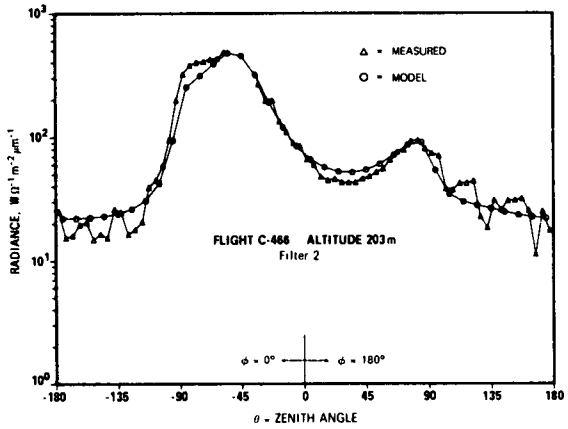

Fig. 10. Comparison of Measured and Calculated Sky and Terrain Radiance Distributions at 200m.

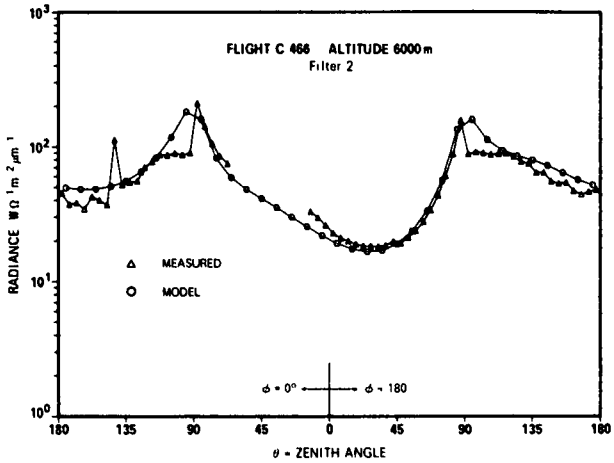

Fig 11 Comparison of measured and calculated sky and terrain radiance distributions at 6000 m

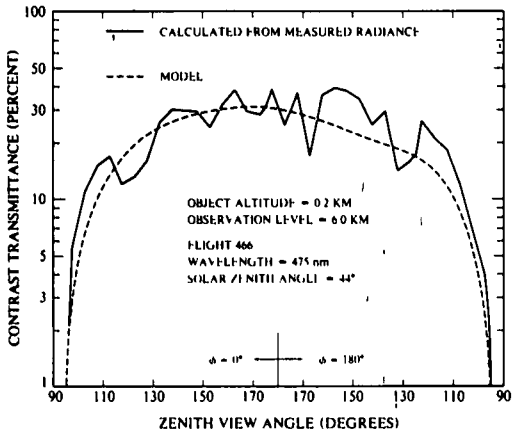

Fig 12 Comparison of contrast transmittance distributions calculated from measured and observed sky and terrain radiance distributions

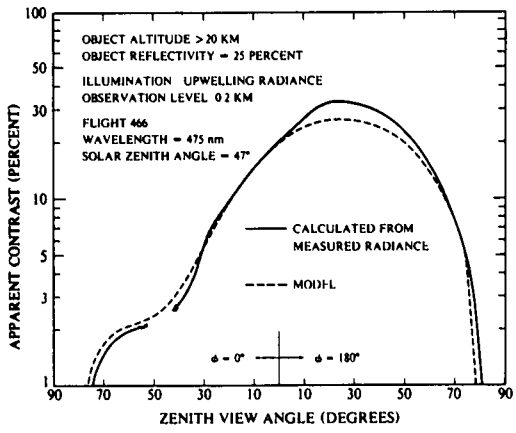

Fig 13 Comparison of apparent contrast distributions calculated from measured and model sky radiance distributions

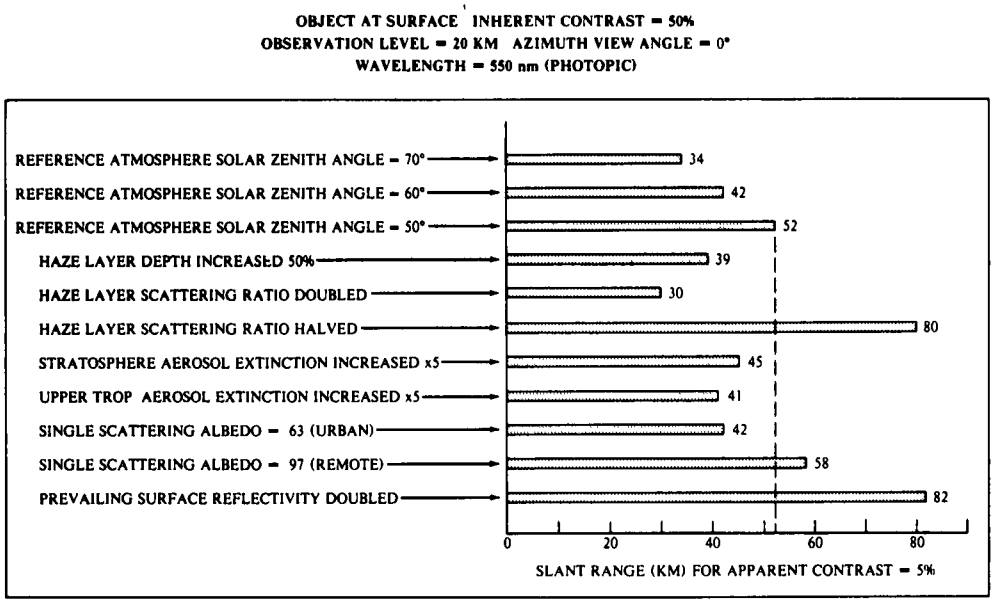

Fig 14 Comparison of the slant range corresponding to apparent contrast of 5 percent for reference atmosphere and selected changes in the reference atmosphere

Table 1.

Geographical and Seasonal Distribution of OPAQUE Related Data Flights

Flight Location (Fig 1)	Attempted Data Sequences				Totals
	Spring 1976	Fall 1976	Summer 1977 & 1978	Winter 1978	
Sicily	0	0	4	5	9
France	0	5	3	0	8
So Germany	0	0	5	8	13
No Germany	5	4	9	3	21
Netherlands	1	0	3	2	6
England	5	0	3	7	15
Denmark	2	4	6	2	14
Totals	13	13	33	27	86
Data Reports	AFGL-TR-77-0078	AFGL-TR-77-0239	AFGL-TR-78-0168 AFGL-TR-80-0207	AFGL-TR-79-0159	AFGL-TR-79-0285

Table 2.

Reference Atmosphere (Photopic, $\lambda = 550m$)

NUMBER OF LAYERS	3
ALTITUDE OF TROPOPAUSE	10 km
DEPTH OF HAZE LAYER	1 3 km
OPTICAL SCATTERING RATIO	
STRATOSPHERE	1 3
UPPER TROPOSPHERE	1 3
HAZE LAYER	16 0
SINGLE SCATTERING ALBEDO	
STRATOSPHERE	0 99
UPPER TROPOSPHERE	0 97
HAZE LAYER	0 83
SURFACE REFLECTANCE	0 07

Table 3.

Parametric Changes Inducing 20% Decrease in Apparent Contrast

Item	Parameter	Change	Amount
a	Haze layer depth, Z	increase	30%
b	Haze layer scattering ratio, $Q(z)$	increase	25%
c	Haze layer single scattering albedo, $\omega(z)$	decreased	24%
d	Mid-Troposphere Aerosol Scattering Coeff $\sigma(z)$	increase	factor of 3
e	Stratosphere Aerosol Scattering Coeff $\sigma(z)$	increase	factor of 5 7

Airborne measurements of European atmospheric scattering coefficients

Richard W Johnson
University of California San Diego
Scripps Institution of Oceanography
Visibility Laboratory
San Diego California 92132

Abstract

A discussion of a series of airborne measurements of atmospheric optical properties in Europe Visible spectrum measurements made using an instrumented C-130 aircraft between 0 5 and approximately 6 km above ground level are described with respect to experimental procedures, results and application of the data to the determination of atmospheric contrast transmission Data locations are illustrated as are the primary radiometer systems utilized to make the measurements Sample data from flights conducted during 1976 and 1977 are presented illustrating irradiance levels beneath scattered to broken cloud decks, and total volume scattering coefficient variations as a function of altitude above ground level Comparisons between scattering coefficient and relative humidity profiles are illustrated and the data base availability is reviewed

Introduction

The Visibility Laboratory, a sub-division of Scripps Institution of Oceanography at the University of California, San Diego, has for a good number of years conducted an airborne measurement program in cooperation with and under the sponsorship of the Air Force Geophysics Laboratory This jointly conducted experimental program has for the most part, been directed toward developing a body of data suitable for applications requiring the determination of visible spectrum contrast transmittance through the lower atmosphere For the last several years it has been conducted as an independent but cooperative effort in conjunction with the NATO OPAQUE Program where OPAQUE is the acronym for OPTICAL ATMOSPHERIC QUANTITIES IN EUROPE And in that context, five two-month deployments have been made to the European area, the first in the Spring of 1976, and the most recent in the Summer of 1978

The purpose of this paper is to present a short review of the program's general procedures, its primary instrumentation, and a sample of some typical results

Flight Procedures

The basic procedure has been to put an instrumented C-130 aircraft into the test environment, and measure those optical atmospheric properties that will most influence visual or electro optical performances with respect to image transmission through that environment For this visually oriented program, the C-130 system was designed to acquire the data necessary for the determination of universal contrast transmittance as defined in Eqs (1) and (2), the derivations for which are described most recently in Duntley, *et al* 1978a[1]

$$R_r^*(z,\theta,\phi) = \frac{\pi\ N_r^*(z,\theta,\phi)}{H_{(z_t)}\ T_r(z,\theta,\phi)} \tag{1}$$

Eq (1), for directional path reflectance, R_r^*, illustrates those optical atmospheric properties which must be determinable from the airborne measurements in order to generate the desired contrast transmittances They are, path radiance along the path of sight $N_r^*(z,\theta,\phi)$ total downwelling irradiance, $H_{(z_t)}$ and beam transmittance along the path, $T_r(z,\theta,\phi)$, where the parenthetical modifiers in all cases, define altitude, z, and the zenith angle θ and azimuth ϕ of the path of sight

$${}_b\tau_r(z,\theta,\phi) = \frac{1}{1 + \dfrac{R_r^*(z,\theta,\phi)}{{}_bR_o(z,\theta,\phi)}} \tag{2}$$

Eq (2), for contrast transmittance, ${}_b\tau_r$, is in a ratio form that is found convenient for use, in that the two reflectance terms R_r^* and ${}_bR_o$, isolate the properties of the transmitting medium, and the properties of the background into two separate quantities which can be independently determined The R_r^* term characterizing the atmospherics, and the R_o term the inherent directional reflectance of the background

The flight program's goal therefore, has been to acquire a set of measurements, suitable for use in these generalized equations, which represent a broad spectrum of geographical and temporal situations. In the recently completed series of OPAQUE deployments, data flights were accomplished in the areas illustrated in Fig. 1. Data missions were flown as far south as the west coast of Sicily in the Mediterranean, and as far north as the southern coast of Denmark in the Baltic. The geographical distribution of the data flights and their related ground based measurements is further identified in Table 1, where each site is listed in order of increasing latitude.

Table 1.

Project OPAQUE Flight Track & Ground Sites Location & Ground Elevations

Geographical Reference and Site Identification Code		Center of Flight Track		Ground Site		Approx Gnd Elev along track
		Latitude	Longitude	Latitude	Longitude	
Ground Sites						
Catania, Sicily	(CT)	-	-	37°24'N	14°55'E	-
Trapani, Sicily	(TR)	-	-	37°55'N	12°29'E	-
Bruz, France	(BR)	-	-	48°01'N	1°45'W	-
Birkhof, Germany	(BK)	-	-	48°13'N	9°11'E	-
Yeovilton, England	(YO)	-	-	51°01'N	2°37'W	-
Soesterberg, Netherlands	(SØ)	-	-	52°08'N	5°17'E	-
Meppen, Germany	(MP)	-	-	52°52'N	7°23'E	-
Flight Tracks						
Sigonella, Sicily	(SG)	37°24'N	15°20'E	-	-	Sea Level
Trapani, Sicily	(TR)	37°33'N	12°30'E	-	-	Sea Level
Bruz, France	(BR)	48°01	1°41'W	-	-	50 m
Birkhof, Germany	(BK)	48°15'N	9°05'E	-	-	762 m
Yeovil, England	(YO)	50°56'N	2°27'W	-	-	60 m
Soesterberg, Netherlands	(SØ)	51°56'N	5°35'E	-	-	6 m
Mildenhall, England	(ML)	52°24'N	1°41'E	-	-	Sea Level
Ahlhorn, Germany	(AL)	52°53'N	7°51'E	-	-	18 m
Meppen, Germany	(MP)	53°00'N	7°37'E	-	-	18 m
Rodby, Denmark	(RB)	54°41'N	11°08'E	-	-	Sea Level

Fig. 1: Project OPAQUE Site Location Map

With this introduction to the intent of the general procedures, let us proceed to a brief description of some of the primary instrumentation with which the radiometric measurements were made during each flight. Fig. 2 illustrates the C-130 as it appeared during the OPAQUE III deployment to France in the Summer of 1977. As the annotation implies, the aircraft carried six different varieties of radiometers, two camera systems, several meteorological probes and a Royco particle counting system.

The primary radiometers were the integrating nephelometer used for the measurement of total volume scattering coefficients, and the upper and lower hemisphere radiance scanners used for the measurement of sky and terrain radiance distributions. The nephelometer, upper hemisphere scanner and upper hemisphere camera were mounted in the modified upper radome as a composite assembly illustrated in Fig. 3.

The upper and lower hemisphere scanners are servo controlled 5° field of view telescope assemblies which have been programmed to scan a hemisphere in a series of 18 ten second revolutions. The radiance distribution measurements are later sorted and averaged to yield an average radiance value for each 6° in azimuth and each 5° in zenith angle.

The integrating nephelometer is enclosed in the large shroud assembly in the foreground of Fig. 3. It is a folded path device designed and built at the Visibility Laboratory several years ago for an earlier program, but modified to its present configuration for use on the OPAQUE deployments. The operational components are illustrated in Fig. 4 with the shroud open, showing the projector and detector assemblies, however the system characteristics are more clearly illustrated in the artist's conception shown as Fig. 5. This nephelometer has several features which make it a particularly attractive experimental tool. First, the optical system uses a cylindrically limited projector beam, stopped to provide a rectangular beam cross section which provides a good geometrical definition of the illuminated volume. Second, the detector assembly's primary channel uses a cosine corrected irradiometer head which performs the optical integration over all scattering angles between 5° and 172° minimizing truncation losses. And third, the detector assembly's secondary channels

measure relatively narrow angle directional scattering at both 30° and 150° which allows the determination of a forward to back scattering ratio that can be used to more thoroughly characterize the sample aerosol.

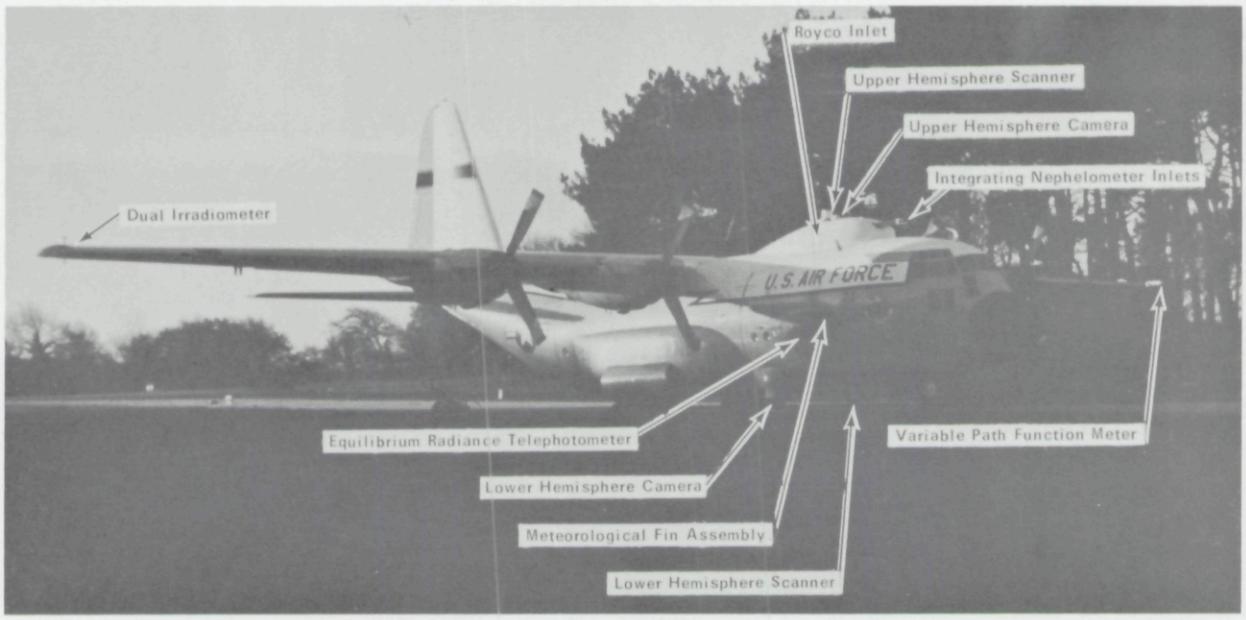

Fig. 2. Airborne Instrumentation System

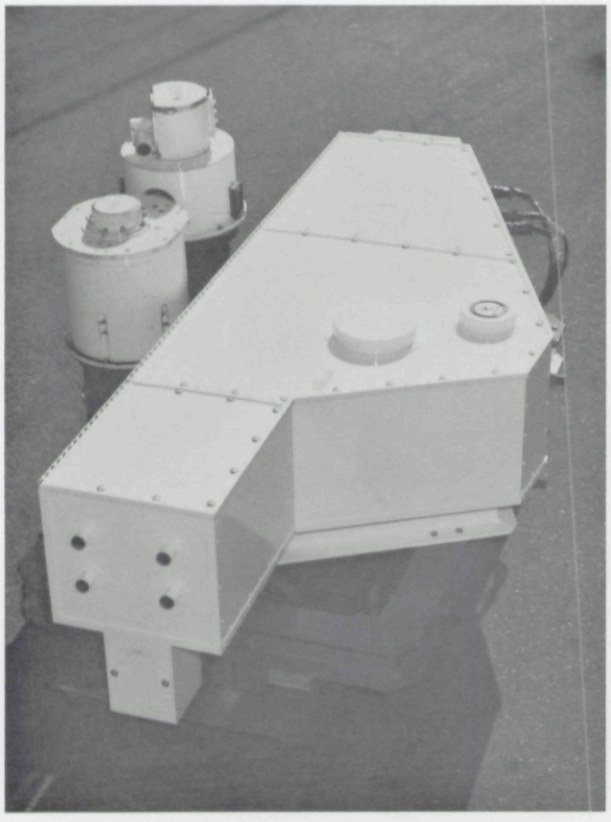

Fig. 3. Integrating Nephelometer Assembly

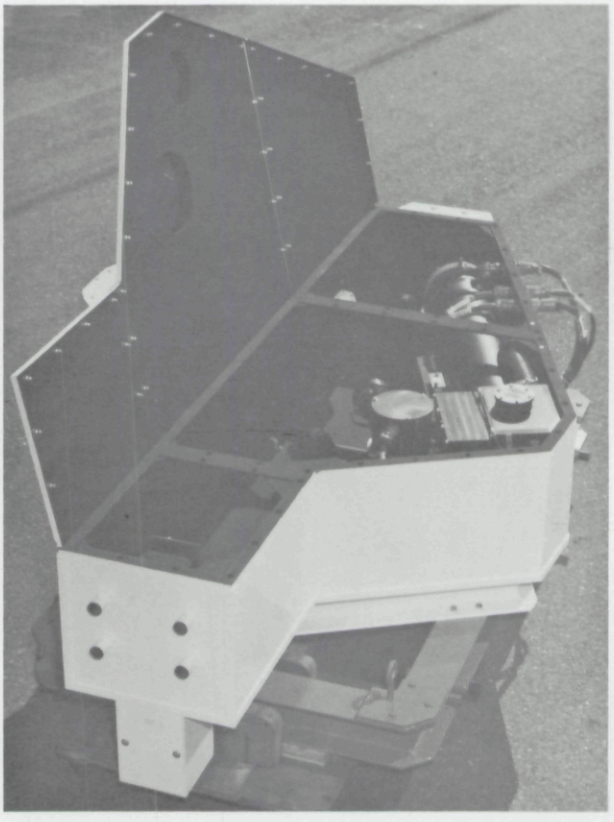

Fig. 4. Nephelometer Internal Arrangement

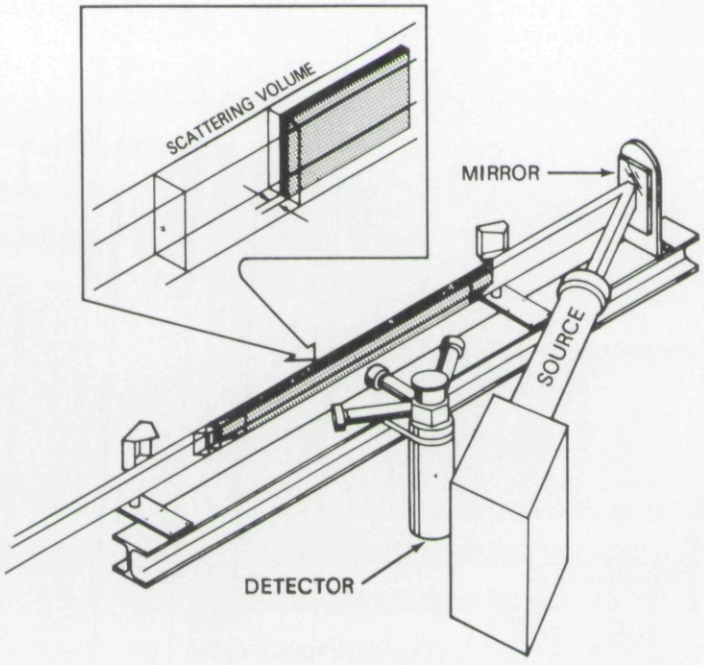

Fig. 5. Nephelometer Schematic Representation

All of the six radiometer channels utilize S-20 photomultipliers fitted with spectral filters to yield the spectral responses illustrated in Fig. 6. The filter number 4 represents the pseudo photopic response which is similar to the response used for many of the OPAQUE ground based measurements. It is also the response which closely approximates the visual response of the human observer, and thus generates the data used in visual search and detection problems.

The nominal flight profile for a clear day mission is shown in Fig. 7. The pattern illustrated requires about an hour and forty-five minutes to complete, and would yield data describing sky and terrain radiances plus scattering coefficient profiles in any two of the four available spectral bands. The flight pattern must be flown twice to acquire equivalent data in all four spectral bands. During the five OPAQUE deployments, the high incidence of low ceilings and generally poor VFR flying conditions precluded the use of this nominal pattern, and restricted data missions to modified profiles that could be completed between ground level and the cloud bases. Consequently, many data flights terminate somewhere between 5 and 10 thousand feet, rather than the twenty shown in the illustration. If one chooses to abandon the requirement for determining contrast transmittance from the data, and is willing to settle for the simpler radiance or beam transmittance, then the automatic scanner data which are used primarily for the computation of path radiances, are not required, and the flight pattern can be simplified to contain only the ascent and descent legs. Under this much less restrictive situation, where nephelometer profile data is the only item of real concern, successful data collection has been accomplished under rather severe weather conditions. These simplified profiles represent just under 30% of the OPAQUE data set.

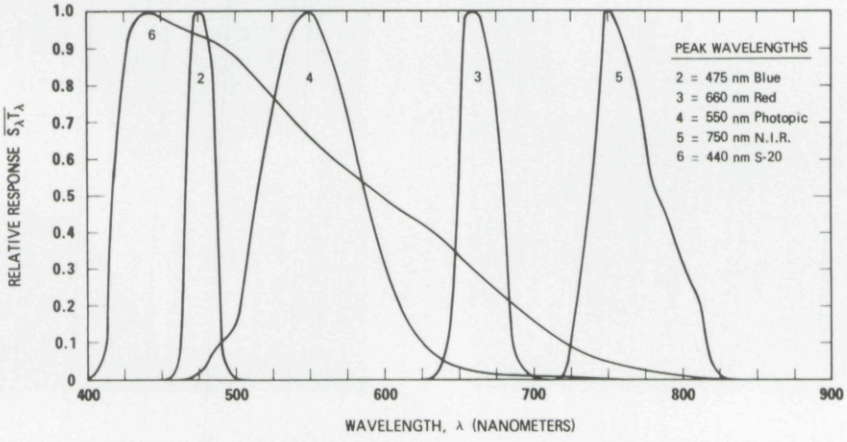

Fig. 6. Radiometer Spectral Response Curves

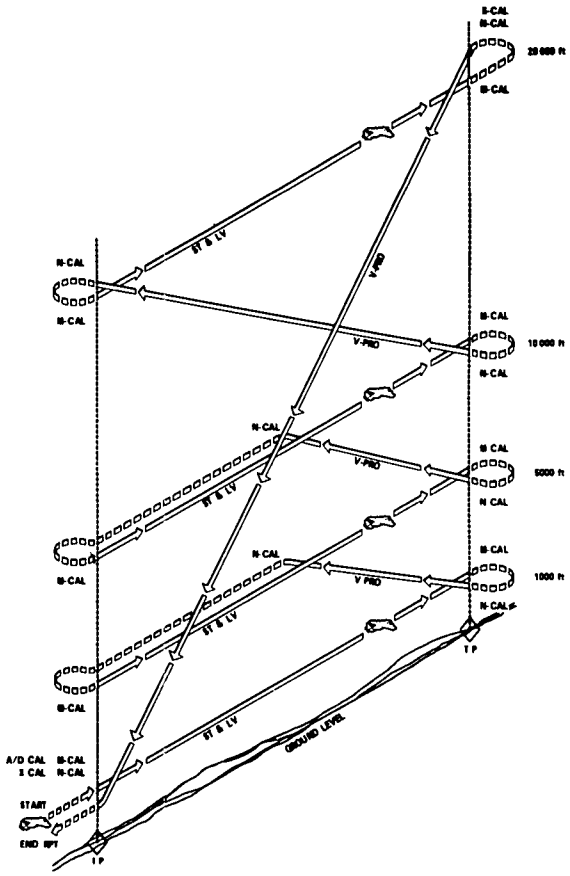

Fig 7 Nominal Clear Day Flight Profile

Data Summary

The following groups of figures have been chosen to represent typical samples of the data collected with the C-130 system during the first three OPAQUE deployments

The first group of three figures are data from flight C-416 which was made on the Rodby track off southern Denmark during OPAQUE III These are typical of data appearing in Duntley, *et al* 1978b[2] Flight C-416 was an afternoon flight with partly cloudy skies There were scattered low cumulus with some high thin cirrus

Fig 8 illustrates measurements of total downwelling irradiance made as a function of altitude in each of the four spectral bands during the ascent and descent portions of the flight The irradiances are generally stable with an occasional downscale kick due to a cloud coming between the aircraft and the sun The photopic illumination, converted from the 1100 $w/m^2\mu$ shown in the plot, is just under 80,000 lux

Fig 9 illustrates the structure of the total volume scattering coefficient as a function of altitude in the same spectral bands Except for the clutter occurring in the middle altitudes around 2 to 3 km where the aircraft was flying through cloud debris, these profiles illustrate the normally anticipated spectral separations That is greater scattering in the filter 2 blue band, scaling down to the lesser values in the filter 3 and 5 red bands The degree of fine structure in the data that is attributable to instrumentation and system noise is generally not more than $\pm 5\%$ of the reading, which at this scale is a band slightly wider than the square symbol used to identify the filter 2 data Radiometer least counts range between ± 0.5 and $\pm 1.5\%$

The low altitude filter 4 scattering coefficient of $1.8 \times 10^{-4} m^{-1}$ or 0 18 km^{-1} indicates an approximate visibility of 17 km with nearby stations calling 15 to 20

The vertical beam transmittances calculated from these scattering coefficient profiles are illustrated in Fig 10 In this presentation the curves represent the vertical beam transmittance from any selected altitude to the ground in each of the four spectral bands The crossover between the filter 3 and 4 curves basically is the result of the nonsimultanaity in the measurement of the scattering coefficient structure This crossover will often occur when a series of measurements is made over a several hour time period under scattered cloud conditions, and can be considered to some degree a measure of the temporal and geographical non-uniformity of the sample environment

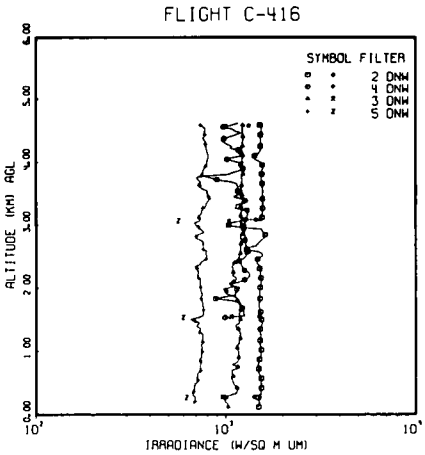

Fig 8

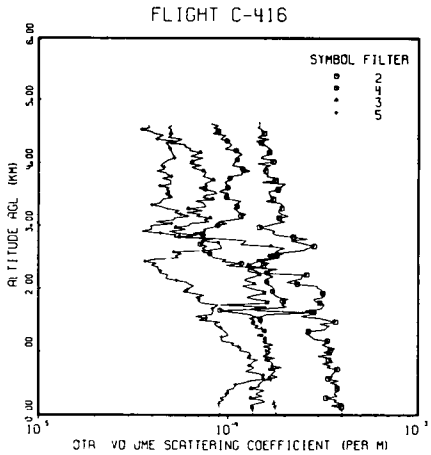

Fig 9

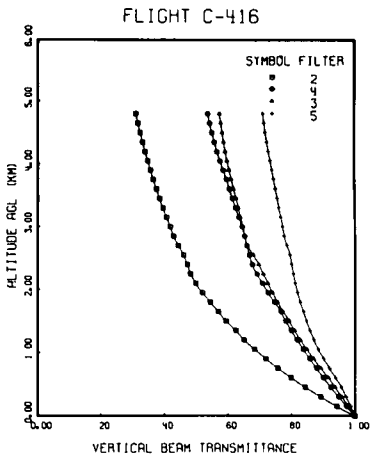

Fig 10

Three Sets of Sample Data from Flight C-416, Rodby, Denmark

The airborne measurements of upper and lower hemisphere radiance distributions made by the automatic scanner systems are not included in the report format currently in use by this program, but they represent a most valuable data resource They are essential, of course, for the computation of the R* directional path reflectance components and the resultant contrast transmittances as illustrated in Eqs (1) and (2) During each standard mission, sky and terrain radiance distributions are measured from four different altitudes in each of four spectral bands Each of these thirty two radiance distributions is represented by an array containing approximately 1000 data points In order to simplify the presentation and possible codification of these arrays we have developed the isoradiance plot illustrated in Fig 11 These data were measured over the Meppen site during an earlier program, but are typical of the 35 sets of flight data in the taped data bank In this polar display the plotted lines represent points of equal radiance with the center of the plot representing the zenith, and the outer periphery the horizon In the matching terrain plot, the center would represent the nadir

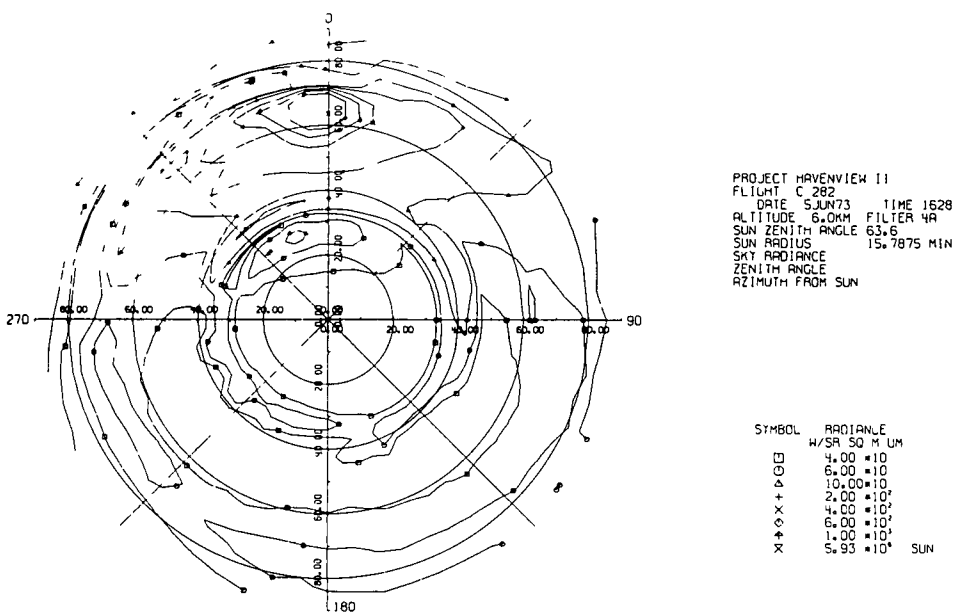

Fig 11 Upper Hemisphere Isoradiance Plot

Typical Comparison Data

This second group of figures represent composite plots which are typical of the summary displays appearing in each of the OPAQUE deployment Technical Reports They contain the same basic data that appears in the individual flight displays, but by grouping several flights together on one plot it is often easier for the analyst to visualize the overall character of the deployment

The first illustration Fig 12, is a grouping of the average temperature profiles measured during each of the OPAQUE I flights These eight profiles are coded by Latitude in the legend and represent data from the flight tracks in the Netherlands, England, northern Germany and Denmark The solid uncoded lines represent the anticipated temperature profiles as listed in the U S Standard Atmosphere Supplements

The second summary plot Fig 13 illustrates total downwelling irradiance profiles measured with the pseudo photopic response during the OPAQUE III flights The generally cluttered structure in the profiles contrasts sharply with the relatively constant values associated with clear day flights The cloud cover coding in the legend for the most part explains the irregularity as all flights were made under scattered to broken or worse cloud conditions The short profile for flight C-422 represents the illumination under full overcast conditions on a Rodby flight made in heavy haze between sea level and the 2 km ceiling

The third and last summary plot Fig 14, represents total volume scattering coefficients measured with the pseudo-photopic response during the OPAQUE II flights The general characteristic best illustrated in this set is the low altitude haze layer that typifies so many of these profiles The low altitude changes in scattering coefficient can easily exceed a factor of ten within the last 1000 meters The magnitude and altitude of this often abrupt haze boundary are obviously major influences upon the determination of slant path transmittances through this lower altitude regime, and can be ignored only at the peril of major error in our determinations

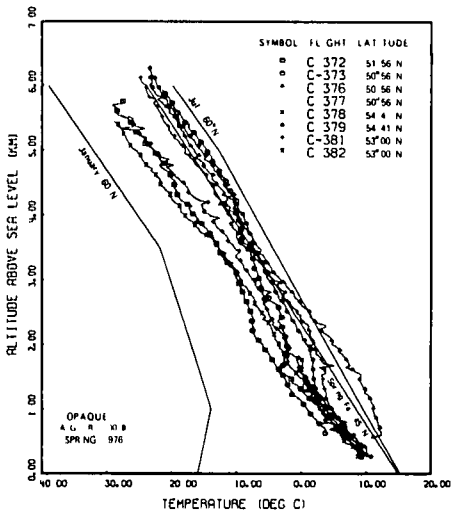

Fig 12

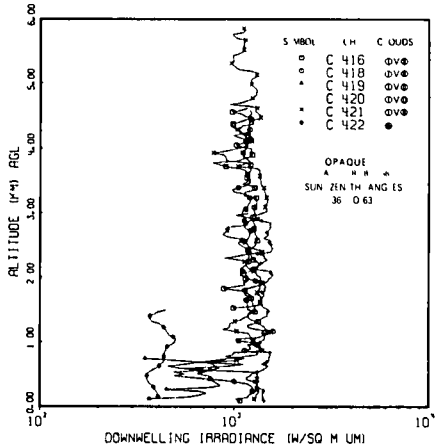

Fig 13

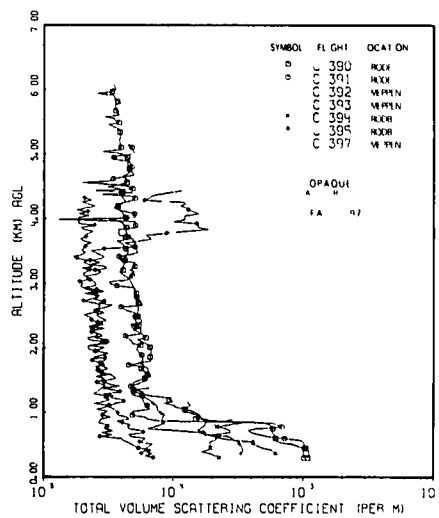

Fig 14

Three Plots of Summarized Data Displays

This final set of three figures illustrates several automatic displays which are being generated to aid in the analysis of the C-130 profile measurements The displays are produced for each flight and are intended to form the data base for further studies into the relationships between atmospheric humidity and aerosol scattering

Figure 15 contains the pseudo photopic scattering coefficient and relative humidity profiles measured on flight C-412 These data were selected to point up the close similarity in the major structural characteristics between the two sets of measurements, a common feature found on many flights both within the OPAQUE and other previously collected data sets

Figure 16 represents the same basic data displayed as a scatter diagram, but with the scattering data pseudo normalized by displaying it as the ratio of the total to the Rayleigh scattering This ratio of "s" to s_R is referred to by some investigators as equivalent ground level scattering If the display were sorted by spectral filter, then the clearly strong correlation could be recognized quite readily

Fig 17 again represents the same basic data, but with the relative humidity converted to absolute humidity and the scattering data adjusted to represent only the Mie component The flexibility and convenience of these automatic displays has provided an increasingly useful and powerful tool in the analysis of these flight data, and the determination of their applicability to the overall task of developing operational optical forecasting

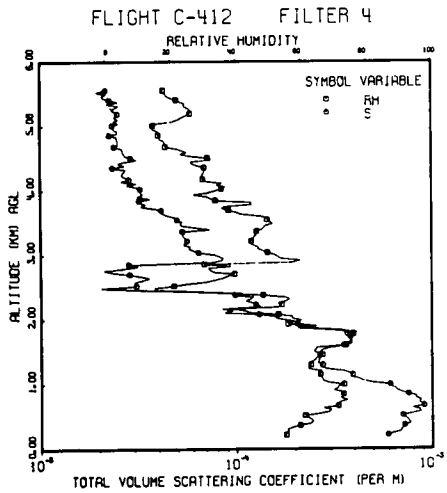

Fig. 15.

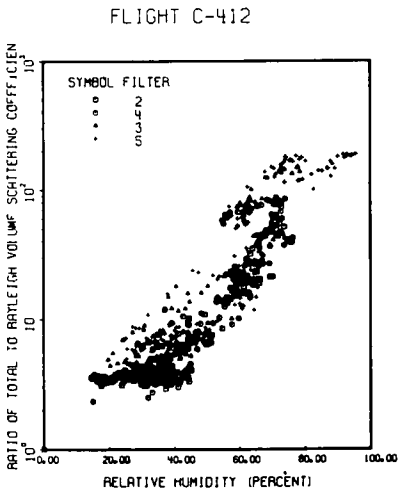

Fig. 16.

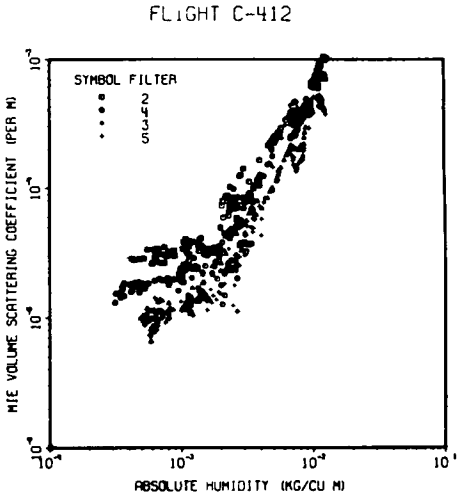

Fig 17.

Three Plots of Alternate Displays for Analysis

Summary

Atmospheric measurements of the type illustrated herein have been made during five European deployments on a total of 10 different flight tracks in six different countries Geographically, the 86 flights are relatively evenly distributed with the minimum of six occurring in the Netherlands, the maximum of 21 occurring in northern Germany, and the remaining five sites averaging 12 flights each Temporally, the flights represent all four seasonal conditions during daylight hours between mid-morning and late afternoon

These vertical profile data in conjunction with the extensive ground based data collected by the European scientific community represent a major step forward in the coordinated documentation of the optical and meteorological properties of the European operational environment They provide a well specified data base upon which extensive analysis will build a more thorough understanding of the linkages between the optical and meteorological conditions and processes

Acknowledgements

This work has been supported by the United States Air Force Geophysics Laboratory under contract F19628-78-C-0200 The author thanks Dr Robert W Fenn and Major Ted S Cress for their encouragement and support throughout the conduct of the program

References

1 Duntley, S Q, R W Johnson, and J I Gordon (1978a), "Airborne Measurements of Optical Atmospheric Properties, Summary and Review III", University of California, San Diego, Scripps Institution of Oceanography, Visibility Laboratory, SIO Ref 79-5, AFGL-TR-78-0286

2 Duntley, S Q, R W Johnson, and J I Gordon (1978b), "Airborne Measurements of Atmospheric Volume Scattering Coefficients in Northern Europe, Summer, 1977", University of California, San Diego, Scripps Institution of Oceanography, Visibility Laboratory, SIO Ref 78-28, AFGL-TR-78-0168